Channel morphology and bedrock river incision: Theory, experiments, and application
to the eastern Himalaya

Noah J. Finnegan

A dissertation submitted in partial fulfillment of the requirements for the degree of

Doctor of Philosophy

University of Washington

2007

Program Authorized to Offer Degree:
Department of Earth and Space Sciences

University of Washington
Graduate School

This is to certify that I have examined this copy of a doctoral dissertation by

Noah J. Finnegan

and have found that it is complete and satisfactory in all respects,
and that any and all revisions required by the final
examining committee have been made.

Co-Chairs of the Supervisory Committee:

_____
Bernard Hallet

_____
David R. Montgomery

Reading Committee:

_____
Bernard Hallet

_____
David R. Montgomery

_____
Gerard Roe

Date:_____

University of Washington

Abstract

Channel morphology and bedrock river incision: Theory, experiments, and application
to the eastern Himalaya

Noah J. Finnegan

Co-Chairs of the Supervisory Committee:
Professor Bernard Hallet
Professor David R. Montgomery
Department of Earth and Space Sciences

The dynamics of incising bedrock rivers are a central focus of geomorphology and

geodynamics because of the primary importance of river incision in the coupling of surface

and tectonic processes, and because of the capacity of river morphology to reveal information

about tectonics. Bedrock channel morphology also remains a challenging fluid dynamical

problem. The components of channel morphology: width, shape, slope, depth, roughness, and

bed cover are central to channel incision because they collectively determine the magnitude

and variation of fluid stresses on the bed, and the ability of fluid stresses and transported

sediment particles to erode the bed. Here, I take two approaches, one experimental and one

theoretical, to investigate the controls on the morphology of incising bedrock channels. I then

apply the results of this work to the problem of estimating the spatial variation of river

incision rates throughout the eastern Himalayan syntaxis. I show that if the process of river

incision is assumed to be scale-invariant, channel width can be cast explicitly in terms of both

river slope and discharge. This scaling relationship is validated for three rivers, two in

California and one in Tibet, and suggests that river incision models can be significantly

improved by accounting for the fact that rivers must occupy smaller channels where they flow faster, in order to conserve mass. For an experimental river eroding due to bedload abrasion, I show that the width of active incision can be cast as a function of sediment supply, grain size and boundary shear stress, suggesting that natural channels may adjust width to accommodate fluctuations in sediment supply. Additionally, I show that channel roughness development due to vertical incision retards sediment transport and incision, and encourages deposition of alluvial cover. The presence of alluvial cover, in turn, forces incision over the lateral and higher regions of the bed. Drawing on my analysis of river morphology, I show that tight spatial co-location of patterns in inferred detachment-limited incision potential, saltation-abrasion potential, topographic relief and mineral cooling ages provide strong evidence for close coupling between river incision and rock uplift in the eastern Himalayan syntaxis.

TABLE OF CONTENTS

Page

LIST OF FIGURES

LIST OF TABLES

iii

Chapter 1

Introduction

1.1 Introduction

This dissertation is focused on understanding what controls the morphology of bedrock channels, and how this, in turn, is related to the ability of bedrock channels to incise their beds. In non-glaciated landscapes precipitation fuels river incision and fluvial sediment transport. The tectonic uplift of rocks, in turn, creates relief and orographic precipitation. Therefore, the growth of topography reflects the competition between the tectonic uplift of rocks and their destruction by climate and slope-driven erosion and sediment transport processes (Davis, 1889,1899; Hack, 1960). Although the idea that mountainous topography is in dynamic equilibrium between rock uplift and erosion is not new (Hack, 1960), only relatively recently have the global implications of the coupling of climate, erosion, and tectonics been explored (e.g., Molnar and England, 1990; Raymo and Ruddiman, 1992). The realization that climate, tectonics and topography are linked has led to an explosion of research related to understanding landscape responses to climatic and tectonic forcing and vice versa. For instance, it is now recognized that rivers can become steeper (Whipple and Tucker, 1999; Snyder et al., 2000; Kirby and Whipple, 2001), wetter (Anders, 2005), and therefore more erosive with faster rates of tectonic rock uplift, leading to the realization that patterns in topography and climate can potentially reveal information about spatial gradients in rock uplift rates (Seeber and Gornitz, 1983; Lavé and

Avouac, 2001; Finlayson et al., 2002; Wobus et al., 2003; Kirby et al., 2003; Vannay et al., 2004; Grujic et al., 2006; Wobus et al., 2006a). Additionally, modeling and field studies indicate that spatial patterns in climate and erosion, from the scale of a rain shadow to a large river valley, may themselves influence the location of deformation in active mountain belts (Willett, 1999; Beaumont et al., 2001; Anders et al., 2002; Koons et al., 2002; Reiners et al., 2003; Stolar, 2006), as well as their width and height (Whipple and Meade, 2004; Stolar et al., 2006; Roe et al., 2006, Willett et al., 2006). Such work has brought to forefront of geosciences the idea that rates of rock uplift with respect to the geoid and surface erosion should be driven towards a dynamic balance in geodynamically active ranges.

Because denudation in non-glacial settings ultimately depends on the ability of rivers to incise through uplifting bedrock, much research has centered specifically on understanding the dynamics of of bedrock incision by rivers (Howard and Kerby, 1983; Seidl and Dietrich, 1992; Wohl, 1993; Wohl et al., 1994; Seidl et al., 1994; Howard, 1994; Kooi and Beaumont, 1994; Rosenbloom and Anderson, 1994; Montgomery et al., 1996; Tucker and Slingerland, 1997; Stock and Montgomery, 1999; Whipple and Tucker, 1999; Whipple et al., 2000; Snyder et al., 2000; Sklar and Dietrich, 2001; Kirby and Whipple, 2001; Roe et al., 2002; Whipple and Tucker, 2002; van der Beek and Bishop, 2003; Tomkin et al., 2003; Lague et al., 2003; Sklar and Dietrich, 2004; Lague et al., 2005; Turowski et al., 2006; Molnar et al., 2006) . Incision undercuts hillslopes and drives landsliding, which is why the rate of sediment

delivered to a channel is commonly believed to depend on its own rate of incision (Burbank et al., 1996). However, depending on sediment supply relative to transport capacity in the channel, landslide derived debris can either promote erosion by providing tools or inhibit erosion when forming a protective alluvial cover (Gilbert, 1877; Sklar and Dietrich, 2001). Thus, the dynamics of bedrock river incision are now understood to be the product of rich but poorly understood feedbacks among climate, erosion and tectonics. Over geologic timescales, these feedbacks ultimately govern the ability of bedrock channels to simultaneously convey sediment and water sourced from upstream, and communicate tectonic base-level changes via incision throughout drainage basins (both up and downstream).

Our perception of how channels respond to variations in sediment supply, rock uplift, and water flux has been strongly influenced by models of bedrock erosion that generally assume rivers adjust to external forcing only via slope changes (e.g., Howard, 1994; Whipple and Tucker, 1999). However, in addition to slope, channel shape, width, roughness, and the extent and texture of bed-cover are also important to dictating channel bed incision for a given discharge and sediment flux because they influence, among other things, the magnitude and distribution of fluid stresses acting on the channel bed, the kinetic energy of transported sediment, and the ability of impacting sediment particles to damage the bed (Sklar and Dietrich, 2004). It is now recognized that channel width varies with rock uplift rate (Lavé and Avouac, 2001; Montgomery et al., 2002; Duvall et al., 2004; Finnegan et al., 2005a; Sklar et al.,

2005), rock strength (Montgomery and Gran, 2001; Wohl and Achyuthan, 2002), and flood stage (Hartshorn et al., 2002). In experiments, Wohl and Ikeda (1997) observed bedrock channel narrowing and deepening with higher channel gradients, while Carter and Anderson (2006) show that such channel narrowing and deepening can suppress bed incision and enhance wall incision, in the absence of bedload sediment. Additionally, recent numerical modeling results suggest that both discharge and slope changes will influence width adjustment in channels where incision is driven by boundary shear stress patterns (Wobus et al., 2006b; Stark, 2006). Laboratory and field studies highlight the importance of roughness in bedrock channels by demonstrating that strong feedbacks between incision and sediment transport can amplify boundary roughness and suppress incision (Shepherd and Schumm, 1974; Wohl and Ikeda, 1997; Wohl et al., 1999; Johnson and Whipple, 2004). Finally, alluvial cover extent and texture has been shown to vary with channel slope (Montgomery et al., 1996; Wohl and Ikeda, 1997), sediment supply (Dietrich et al., 1989; Buffington and Montgomery, 1999a), and channel roughness (Davis et al., 2005), and itself appears to strongly influence the style and location of bed wear (Sklar et al., 2005; Demeter et al., 2005).

Adjustments in channel slope ultimately require changes to the entire relief structure of a range (Whipple and Tucker, 1999), however width, bed-cover and roughness can potentially respond on much shorter time and length scales. Therefore an understanding of the specific controls on these factors is essential to understanding

how channels accommodate variability in climate, sediment supply, and rock uplift on geologic timescales. Additionally, because channel width and bed-cover, in particular, are straightforward to measure in the field, an increased understanding of how they influence channel incision may improve our ability to use geomorphic information to estimate the spatial distribution of incision rates in active orogens, which is of particular interest to many studies of active tectonics.

1.2 Chapter 2

In chapter 2 of this dissertation, I begin by focusing on the problem of what controls the width of an incising bedrock channel. I derive a simple relationship for the steady-state scaling of channel width. I then evaluate the proposed model for three rivers that are incising bedrock under both uniform and spatially variable rock-uplift. Next, I evaluate the sensitivity of river incision models to assumptions about channel width by comparing how both conventional width scaling laws and the proposed model predict spatial patterns in erosive potential when incorporated in a calculation of stream-power.

I show that on the basis of the Manning equation and basic mass conservation principles, the steady-state width (W) of river channels can be cast as a function of discharge (Q), channel slope (S), roughness (n), and width-to-depth ratio (α). Additionally, I propose that channel width-to-depth ratio, in addition to roughness, is a function of the material in which a channel is developed, and that where a river is

confined to a given material, width-to-depth ratio and roughness can be assumed

constant. Given these simplifications, the proposed width expression emulates

traditional width-discharge relationships for rivers incising bedrock with uniformly

concave fluvial long profiles. More significantly, this relationship also describes river

width trends in terrain with spatially varying rock-uplift rates, where conventional

discharge-based width scaling laws are inadequate. I suggest that much of observed

channel width variability in river channels incised in bedrock is a simple consequence

of the tendency for water to flow faster in steeper reaches and therefore occupy

smaller channel cross-sections. I demonstrate that using conventional scaling

relationships for channel width can result in underestimation of the variability of

stream-power in channels incising bedrock and that the proposed model improves

estimates of spatial patterns of bedrock-incision rates.

1.3 Chapter 3

In chapter 3, I report the results of an experiment designed to enable detailed

observations of how sediment supply and cover control the morphologic evolution and

incision rate of a bedrock channel. The intention of this chapter is to begin to embrace

the complexities of natural bedrock channel systems in an effort to move beyond some

of the commonly employed simplifications made in bedrock incision models. In my

experiments, I used a laboratory flume to investigate experimentally how bedrock

channel slope, width, roughness, alluvial cover, and incision rate collectively evolved

during the transient incision of an initially smooth channel with a varying bedload supply rate. Hence, channel slope, roughness, width, bed-cover and incision rate were free to adjust both to the supply of sediment and to the evolving morphology of the channel itself during the transient incision of the experimental channel.

The results of the experiments demonstrate that when the channel was free of alluvial cover, incision was focused over a fraction of the bed width that varied strongly with both bedload supply and bedload transport capacity. Non-dimensionalization yields a relationship for the width of active incision that explicitly incorporates bedload supply rate, sediment grain size, and bed shear stress, which suggests that in natural channels width may respond dynamically to accommodate changes in bedload sediment supply. Because increases in sediment supply widened the band of active bedload sediment transport and thus the width over which incision took place, mass removal from the bed scaled with sediment supply when the bed was free of cover, consistent with the number of available tools limiting incision rate. However, bed roughness growth due to the progressive incision of the bed during the experiment eventually led to deposition of alluvial cover and the suppression of incision on the bed at high sediment supply rates, consistent with a alluvial cover limiting incision rate. The dynamics of roughness creation and alluvial cover deposition can therefore drive both negative and positive feedbacks on incision rate change following sediment supply perturbations. These experimental results offer several potentially field-testable hypotheses that together are likely to help explain

variability in the width, slope, and bed roughness of bedrock river channels in transient landscapes.

1.4 Chapter 4

In chapter 4, I build on the analyses presented in chapters 2 and 3 in order to use river morphology to estimate spatial patterns in river incision potential in southeastern Tibet. Specifically, I compare patterns in river power, inferred excess fluvial transport capacity, topographic relief, precipitation, zircon (U-Th)/He ages, and biotite $^{40}Ar/^{39}Ar$ ages to assess the coupling between surface erosion and rock uplift in the eastern Himalayan syntaxis.

The analysis reveals a tight spatial correspondence of fluvial incision potential, high relief, and young biotite and zircon cooling ages. The spatial coincidence is most easily explained by a sustained balance between rates of vertical rock ascent and erosion at the surface over at least the last ~ 1 Ma. Only patterns in precipitation appear uncorrelated with exhumation, suggesting precipitation does not directly drive erosion in this region. I identify two regions along the lower Parlung Tsangpo and the upper Yarlung Tsangpo where I observe low river power and rapid mineral cooling in a manner locally inconsistent with a detachment-limited view of long-term river incision. Using the framework of the saltation-abrasion model (Sklar and Dietrich, 2004), however, this conflict may be reconciled in a manner that is self- consistent with both the model and field observations of these reaches. The Yarlung Tsangpo-

9

Brahmaputra River is the largest and most erosive river in the Himalaya, and two lines of evidence point to its role in the dynamic interaction of local erosion, rock uplift, thermal weakening of the lithosphere, and deformation: 1) Whereas along the rest of the Himalaya front, high relief and high rock uplift rates are essentially continuous, the high relief of the syntaxis is restricted to a "bullseye" pattern centered on the region where the largest river in the Himalaya, the Yarlung Tsangpo-Brahmaputra, is at its most erosive. 2) The location of rapid incision on the Tsangpo has been pinned for at least 1 million years, and without compensatory uplift of the Namche Barwa-Gyala Peri massif during this time, the Yarlung Tsangpo knickpoint would have eroded headward rapidly, incising deeply into Tibet.

1.5 Chapter 5

In chapter 5, I present basin-wide erosion rate estimates derived from measurements of cosmogenic ^{10}Be from river sediments in the eastern Himalayan syntaxis. While not directly pertinent to the question of channel morphology and river incision, the analysis provides a quantitative estimate of erosion rates across the eastern Himalayan syntaxis. These data, in turn, are helpful to the analysis of the dynamics of the eastern Himalayan syntaxis in chapter 4 because they provide constraints on the spatial distribution of erosion to compare with patterns in river morphology and exhumation. In chapter 5, I use ^{10}Be measurements (1) to map the spatial pattern of erosion rates across the eastern Himalayan syntaxis, (2) to make an

estimate of the volumetric sediment flux of the Brahmaputra river near where it exits the Himalaya, (3) to examine the relationship between topography and erosion rates within the sampled region, and (4) to assess the relative contributions of the Tibetan plateau, Tsangpo Gorge and Nyainqentangla Range to the sediment load of the Brahmaputra River.

Results reveal an order of magnitude increase in erosion rates from 0.13 – 0.24 mm/yr for the southern Tibetan plateau to 1.07 – 3.57 mm/yr for the Namche Barwa-Gyala Peri massif and Nyainqentangla Range. Samples from 1 – 30 km^2 sub-catchments display less than a two-fold variation in erosion rates. The observed regional increase in erosion rates across the study area is correlated with regional increases in topographic relief (R^2 = 0.81). Based on the data, 62 +/- 9 % of the flux of the Yarlung Tsangpo-Brahmaputra River at Medoc, Tibet is sourced from the 14 % of the catchment within the eastern syntaxis. Given uncertainties in [10]Be production rates due to glaciers within the study region, the analysis allows for erosion rates as high as 6 mm/yr within the Tsangpo Gorge and its direct vicinity.

Chapter 2

Controls on the channel width of rivers: implications for modeling fluvial incision of bedrock

2.1 Introduction

The role of bedrock-channel incision on the evolution of mountainous topography has become a central concept in geomorphology (e.g., Seidl and Dietrich, 1992; Burbank et al., 1996). Considerable attention to rivers incising bedrock in tectonically active landscapes (e.g., Whipple and Tucker, 1999) has led to the use of river morphology in interpreting the scale, magnitude, and timing of rock uplift, for which other evidence is often sparse or equivocal (e.g., Lavé and Avouac, 2001; Finlayson et al, 2002; Kirby et al., 2003). Collectively, this work has highlighted the stream-power model of river incision as a valuable tool for exploring the dynamics of fluvial erosion of bedrock.

The stream-power model generally casts bedrock incision rate, E, as a function of river slope, S, and river discharge, Q: $E = kQ^m S^n$, where k represents bedrock-specific erosivity, and m and n are empirically determined or selected on the basis of the hypothesized control on incision rate, e.g., power or shear stress (Whipple and Tucker, 1999). Estimation of river power per unit bed area or shear stress requires direct knowledge of channel width, typically approximated as bank-full channel width. However, spatially continuous width measurement necessitates high-resolution imagery and/or labor-intensive ground surveying. For this reason, models of bedrock

incision often do not treat width explicitly, but instead rely on the assumption that channel width is a power-law function of discharge where $W \propto Q^b$. This substitution subsumes width variations into the exponent m on Q in the stream-power model. Substantial empirical work does suggest that discharge-based width-scaling relationships are valid for alluvial rivers and that $b \approx 0.5$ (e.g., Knighton, 1998). Examples where these relationships have been evaluated for bedrock channels typically exhibit exponents on area or discharge of 0.3 to 0.5 (e.g., Whipple, 2004).

Field-based studies provide evidence for the alternative view that channel width varies locally, much like channel slope does, in association with spatial changes in rock uplift rate and erodibility. Lavé and Avouac (2001) and Montgomery and Gran (2001) demonstrate downstream narrowing of river channels in bedrock associated with a downstream increase in rock uplift rate and bedrock hardness, respectively. Additionally, Duvall et al. (2004) show that variation in channel width, as well as slope, can account for inferred differences in long-term fluvial incision rates between two neighboring rivers experiencing different uplift. These studies show that simple scaling relationships between width and discharge alone are not adequate in precisely those situations where it is most interesting to be able to estimate bedrock incision rates: where rates of uplift or rock erodibility vary spatially. Additionally, in an effort to provide a theoretical basis for the empirical equations of downstream hydraulic geometry, Griffiths (2003) derived a series of analytical expressions that relate channel width, roughness, depth, slope and discharge. However, because the

analysis relies on the constraint that width scales linearly with downstream distance, the Griffiths model cannot address the downstream narrowing of channels. Generally, it remains unknown whether adoption of the traditional assumptions of hydraulic geometry has hindered understanding of the coupling between bedrock incision and tectonic processes.

Below I derive a simple relationship for the steady-state scaling of channel width. I then evaluate the proposed model for three rivers that are incising bedrock under both uniform and spatially variable rock-uplift. Under the simplifying assumption of constant channel width-to-depth ratio and Manning's n, I compare how conventional width scaling laws and the proposed model predict spatial patterns in erosive potential when incorporated in a stream-power calculation. I conclude that bedrock channel width varies with both discharge and river slope, and that scaling channel width with only discharge, as is common, underestimates unit stream-power in areas where rivers steepen downstream.

2.2 Model

The Manning equation (Manning, 1891), which is widely accepted as an empirical flow law for rough, steady, and uniform channel flow, states that the cross-section average water velocity, U, is given by:

$$U = R^{2/3}S^{1/2}/n, \tag{1}$$

where R is hydraulic radius, S is bed slope, and n (Manning's n) is an empirical roughness coefficient. The hydraulic radius of the flow is its cross-section area, A, divided by the wetted-perimeter, W_p. For a rectangular channel where bank-full width, W, and depth, D, are related by the width-to-depth ratio $\alpha = W/D$ (referred to hereafter as α), area and wetted perimeter are easily rewritten in terms of bank-full channel width

$$W_p = W + 2D = W(2/\alpha + 1), \tag{2}$$

and

$$A = W^2/\alpha. \tag{3}$$

Substituting equations 2 and 3 for R in equation 1 and simplifying yields

$$U = (\alpha+2)^{-2/3}W^{2/3}S^{1/2}/n. \tag{4}$$

It is straightforward to show that equation 4, although derived here for a rectangular channel, is valid for all rivers where W and R are linearly related, i.e., for channels where α is constant. In natural channels, α appears to be relatively constant for a given channel-bed material (Figure 1), suggesting that the assumption of constant width-to-depth ratio is an acceptable simplification for a channel developed in a particular material. From mass conservation, the flow discharge can be expressed as $Q = UA$. Multiplying equations 4 and 3 and solving for W therefore leads to

$$W = [\alpha(\alpha+2)^{2/3}]^{3/8}Q^{3/8}S^{-3/16}n^{3/8}. \tag{5}$$

Equation 5 thus states that channel width naturally increases with discharge (and therefore drainage area), as is widely recognized. The equation explicitly incorporates the effects of α and n, the latter of which by impeding flow increases cross-section area. Importantly, the equation also states that width can decrease with increasing channel slope, creating the potential for narrowing of channels where rivers steepen, for instance where they enter regions with faster rock-uplift rates or more resistant rock (e.g., Seeber and Gornitz, 1983; Kirby et al., 2003).

2.3 Methods

I tested the proposed model's predictions for two relatively simple, concave-up streams incising bedrock and experiencing spatially uniform uplift. Oak Creek and Kinsey Creek drain the coastal King Range in northern California and have each been intensively surveyed for channel width (Snyder et al., 2003). I also tested the proposed model against data from the bedrock-channel part of the more complex Yarlung Tsangpo River in southeastern Tibet, where it traverses a major antiformal uplift in the eastern Himalayan syntaxis. As it crosses this structure, the river steepens and narrows considerably within its bedrock gorge.

I restricted the analysis of the Yarlung Tsangpo to the region where it is clearly incising bedrock and sampled width every 100 m from a continuous map of channel width created by digitizing channels from 28.5 m pixel resolution Landsat 7 Thematic Mapper images of the river at high flow. Channel elevation profiles and slopes were

derived from the 3-arc second (~90 m) Defense Mapping Agency Digital Terrain

Elevation Data (DTED) for Asia. Mean annual discharge was obtained by routing

annual accumulated TRMM (Tropical Rainfall Measuring Mission) satellite-derived

rainfall on the 30-arc second GTOPO 30 DEM of Asia. Estimates of discharge using

TRMM data have been shown to agree with gauged mean annual discharges for 21

Himalayan catchments to within 15% (Anders et al., 2005). Due to the relatively

coarse DEM used for the Yarlung Tsangpo, it was necessary to segment the river into

10 km reaches in order to remove noise in the river elevation profile. For each reach,

mean elevation, mean channel width, and slope were calculated.

I used Snyder et al.'s (2003) field-measured bank-full width data for Oak

Creek and Kinsey Creek. Elevation and slope data were derived from 10-m-resolution

USGS digital elevation data as reported in Snyder et al. (2003). I calculated mean

width, elevation, and slope for every 3 data points in the dataset, resulting in mean

values spaced at roughly 100 m intervals. Mean annual discharge was estimated for

Oat Creek and Kinsey Creek by applying the relationship between mean annual

discharge and drainage area for nearby Honeydew Creek (Snyder et al., 2003).

Errors in slope data for all rivers were calculated using the root mean square

error (RMSE) of 7 m for the 10-m-resolution DEM and 18 m for 3-arc-second-

resolution DEM (EROS Data Center, 2000; Gesch and Larson, 1998). These

uncertainties were propagated through the various calculations of mean width and

mean stream-power below and are represented in the figures. It is important to keep in

mind that the uncertainties shown in the figures apply only to values averaged over 10 km for the Yarlung Tsangpo, and roughly 100 m for the rivers in the King Range.

2.4 Model Evaluation

Like alluvial rivers, many rivers incising bedrock also exhibit relatively simple, concave-up elevation profiles, where slopes decrease steadily in a downstream direction. For this class of rivers, elevation profile data can be fit into the form

$$S = kQ^{-\theta}, \tag{6}$$

where θ is referred to as the concavity index (Flint, 1974). Substitution of equation 6 into 5 yields the following expression for the dependence of the width of a river on concavity and discharge, with constant α

$$W \propto Q^{3/8 + 3\theta/16} n^{3/8}. \tag{7}$$

For a typical concavity index of ½ and constant roughness, equation 7 yields

$$W \propto Q^{15/32} \approx Q^{0.47}. \tag{8}$$

Hence for rivers with uniform concavities, the model accounts for the discharged-based downstream width relations typically observed for alluvial channels. More significantly, the similarity of the proposed relationship to traditional width empiricisms is confirmed for bedrock channels after plotting measured channel width, channel width determined from equation 5 with constant n and α ($kQ^{3/8}S^{-3/16}$), and channel width determined from assuming width scales with $Q^{1/2}$ along Kinsey Creek and Oat Creek in northern California (Figure 2). Notably, the simplified version of

equation 5 is indistinguishable from a simple relationship in which width scales only with $Q^{1/2}$.

Equation 5 also predicts that anomalously steep reaches will have higher water velocities— provided that changes in channel bed roughness do not offset those in slope—and, in order to conserve water flux, smaller cross-sections. Under the assumption of constant α, channel width and depth are proportional to the square root of cross-section area, and so these reaches should both shallow and narrow. Rivers incising bedrock in tectonically active or lithologically variable regions frequently lack consistent and uniform concavities, and local convexities are commonplace (Seeber and Gornitz, 1983; Kirby et al., 2003). In such locales, equation 5 indicates that simple width-discharge scaling relations should lose their predictive power.

To evaluate this analytical prediction in more tectonically complex terrain, I applied the proposed width model to the Yarlung Tsangpo River. For the Yarlung Tsangpo, I calculated linear regressions (forced through the origin) of measured channel width vs. $Q^{1/2}$ and of measured channel width vs. $Q^{3/8}S^{-3/16}$ (equation 5 with constant n and α). For the Yarlung Tsangpo, regression of width against $Q^{3/8}S^{-3/16}$ yielded better fits ($R^2 = 0.68$) than did a model that scaled width with only $Q^{1/2}$ ($R^2 = 0.40$) (Figure 3A). The extent to which the model matches the data supports the idea that channel shape tends towards self-similar adjustments when confined to bedrock. These changes depend primarily on discharge and slope, which are themselves

externally modulated by factors such as regional base-level, rock uplift rate, bedrock resistance to erosion, and climate.

2.5 Modeling River Incision

River long profile analyses, which typically rely on width-discharge scaling relationships, have become an important tool for inferring spatial and temporal patterns in rates of bedrock incision and, where steady-state is assumed, rates of rock uplift. In order to explore the sensitivity of river incision models to different methods for estimating channel width, I compared how conventional width scaling laws and the proposed model predict spatial patterns in unit stream-power (Figure 3B). For the Yarlung Tsangpo, unit stream-power ($\Omega = \rho g Q S / W$) was calculated using mean annual discharge, slope, and channel width obtained in three ways: (1) measured; (2) determined from a conventional width relationship of the form $W \propto Q^{1/2}$, which yields an expression of the form $k Q^{1/2} S$; and (3) determined from equation 5, which with constant n and α, yields an equation that takes the form

$$\Omega = k Q^{5/8} S^{19/16}. \tag{9}$$

For the Yarlung Tsangpo, use of a simple width-discharge scaling law results in as much as a 40% underestimate of unit stream-power along the sections of the river that steepen downstream. In general, such an approach also tends to damp the spatial variability in erosive power because it does not reflect the tendency for channels to narrow where they steepen. Equation 5 comes closer to describing the full

downstream variability in the width of the Yarlung Tsangpo and hence the actual unit

stream-power (Figure 3B). The proposed model thus has important implications for

fluvial responses to variable rock uplift and lithology, which are of particular interest

in most active orogens. Because width appears to narrow as slope increases, a channel

requires less of a change in slope (and therefore fluvial relief) than it would if slope,

alone, responded to a particular forcing such as rock uplift rate, bedrock resistance to

erosion, or climate. This tendency for channels to narrow as they steepen thus

provides a negative feedback on fluvial relief change and results in the non-linear

exponent on slope in equation 9.

2.6 Discussion

Equation 5 highlights the relative complexity of modeling channel width when

flow velocity is considered. However, it's worth noting that all stream-power incision

models make implicit assumptions about velocity. For example, Whipple and Tucker

(1999) assume roughness is constant by inserting the dimensionless friction factor, C_f,

from their momentum equation into the rate constant, K, in their erosion equation.

Additionally, in their derivation width is assumed to vary only with discharge. These

constraints force flow depth, and therefore α, to accommodate all variation in cross-

sectional area due to changes in velocity dictated by the momentum equation.

Although this model was clearly not developed with the intention of predicting reach-

scale morphology, it provides an example of how stream-power models make implicit

requirements of the morphology of rivers. In order to explore the particular

phenomenon of width scaling observed in bedrock channels, I have explicitly coupled

width and depth in this analysis, and thereby allow changes in cross-sectional area to

be accommodated by both depth and width.   While I provide justification that α

remains relatively constant for channels confined to a particular material (Figure 1), I

acknowledge the fundamental control that my choice of treating the width-to-depth

ratio imposes on the scaling of behavior of channel width in this analysis. Given the

lack of a clear consensus on the controls on width-to-depth ratio in natural channels, I

stress that other ways of scaling α can easily be accommodated in my framework.

Nonetheless, equation 5 should be applied cautiously as it requires that R (hydraulic

radius) and W (channel width) be linearly related.

From Figure 1 it is also clear that significant changes in channel width are to

be expected at boundaries between different types of channels, for instance where a

river transitions from alluvium to bedrock. Such width transitions do not result from

flow velocity changes alone, and it is for this reason that I avoid alluvial reaches in

this analysis. I speculate that the systematic changes in α shown in Figure 1 reflect

different critical shear stresses for mobilization or erosion of channel boundaries

developed in different materials. Specifically, bedrock channels can support much

higher wall shear stresses than gravel channels. Hence a river can likely maintain a

narrower channel in bedrock than in gravel at the same discharge.

Because channel roughness, bed-material, and caliber are inextricably linked, it is difficult to consider any of these factors independently, particularly for channels with mobile beds. Without knowledge of Manning's n, I have assumed in all of the regressions and modeling that n is constant. As noted earlier, all stream-power formulations make the same implicit assumption of constant roughness. However, there is significant work that suggests Manning's n may scale strongly with bed slope in alluvial rivers. For instance, Dingman and Sharma (1997) report that n varies with bed slope to a power of $0.3 - 0.4$ in alluvial channels. Adoption of such a relation for roughness would effectively cancel out any slope dependency in the proposed width model, thus reducing width to a simple function of discharge and α. This further simplification provides a good explanation for the observation that significant narrowing and changes in flow velocity are generally absent in alluvial channels (Leopold and Mattock, 1953), but it is unable to explain the downstream narrowing observed in natural channels confined in bedrock.

Whereas alluvial channel roughness can vary as bed coarsening occurs at higher shear stresses, a channel bounded by bedrock lacks an obvious mechanism to change boundary roughness as boundary shear varies. Therefore, I suggest that for the end-member case of a channel truly confined within bedrock boundaries, increases in flow velocity and narrowing will tend to occur where channels steepen because the flow feedbacks that operate in alluvial channels are suppressed. On the Yarlung Tsangpo, it appears that any downstream increases in roughness along the steeper

23

reaches of the river are not sufficient to prevent flow acceleration and the ~50% channel narrowing observed along the river, unless width-to-depth ratio systematically decreases downstream.

2.7 Conclusions

I have developed a scaling relationship for the width of river channels that depends on channel slope, river discharge, roughness, and channel width-to-depth ratio. A simplified version of this relation applied to longitudinally simple, uniformly concave bedrock rivers mimics traditional width-discharge relations that scale river width with only the square-root of discharge. However, equation 5 is considerably more versatile as it also describes river width trends in more complex terrain with spatial variations in rates of rock uplift.

Application of conventional discharge-based width scaling relationships to bedrock channels tends to underestimate erosive power along reaches that steepen downstream. On the Yarlung Tsangpo, unit stream-power calculated with a common discharge-based power-law for channel width is as much as 40% lower than estimates made from satellite-based width measurements and from my model. The analysis presented above indicates that modeling of bedrock channel incision would be improved simply by accounting for adjustments in channel width due to the tendency for water flowing faster through steeper reaches to occupy smaller channels.
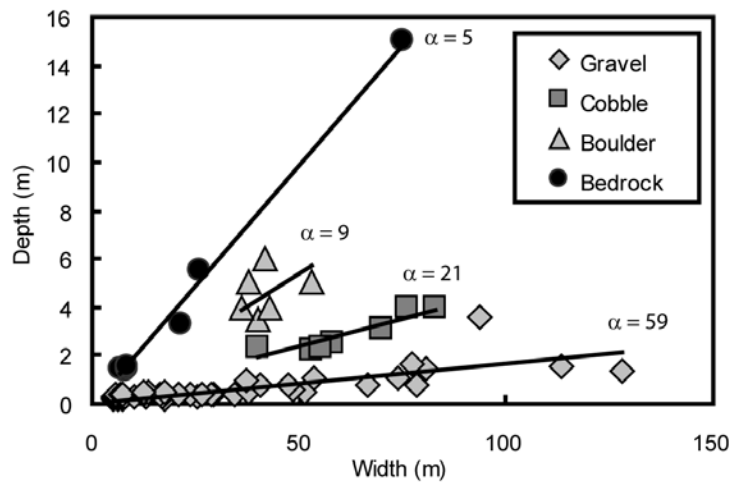
Figure 1: Plot of α for different dominant channel substrates
Gravel data are from the Yellowstone River, Wyoming (Leopold and Mattock, 1953),
and the largest bedrock width data point is from the LiWu River, Taiwan (Hartshorn et
al., 2002). Otherwise, data are from field surveys in the Cascades of Washington
State. While gathered from various locations, all bedrock data are from channels
incised in high-grade metamorphic or granitic rocks.
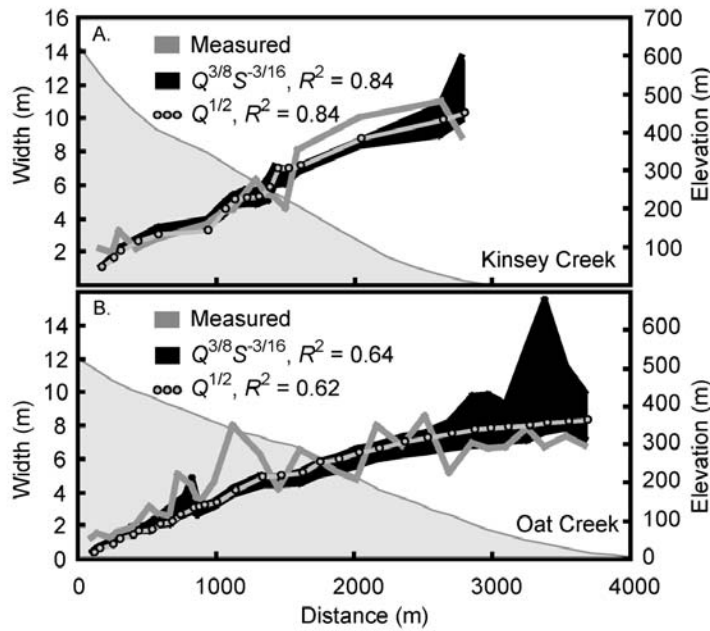
Figure 2: Channel width for Kinsey Creek and Oat Creek
River long profiles and comparisons of measured channel width (Snyder et al., 2003), channel width derived from a $Q^{1/2}$ relationship, and channel width derived from equation 5 for A: Oat Creek and B: Kinsey Creek, CA, USA. Uncertainties due to errors in width measurement and DEM-derived river slopes are represented by line thickness.
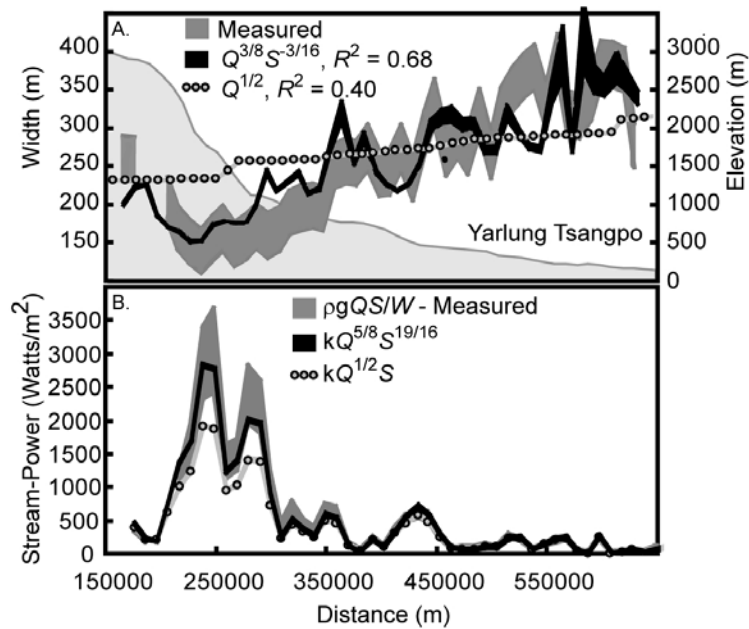
Figure 3: Channel width and river power for the Yarlung Tsangpo
A) River long profile and comparison of measured channel width, channel width derived from a $Q^{1/2}$ relationship, and channel width derived from equation 5 for the Yarlung Tsangpo, SE Tibet. B) Comparison of unit stream-power ($\rho g Q S/W$) for the Yarlung Tsangpo using measured channel width, width derived from equation 5, and width derived from a $Q^{1/2}$ relationship. Uncertainties due to errors in width measurements and DEM-derived slopes are represented by line thickness for both A and B.

Chapter 3

Interplay of sediment supply, river incision, and channel morphology revealed by the transient evolution of an experimental bedrock channel

3.1.0 Introduction

In mountainous landscapes, rivers convey sediment and water sourced from upstream, and communicate downstream base-level changes via incision. Consequently, bedrock river channels are thought to be a key link between climate, tectonics, and topography (e.g., Molnar and England, 1990). In landscapes undergoing transient evolution due to changes in climatic or tectonic forcing, the rate and style of topographic response will be strongly influenced by adjustments in the efficiency with which channels incise into bedrock and transport the coarse sediment load. At the scale of a river reach, changes in tectonic and climatic forcing will be felt at the downstream boundary through changes in the rate of local relative base-level lowering, and at the upstream boundary by changes in the rate and grain size of sediment supply and in the supply of water. Understanding the transient response of bedrock channels thus requires insight into the interplay between incision rate, bedload sediment transport, and the morphologic attributes that control the efficiency of these key processes.

Where bedload abrasion is the dominant incision mechanism, material carried by bedrock rivers – depending on sediment supply relative to transport capacity – can either promote incision by providing tools, or inhibit incision when deposited as a

protective alluvial cover (Gilbert, 1877; Sklar and Dietrich, 1998). Hence, many

incision models have some representation of both bedload transport and incision (e.g.,

Kooi and Beaumont, 1994; Lavé and Avouac, 2001; Whipple and Tucker, 2002;

Lague et al., 2005, Gasparini et al., 2006). The most mechanistically explicit model

developed to-date incorporates the physics of incision by bedload abrasion and the

physics of transport by saltating bedload (Sklar and Dietrich, 2004).

The ability of a channel to convey bedload is governed by channel slope,

shape, width, and roughness because together they control the magnitude and spatial

distribution of fluid stresses acting on alluvial sediments for a given discharge.

However in bedrock channels incised dominantly by bedload abrasion, these

components of channel morphology are themselves formed by the transported bedload

incising the channel boundary. Hence feedbacks must operate between incision,

sediment supply, and channel morphology to enable channels to transmit varying

sediment loads and incise their beds in response to relative base level lowering.

However, our understanding of how mountain channels respond to variations in

sediment supply is strongly influenced by models of longitudinal profile evolution that

assume that changes in channel slope are the primary way rivers adjust to changes in

external forcing (e.g., Howard, 1994; Whipple and Tucker, 1999; Whipple and

Tucker, 2002). Nevertheless, numerous studies suggest that in addition to slope,

channels can also adjust width, roughness, and the extent and texture of alluvial cover,

all of which also influence the ability of a channel to transmit bedload and incise its bed.

Field studies have documented channel width changes associated with variations in rock uplift rate (Lavé and Avouac, 2001; Montgomery et al., 2002; Duvall et al., 2004; Finnegan et al., 2005a; Sklar et al., 2005), rock strength (Montgomery and Gran, 2001; Wohl and Achyuthan, 2002), and flood stage (Hartshorn et al., 2002). In experiments simulating incision of a cohesive substrate by sand abrasion, Wohl and Ikeda (1997) observed bedrock channel narrowing and deepening with higher channel gradients, while Carter and Anderson (2006) show that such channel narrowing and deepening can suppress bed incision and enhance wall incision, in the absence of bedload sediment. Additionally, recent numerical modeling results suggest that both discharge and slope changes will influence width adjustment in channels where incision is driven by boundary shear stress patterns (Wobus et al., 2006b; Stark, 2006). However, the effects of sediment on incision are not considered in these models. Laboratory and field studies emphasize the importance of roughness in bedrock channels by demonstrating that strong feedbacks between incision and sediment transport can amplify boundary roughness and suppress incision (Shepherd and Schumm, 1974; Wohl and Ikeda, 1997; Wohl et al., 1999; Johnson and Whipple, 2004). Finally, alluvial cover extent and texture has been shown to vary with channel slope (Montgomery et al., 1996; Wohl and Ikeda, 1997), sediment supply (Dietrich et al., 1989; Buffington and Montgomery, 1999a), and

channel roughness (Davis et al., 2005), and itself appears to strongly influence the style and location of bed wear (Sklar et al., 2005; Demeter et al., 2005).

Whereas watershed-scale adjustments in channel slope to changing tectonic or climatic boundary conditions ultimately require changes to the entire relief structure of a mountain range (e.g., Whipple and Tucker, 1999), channel width, alluvial cover, and roughness might respond on much shorter temporal and spatial scales. The potentially significant role of these other modes of channel adjustment has important implications for understanding both transient and steady-state landscapes. If channel slope change is a relatively minor component of overall channel adjustment, and morphological adjustments can occur at rates similar to the rate of change in climatic or tectonic forcing, then river profiles may remain close to a state of dynamic equilibrium during transient evolution of other properties of the landscape, such as drainage density, ridge-top curvature, or the frequency of landslides. Conversely, if feedbacks between morphologic attributes such as channel width, roughness, alluvial cover and sediment transport capacity inhibit overall channel adjustment, then landscape transients may be longer-lived and result in greater topographic change.

To explore the interplay among channel morphology, bedload sediment transport, and bedrock incision, I conducted an experiment to observe the transient evolution of a laboratory bedrock channel in which channel slope, width, roughness, alluvial cover, and incision rate were free to adjust. I focus on transient response because steady-state channel morphology alone reveals little about the dynamics

governing channel evolution (e.g., Whipple and Tucker, 2002; van der Beek and Bishop, 2003). Adjustment of the experimental channel was designed to occur in response to two factors, the initial, non-equilibrium channel morphology, and systematic variations in sediment supply. I treat sediment supply as the independent variable because the entire model channel experiences supply changes essentially simultaneously, unlike changes in local base-level lowering rate, which must propagate upstream through the reach. Also, by varying sediment supply I can focus specifically on how changes in channel morphology influence the efficiency with which channels transport bedload and incise bedrock by bedload abrasion.

The balance of the paper is divided into four sections. Section 2 is a description of my experimental methods and design. In section 3 I present results of the specific responses of incision, alluvial cover, channel slope, channel roughness, and channel width during the experiment. In section 4 I synthesize and discuss the observations related to each of the transient response variables, and present a non-dimensional collapse of the width data. In section 5 I derive a scaling relationship for channel width that explicitly incorporates sediment supply and discuss its implications for understanding the controls on bedrock channel width.

3.2.0 Experimental Approach

3.2.1 Experimental methods

I conducted the experiment in a 7.2 m long, 1.2 m wide, and 0.33 m deep tilting flume, located at the University of California Berkeley Richmond Field Station. The flume was filled to a depth of about 30 cm with an artificial bedrock composed of a custom mix of cement, fine sand, and fly ash, delivered by a commercial concrete supplier. Tensile strength tests indicated that after an initial curing period the model bedrock had a tensile strength of approximately 0.05 MPa, which did not change significantly for the short duration of the experiment. The model bedrock formed a brittle-cohesive, massive block, for which the resistance to abrasion can be scaled using the method of Sklar and Dietrich (2001). The model bedrock did not erode by either clear water flows or by wetting-drying cycles. The flume has a motor-driven-auger sediment feed at the upstream end capable of delivering gravel to the channel at a fixed rate, and at the downstream end, a submerged basket suspended from a load-cell for measuring bedload sediment mass flux out of the flume. A pump circulates water up to a maximum discharge of 0.05 m^3/s. Mounted on a carriage above the flume is a laser scanning system for measuring high-resolution surface topography (Huang et al., 1988). The nominal vertical precision of the laser scanning system is 0.2 mm and the total scanned area of the flume is 350 cm by 65 cm. I used the laser to create-high resolution (5 mm grid size) digital elevation models (DEMs) during the experiment. By differencing the DEMs it was possible to create maps of incision for

each scan interval. Overhead-mounted, remotely-triggered digital cameras periodically recorded alluvial cover on the bed of the flume during the experiment.

I excavated an initial channel with a slope of about 1.6 % along the upstream half and a slope of about 2.6 % along its lower half (Figure 4A), with a trapezoidal cross-section with a top width of ~38 cm, a bottom width of ~22 cm, and a depth of ~12 cm consistently along the length of the flume (Figure 4B). I had initially intended to cut a uniform slope of 2% but due to changes in my excavation methodology as I moved downstream, I instead created the two slope segments; as discussed below this proved fortuitous because in the experiment differential adjustment of the upstream and downstream segments was observed. Over the course of the experiments $5.6 - 6.0$ mm diameter gravel was supplied to the channel at a rate varying between 0.011 kg/s - 0.059 kg/s. Discharge was fixed at 0.04 m^3/s and generally resulted in a flow depth of about 10 cm on the initial bed. Surface flow velocities ranged between $1.2 - 1.4$ m/s, and flows were super-critical throughout the experiments.

3.2.2 Experimental Design

In selecting the initial channel geometry, bed slope and sediment grain size I attempted to balance several sometimes conflicting goals. First, I sought a mean dimensionless shear stress (τ^*) well in excess of the high end of the range for the threshold of particle motion in alluvial channels ($\tau^*_c \sim 0.08$, Buffington and Montgomery, 1997), so that the channel could transport a wide range of sediment

supply rates without significant bed aggradation. Second, I selected a relatively large,

uniform grain size to maximize sediment impact kinetic energy in order to drive rapid,

measurable bed incision, and suppress erosion by suspended sediments. Third, the

flow was designed to be supercritical to be consistent with field observations of flood

discharges in bedrock channels (e.g., Tinkler, 1997) and to prevent backwater effects

at the downstream end of the flume. Finally, within the above constraints, I sought the

largest width to depth ratio to allow for lateral variation in the location of sediment

transport, partial bed cover, and bed incision.

Because I wanted both bedrock incision rate and channel slope to freely adjust

to the initial and upstream boundary conditions, I intentionally did not attempt to drive

incision by imposing a local base-level lowering rate at the downstream boundary.

Rather, the experimental design called for lowering the floor of the exit chute after

each run segment by an amount equal to the mean channel bed incision. As described

in detail below, these increments of downstream boundary lowering had no

discernable effect on incision rate or other morphologic responses in the portion of the

flume where measurements were made. Because flow remained supercritical

throughout the flume and the exit chute, the elevation of the downstream overflow

gate exerted no control on the flow depth or velocity upstream.

I divided the experiment into a sequence of run segments, each lasting six

hours. This interval corresponded to the minimum amount of time necessary to obtain

a clearly measurable incision signal on the bed of the flume. I scanned the elevation of

the bed at the end of each six-hour interval, after vacuuming any deposited sediment

out of the channel. I held sediment supply constant over multiple six-hour intervals in

order to determine how channel morphology evolved with a steady rate of sediment

supply, changing the sediment supply rate after either 12 or 18 hours. As described

below and listed in Table 1, I varied the sediment supply between three rates, in a

sequence designed in response to observations of the dynamic channel evolution. I

ended the experiment after 10 six-hour run segments (60 hours total run time) when a

thick alluvial cover formed at all sediment supply rates.

3.3.0 Results

3.3.1 Overview

Here I provide a brief overview of the experimental results, followed below by

a more detailed report of the response of each of the individual adjustable channel

attributes, including slope, incision rate, alluvial cover, roughness and width. Over the

course of the 60-hour run time of the experiment, a gently meandering slot 2 to 20 cm

wide and 2 to 10 cm deep formed along the length of the bed of the initial channel

(Figure 4B and 4C). The entire bed lowered by an average of about 2 cm over the

experiment (Figure 4A), but locally incision was as high as 9 cm (Figure 4C). After

60 hours, even at its most deeply incised point, the channel was still over 8 cm from

incising to the base of the cement mixture. The erodible walls of the initial trapezoidal

channel remained essentially un-incised during the experiment (Figure 4B and 4C),

except for in a few locations where lateral erosion occurred at the base of the channel walls. The spatially non-uniform vertical incision increased the channel bed roughness and the tendency for alluvial deposits to form, coincident with a reduction in incision rate for a given sediment supply rate. I observed a consistent pattern of variation in slot width in which lower sediment supply rates and higher excess shear stresses corresponded with narrower slot widths.

3.3.2 Slope

Channel slope scales bed shear stress and is therefore central to a channel's ability to transport sediment and incise its bed. Slope change is generally modeled as the primary mechanism by which bedrock channels adjust to changes in the rate of relative base-level lowering (e.g., Whipple and Tucker, 1999). However, in addition to responding to the rate of base-level fall, mountain rivers also transport coarse sediment as bedload. This observation has led to debate about the extent to which bedrock channel slope adjusts in order to transport sediment, such as is observed in alluvial channels (e.g., Ikeda and Iseya, 1988), and the extent to which it responds to base-level lowering (Sklar and Dietrich, 1998; Whipple and Tucker, 2002; Sklar and Dietrich, 2006).

Despite the short duration of the experiment, meaningful slope change did occur in the upstream and downstream segments that were initially excavated to different slopes. As a result, the initial slight convexity in the channel was erased over

the experiment so that the entire channel approached a uniform gradient. As shown in Figure 5, the downstream portion of the channel decayed in slope from 0.0264 to 0.0208, while the upstream portion of the flume increased its gradient from 0.0159 to 0.0192. These changes in gradient are consistent with the initial convexity rotating or diffusing into the upper in portion of the flume as the experiment progressed in time. For the flume as a whole, however, the average slope remained essentially unchanged. The mean slope of the channel declined from 0.0209 to 0.0202 over the course of the experiment, a change of only 3% of the initial value.

The changes in slope in the upstream and downstream portions of the flume were due primarily to the locally higher incision at the crest of the convexity, and were not driven by base-level fall imposed on the channel from downstream. I was unable to measure incision at the downstream-most portion of the flume because the laser scanner could not move closer than 70 cm from the exit chute, where I attempted to lower base level to keep pace with upstream incision. Visually, I observed formation of small pulses of accelerated incision at the downstream boundary, however these did not appear to propagate further than a few decimeters upstream, and did not propagate into the area of the channel where elevation measurements were made with the scanner. My interpretation is that the region scanned during the experiment was disconnected from the downstream boundary condition and that incision of the channel was driven by the initial slope and not by base level lowering.

3.3.3 Incision rate

To highlight specific ties between channel incision, morphology, and sediment supply, I distinguish two ways of measuring vertical wear in the experiments: slot-averaged incision, and bed-averaged incision. Slot-averaged incision is calculated by averaging vertical incision only over the bed area of the actively incising slot. Because slot growth was inhibited by the formation of alluvial cover, slot-averaged incision only took place when alluvial cover was largely absent from the bed and incision was focused along a single well-defined zone. It records the ability of the channel to incise vertically and thereby to transmit base-level changes upstream. Bed-averaged incision is an integrated measure of incision averaged over the entire width of the flume during the experiment. It is therefore sensitive to the changing area of incision during the experiment, and serves as an index of total channel incision and as a proxy for the volume eroded out of the flume.

Figure 6 shows the time sequence through the experiment of the sediment supply rate, the bed-averaged and slot-averaged incision rates for each six-hour interval, and the cumulative bed-averaged and slot-averaged incision depths. Examination of Figure 6 reveals fundamental differences in the evolution of slot-averaged incision compared to the evolution of bed-averaged incision during the experiment. Figures 6A and 6E show that slot-averaged incision rate declined steadily for each period of time during which the flume was at a fixed sediment supply. When sediment supply was fixed during hours 0 to 12, 12 to 24, and 52 to 60,

slot-averaged incision rate declined from 1.9 mm/hr to 1.5 mm/hr, from 2.0 to 1.6

mm/hr, and from 1.8 mm/hr to 1.3 mm/hr, respectively. Additionally, reductions in

the rate of sediment supply led to increases in slot-averaged incision rate, as shown by

the spikes in slot-averaged incision rate following drops in bedload supply at hours 12

and 42. The increase in the rate of bedload supply at hour 24, in contrast, led to no

measured slot incision due to the formation of a thick alluvial cover during this period.

Bed-averaged incision rate, in contrast, steadily decayed throughout the

experiment (Figure 6B and 6C). In contrast to slot-averaged incision, the trend in bed-

averaged incision was apparently less affected by the formation of alluvial cover, as

indicated by the continuation of bed-averaged incision during hours 24 to 42 of the

experiment. The incision of the bed during this time, although restricted to the

margins of the channel, was nevertheless measurable as bed-averaged erosion.

3.3.4 Alluvial cover

Alluvial cover is of fundamental importance to bedrock incision because it

armors the bed from the erosive forces of both water and mobile sediment and thereby

inhibits incision (Gilbert, 1877; Seidl et al., 1994; Wohl and Ikeda, 1998; Sklar and

Dietrich, 2001). Consequently, a clearer understanding of the controls on spatial and

temporal patterns of alluvial deposition, and their influence on rates and modes of

channel incision is desirable. I used photographs to record alluvial cover extent

periodically in the experiments, and I documented its impact on the style and magnitude of incision of the experimental channel.

I observed that after 12 to18 hours at a given bedload feed rate, the declining rate of slot incision culminated in the deposition of alluvial cover in the slot and cessation of further slot incision. Figure 7 shows photographs of alluvial cover during the experiment that reveal the transition from a relatively cover-free condition to a largely covered bed by hour 12 of the experiment. As discussed below, this transition was likely due to the growth of roughness on the bed and its role in inhibiting bedload transport. During periods of higher rates of slot incision, transient and isolated patches of alluvial cover formed along the bed, but the bed was predominately free of cover and the transported sediment contacted the bedrock directly.

The two reductions in sediment supply during the experiment led to temporary removal of alluvial cover followed by pulses of renewed slot cutting and narrowing. This renewal of incision is seen in the spikes in slot incision rate in Figure 6E associated with drops in sediment supply at hours 12 and 42. The increase in sediment supply at hour 24, on the other hand, resulted in negligible slot incision. This is because the narrower slot formed during the previous, lower sediment supply regime was rapidly filled with sediment, and led to the formation of a thick, protective alluvial cover that persisted from hour 24 to 42 of the experiment.

As the experiment progressed and the model bedrock became more deeply incised, the bed required progressively lower sediment feed rates to remain free of

alluvial cover. By the end of the experiment, alluvial cover formed at even the lowest bedload supply rate. When significant alluvial cover was present on the bed, bedload transport was concentrated in two narrow zones on either side of the alluvial deposit, where it was in contact with the relatively un-incised and thus smoother surface of the channel bed margins. In these instances, incision was focused along the edges of the alluvial deposit. Although incision still occurred on the bed of the flume after alluvial deposition (Figure 3C), there was no slot cutting because of the extensive alluvial cover filling the previously incised slots (Figure 3E).

3.3.5 Roughness

Roughness is important to incision by bedload abrasion for at least three reasons. First, roughening of the channel increases the probability that mobile sediment grains will come to rest where they are shielded from the flow by individual roughness elements (e.g., Kirchner et al., 1990; Buffington and Montgomery, 1999b). Second, roughness will locally increase the friction angle for stationary grains on the bed, thereby increasing grain resistance to motion (e.g., Kirchner et al., 1990). Third, roughness in channels increases the drag on conveyed fluid. Therefore, the growth of roughness in a channel results in the progressive reduction in shear stress available for bedload transport (e.g., Manga and Kirchner, 2000). For these reasons, the growth of roughness in bedrock channels, due to spatially variable incision, represents a

potentially important negative feedback on incision rates (e.g., Wohl and Ikeda, 1997; Wohl et al., 1999; Johnson and Whipple, 2004).

Channel roughness is commonly quantified with empirical friction coefficients back-calculated from measurements of flow velocity or by metrics based on characteristic length scales, such as grain diameter or bar height (see reviews in Wohl (2000) and Dingman (1984)). For the purpose of illuminating feedbacks between bedrock incision and bedload sediment transport I prefer a roughness measure that is based on direct measurement of the evolving bedrock surface topography and which characterizes the bed surface over a range of length scales. Therefore, I quantified roughness in the experimental channel by calculating the extent to which both the bed and the walls of the channel deviated from perfectly planar surfaces. Specifically, I calculated a planar least-squares fit to the bed and each wall of the channel for every time step. For each surface, I then subtracted the actual topography from this plane and calculated the standard deviation of the distribution of differences between the plane and the actual topography. Because the deviations from a planar surface tended to be normally distributed (Figure 8), the standard deviation is an appropriate measure for the degree of surface irregularity. I note that spatially uniform incision will result in no apparent roughness growth according to this roughness metric. Therefore, changes in roughness are directly attributable to spatial variations in channel incision rates.

In Figure 9, I plot bed roughness and wall roughness during the experiment. Figure 9 indicates that roughness on the bed quadrupled over the experiment, whereas wall roughness was essentially unchanged. This is consistent with observations that incision in the channel was confined to the bed of the channel, where active bedload transport took place. Figure 9 also shows that roughness was generated only when the bed was incising vertically and free of significant alluvial cover. During hours 24 to 42, when the bed was mostly covered, bed roughness did not increase, despite the fact that incision was still taking place on the margins of the channel (Figure 6C).

Channel sinuosity is an additional source of roughness that increases drag by forcing lateral accelerations that extract fluid momentum. Hence, growth of sinuosity in transient channel evolution represents another potentially important negative feedback on incision rate. The slot carved after the first time step of the experiment had a very subtle meandering pattern to it, which although visually apparent had a sinuosity of only 1.01. This incisional meandering closely mimicked the meandering pattern in the high velocity, super-critical core of flow set up by lateral irregularities in the excavation of the initial channel. In subsequent time steps the slot sinuosity did not change from the initial value of 1.01, and the overall channel sinuosity did not change because there was negligible erosion of the channel walls. Thus, although sinuosity contributed to the total drag on the flow, it did not contribute to changes in bed roughness over the course of the experiment.

3.3.6 Width

The width of a channel is important to river incision into bedrock because it determines bed area over which sediment can be transported and influences both the magnitude and spatial variation of fluid stresses applied to the bed. However, the controls on channel width and its relation to both sediment transport and incision in bedrock channels remain poorly understood. Bedrock channel width adjustment can occur by widening due to lateral wear of channel walls and narrowing due to focused incision over only part of the channel cross-section. Thus the variability in the spatial distribution of incision directly influences the extent and rate of channel width adjustment.

In Figure 10 I plot spatial patterns and magnitudes of incision for the three 12-hour periods during which the flume was incising its bed at a fixed sediment supply rate and remained relatively cover free. For each period, incision was concentrated in a band that grew increasingly narrow as sediment supply was reduced. The changes in the width of the incising slot resulted from the fact that bedload transport was not spread evenly across the channel bed, but instead occurred over a fraction of the bed width, which varied strongly with the supply of sediment itself. Incision was concentrated in this zone of active transport, leading to a positive feedback in which the deepening slot become increasingly efficient at capturing and retaining mobile sediment, thus starving the region of the bed outside the slot of abrasive tools. As a

result of this feedback, the width of the incising slot evolved to match the width of the region of bedload transport.

I note that each of the slots shown in Figure 10 was not incised independently on an initially smooth bed. Rather, they were incised as the bed morphology evolved progressively through the experiment. Hence the initial conditions are not equivalent between each of the panels. Note also that the sinuosity of the slots shown in Figure 10 is visually exaggerated by the differing length scales of the horizontal and vertical axes in the plot.

The initially steeper slope in the downstream portion of the channel (Figure 4A) is spatially coincident with a narrowing downstream of the incising slot, clearly observed at both intermediate and high sediment feed rates. To explore this width variation in more detail, in Figure 11 I plot the longitudinal variation in the width of the slots formed at three sediment feed rates, along with the channel slope, slot-averaged incision rate, and bed-averaged incision rate along the flume. Figure 11B shows a strong difference in the mean width of the incising slot associated with the changes in sediment supply rate, as well as a clear downstream narrowing of the incising slot associated with the initially steeper channel gradient of the lower half of the flume (Figure 11A). Notably, Figure 11C indicates that the rate of slot incision was independent of the width of the slot. This is because changes in sediment supply did not clearly affect the rate of incision in the slot, but instead changed the region over which bedload transport and incision took place. This is evident in the bed-

averaged incision rate (Figure 11D), which shows the strong influence of the reduction of total incising area as a function of sediment supply.

As noted above, as the experiment progressed in time, the channel became rougher and alluvial cover was deposited at decreasing bedload supply rates until significant cover was present at all sediment feed rates. In Figure 12 I show patterns of bed incision for the same sediment supply rate at different times in the experiment to highlight the effect of the formation of alluvial cover on the spatial distribution of bed incision. In the early stages of the experiment there was no alluvial cover when the bedload supply rate was 0.059 kg/s, and I observed incision to be confined within a single well-defined zone on the bed (Figure 12A), particularly in the downstream portion of the channel. However, after significant morphologic evolution of the channel bed, deposition of a thick alluvial cover in the more deeply-incised central portion of the bed resulted when the high sediment feed rate of 0.059 kg/s was returned. When cover was present on the bed, bedload transport and incision were concentrated in two narrow zones on either side of the alluvial deposit, along the relatively smoother surface of the channel margins (Figure 12B).

To illustrate in more detail the effect of alluvial cover on the pattern of incision on the bed of the flume, I plot a time sequence of cross-channel elevation and incision profiles at one location along the bed of the flume (Figure 13). The figure depicts the initial pulse of incision at the first sediment supply rate between hours 0 and 12, followed by narrowing and continued incision, after the reduction in sediment feed

rate, between hours 12 and 24. When the sediment supply rate was returned to its

initial value between hours 24 and 42 and extensive alluvial cover was deposited,

there is negligible incision in the slot itself. Instead, vertical incision is concentrated

where the alluvial deposit intersects the channel boundary, and results in the widening

of the slot created under the first sediment supply regime.

3.4.0 Discussion of Results

3.4.1 Channel Slope

The modest change in mean bed slope over the 60 hours of experimental run

time, compared to the far more dynamic changes in roughness and alluvial cover,

highlights that fact that channel slope changes happen slowly. This is because the

time scale for slope adjustment is set not by the absolute incision rate but by the

magnitude of sustained longitudinal differences in incision rate through a reach. The

net reduction in mean bed slope in the experiment, from 0.0209 to 0.0202, is

equivalent to a difference in incision depth of 2.5 mm between the ends of the 3.5 m

length of scanned bed (Figure 4A), only about 14% the bed-averaged incision depth of

17 mm. In effect, 86% of the incision during the experiment did not contribute to

slope change.

It is anticipated that decline in mean slope, although modest, might

nevertheless reduce the efficiency of incision, particularly if slope adjustment is the

dominant way transient channels evolve toward a dynamic equilibrium. Figure 14

shows the variation in slot-averaged incision rate over the range of mean slope values for which the bed lacked significant cover. Slot-averaged incision is plotted because it represents erosional efficiency per unit slot width, and thus normalizes for the changes in sediment feed through the experiment. The data do show a weak positive correlation between slope and slot-averaged incision rate, however the linear regression slope is not significant ($P \sim 0.23$). I therefore interpret the large scatter as evidence that changes in bed roughness (discussed below) have a larger effect on incisional efficiency and thus dominate the transient evolution of incision rates.

The primary slope adjustment observed was the elimination of the slight profile convexity created in the initial channel excavation. The response of the channel to this initial slope perturbation can provide insight into relative roles of the efficiency of bedrock incision and bedload sediment transport in channel evolution. On the basis of numerical modeling, Whipple and Tucker (2002) argue that the long-profile evolution of a channel in response to a transient incision wave is diagnostic of whether it is a channel where incision is limited by the ability to move sediment or by the ability to detach bedrock. Specifically, these two cases can be distinguished by the observation that a pulse of relative base-level lowering in a transport-limited channel will diffuse upstream, whereas in a detachment-limited channel it will be translated as a discrete knickpoint. Because the initial profile convexity diffused upstream (Figure 5) and was not translated as a knickpoint, incision in our experimental channel could be interpreted as transport-limited.

Sklar and Dietrich (2006) offer an alternative framework for considering the roles of sediment transport and rock detachment in controlling bedrock incision. Rather than considering incising channels as either transport or detachment limited, Sklar and Dietrich (2006) suggest that channels incising by bedload abrasion occupy a middle ground between these end-members, where the relative efficiency of both transport and detachment contribute to the steady-state channel slope that transient channels are presumably adjusting towards. Specifically, the steady-state slope (where incision rate and relative base level lowering rate are equal) can be considered a sum of the slope required to transport the imposed sediment load and an additional slope increment that creates excess transport capacity, which in turn causes bedrock exposure and detachment.

Early in the experiment, when the bed was relatively smooth and little or no alluvial cover formed even at high sediment supply rates, the channel slope was clearly steeper than the transport slope (the minimum slope needed to transport the load). Thus the channel could be considered primarily detachment limited in that the incision rate would have been greater if detachment were more efficient, due to weaker rock for instance. In this framework, the transient evolution of the channel to a rougher, more easily alluviated bed can be interpreted as a shift toward more transport limited conditions. Even though the mean slope was essentially unchanged during the experiment, the effective transport slope got steeper and approached the

actual channel slope by the end of the experiment, due to reductions in the efficiency of bedload transport.

3.4.2 Incision, Bed Roughness and Alluvial Cover

The evolution of bed roughness, alluvial cover and the rate of incision over the course of the experiment were highly interdependent. Therefore, in this section I discuss these three factors together, and focus on how changes in roughness and cover affect the efficiency of incision and bedload transport. A key goal is to explore possible feedbacks in channel adjustment as the channel evolved away from the initially smooth bed configuration and in response to the changing sediment supply. I note that channel width, apart from roughness, alluvial cover, and slope (discussed above), will influence the efficiency of transport and incision. Although the width of the channel didn't change appreciably because of the relatively short duration of the experiment, there was a very strong response of the width of the incising slot to variations in sediment supply over the experiment. I address channel width separately in next section.

I observed that the creation of roughness occurred only when the bed was incising and free of significant alluvial cover, as shown in Figure 9. After alluvial cover was deposited on the bed, roughness remained nearly constant (Figure 9), despite the fact that erosion of the bed continued (Figure 6B and 6C). These observations are consistent with the results of Demeter et al. (2005), who found that

partial alluvial cover focused incision on the exposed highpoints on the channel bed, resulting in either no increase or even a decrease in channel bed roughness, using the same roughness metric as we use here.

I infer that low roughness, cover-free channels, such as the initially smooth bed, are likely to be unstable. This is because smooth conditions favor slot cutting, which creates bed roughness, which in turn decreases the efficiency of bedload transport and eventually encourages deposition of alluvial cover. In Figure 15 I plot the sediment supply rate that corresponded with the onset of cover deposition as a function of the channel roughness, for each of the six-hour intervals during which I observed alluvial cover to form. The line connecting the three points in effect separates the cover-free from the dominantly-alluvial parameter space for the experiment. The figure illustrates that as sediment transport efficiency decreases due to the growth of bed roughness over the entire channel, the deposition of alluvial cover will occur at progressively lower sediment supply rates.

Increasing roughness also had the effect of reducing incision rates, even in the absence of significant alluvial cover. Figure 16A shows the variation in slot-averaged incision with bed roughness for the three constant-feed periods where the bed of the slot remained largely cover-free. I plot slot-averaged incision rate here because it enables examination of the effect of roughness on incisional efficiency for multiple supply rates, without the confounding effect of the changing width of bedload transport on bed-averaged incision. The rate of change of slot-averaged incision rate

with roughness creation was remarkably consistent over the experiment, -0.14 to -0.16 (mm/hr)/(mm).

The combined effects of roughness and alluvial cover formation on incision rates are shown in Figure 16B. In the figure, I plot the reduction in bed-averaged incision rate due to increasing bed roughness for the two periods of high sediment feed rate (0.059 kg/s), including when I observed active bed incision at the margins of an extensive alluvial cover (Figures 9 and 10). During the initial period (hours 0-12, closed circles) increasing roughness lowered the bed-averaged incision rate from 0.89 to 0.58 mm/hr, in part due to the growth of partial alluvial cover on the slot bed (Figure 7). In the second period (hours 24-42, open circles), larger bed roughness combined with the high sediment feed created an extensive alluvial cover that limited bed averaged incision rates to an average of 0.11 mm/hr, nearly an order of magnitude less than the smooth bed case.

To explore potential feedbacks between roughness, cover and incision rate, and their impact on how channels adjust to external forcing, I use the conceptual framework of the saltation-abrasion bedrock incision model (Sklar and Dietrich, 1998; 2001; 2004; 2006). As Gilbert first hypothesized in 1877, incision by bedload abrasion should be most efficient at a moderate sediment supply relative to transport capacity. Incision efficiency declines away from this maximum if supply is reduced, due to a shortage of abrasive tools (the tools effect), and also declines if supply is increased, due to an increase in the extent of alluvial coverage of the bedrock bed (the

cover effect). A key distinction between the saltation-abrasion model and the analysis presented here is that I am able to distinguish between local incisional efficiency, as represented by slot-averaged incision, and the bed-averaged incision rate. The saltation-abrasion model does not account for cross-sectional variations in incision rate and thus only predicts a bed-averaged incision rate. Here, I consider both slot-averaged and bed-averaged incision rates and ask how the channel responds to changes in both types of incision due to perturbations in sediment supply and bedload transport capacity.

Bed-averaged incision rates in the experiment show a clear tools-effect type dependency on sediment supply, as shown in Figure 17. Increasing sediment supply widens the band of active bedload sediment transport and thus the width over which incision takes place, leading to increased mass removal from the bedrock bed. However, as roughness increases, particularly for high sediment supply rates, a cover-effect type dependence takes over, decreasing sediment transport efficiency and driving incision rates down. The dependence of slot-average incision rates on sediment supply is less-clearly revealed in my experimental results because of the co-variation of sediment supply and evolving bedrock roughness. Figure 16A suggests, however, that the efficiency of slot-averaged incision may be greater for lower sediment feed rates, which is consistent with a cover-effect type relationship. This can be seen by assuming, for a given sediment supply, that the linear decline in slot-averaged incision with increasing roughness might extend to lower roughness values

and higher rates of incision. Then, for a given bed roughness, lower sediment supply rates would correspond with higher rates of slot-averaged incision.

For transient channel adjustment initiated by perturbations in the supply rate of bedload sediments, a cover-effect dependence of incision rate on sediment supply will lead to a negative feedback, mediated by roughness and cover adjustments. Negative feedbacks in this context are channel responses that tend to oppose the effect that the sediment supply perturbation would otherwise have on the channel, and they therefore tend to restore the pre-disturbance efficiency of incision. For example, with a cover-effect dependence of incision on sediment supply, a drop in incision rate due to a reduction in sediment supply will tend to be opposed by the fact that a greater fraction of the bed is exposed to sediment impacts at lower supply rates. Again, in this way the change in incision rate due to the sediment supply perturbation is suppressed via a negative feedback. Evidence for a negative feedback is clear in the response of slot-averaged incision rates to reductions in sediment supply. Reductions in sediment supply (at hours 12 and 42) had the initial effect of increasing erosional efficiency, but because this led to renewed slot cutting and increased bed roughness, slot erosion rates declined back toward the low values that prevailed before the change in supply (Figures 6E and 16A).

When I shift focus to bed-averaged incision rates, and consider the effect of an increase in sediment supply to a bed with substantial roughness, I also see evidence for a negative feedback loop. At hour 24 I increased sediment supply from 0.025 to 0.059

kg/s, and observed slot filling and the formation of an extensive longitudinal swath of alluvial cover. Consistent with a cover-effect response to increased supply, bed-averaged incision rates declined dramatically during the first 6 hour period (hours 24-30). However, the erosion that did occur was concentrated on the higher elevations of the bed, leading to a slight but noticeable reduction in overall bed roughness (Table 1). During the subsequent 6 hour period (hours 30-36) erosion rates rebounded substantially (Figure 6C), presumably because the smoother upper bed surface could sustain more energetic bedload transport with a narrower longitudinal swath of alluvial cover. Although the roughness adjustment led to an increase in bed-averaged incision rate, this represents a negative feedback in that the channel morphologic response tended to oppose the initial reduction of bed-averaged incision rate caused by increasing the sediment supply. The important implication of both of these cover-effect examples is that changes in external forcing can be accommodated by adjustments in roughness and cover, without any adjustment in channel slope.

Alternatively, with a tools-effect dependence of incision on sediment supply, a drop in sediment supply will lead to reduced incision by depriving the bed of tools, whereas an increase in sediment supply will promote incision by providing additional abrasive tools to the flow. Where incision rate has a tools-effect type dependence on sediment supply, positive feedbacks, mediated by roughness and cover adjustments, can therefore reinforce the effects of changes in supply on the efficiency of incision. In the experiments, I see this with the response of bed-averaged incision rates to

reductions in sediment supply, for example after the reduction in sediment feed from 0.059 to 0.025 kg/s at hour 12 (Figure 3A). Even though slot incision rate increased due to the drop in bedload supply (Figure 3E), bed-averaged incision continued to decline because the increase in local incision efficiency was more than offset by the reduction in the width over which incision took place (Figure 11D). The renewed slot cutting increased bed roughness and promoted alluvial deposition within the slot, which further decreased bed-averaged incision and thereby reinforced the lower bed-averaged incision rates initially promoted by the drop in sediment supply. Note that although the channel response involves the mechanism of bed cover formation, from the point of view of bed-averaged incision this is still a tools-effect type response in that lowering supply reduced incision rate. In the field, positive feedbacks that may be characteristic of tools-effect dominated channels would eventually lead to counteracting channel slope adjustments that would tend to restore the previous erosional efficiency. For example, channel reaches in which sediment supply reduction and roughness growth lead to a virtual shutting down of incision, as I observed in the experimental channel, would eventually steepen due to continued relative base-level lowering.

A key implication of the potential feedbacks identified above is that the magnitude-frequency characteristics of the distribution of events that supply both water and coarse sediment will strongly influence the evolution of roughness, alluvial cover, and incisional efficiency of both transient and quasi-steady-state bedrock

channels. Variations in the grain size distribution of bedload sediments should also have first-order effects on the evolution roughness and alluvial cover, which the experiments using uniform-size sediments could not reveal. For example, alluvial deposition within slots will be enhanced by a wide grain size distribution because only a small number of large grains are needed to form slot-spanning sediment jambs. In addition, the style and rate of bedrock roughness adjustment in particular will also depend on rock properties such as strength and jointing (Wohl and Achyuthan, 2002), and on the occurrence and frequency of events capable of resetting roughness, such as debris flows (Stock and Dietrich, 2003).

3.4.3 Channel width

The experimental results suggest that bedload supply exerts a fundamental control on the width of evolving bedrock river channels. Neither bedload transport nor incision was observed to take place uniformly over the available bed area. Instead, the width over which incision and bedload transport occurs can vary significantly depending on the balance between bedload supply and transport capacity. Additionally, when bedload supply approached the transport capacity in our experiments, alluvial cover was deposited on the bed. This led to concentrated transport and incision on the edges of the alluvial deposit, and thereby encouraged channel widening (Figure 13). Observations thus indicate that channels can adjust their width by changing the region over which vertical incision takes place.

According to the results, both the width over which incision takes place and its location in the channel, in turn, are directly related to the balance between bedload supply and transport capacity for a given channel. A similar phenomenon has also been observed in laboratory alluvial channels, in the absence of boundary incision. Specifically, Dietrich et al. (1989) observed experimentally that decreasing the rate of sediment supply to a channel causes a narrowing in the zone of active transport and a coarsening in the immobile channel margins.

The experiments therefore confirm that changes in the width of bedload transport and incision can be driven simply by changes in the rate of sediment supplied to the channel. Additionally, we show that for a fixed sediment supply rate, low transport stages encourage the growth of wider channels, while at high transport stages, incision and bedload transport are focused in the channel center, promoting channel narrowing (Figures 11 – 13). It is speculated that this focusing of transport arises due to a combination of secondary flow and the tendency for bedload transport to be channeled into topographic lows as they are incised (e.g., Johnson and Whipple, 2004).

Although a clear mechanistic understanding of the feedbacks governing this behavior is lacking, I have nevertheless made an effort to generalize the experimental results to further investigate how channel width changes might occur. Recall that transport and incision were observed to be generally focused in the channel center at high slopes and low supply rates, while at low slopes and high supply rates incision

59

and transport spread out across the bed. Bedrock channels could also plausibly
accommodate variation in sediment supply or transport efficiency by adjusting
bedload concentration over a fixed width of active transport. This is in fact an implicit
assumption of coupled bedrock-incision bedload-transport models that use a fixed
width but allow for changes in sediment supply (e.g., Sklar and Dietrich, 2004).
However, in my experiments the region of bedload transport in the channel adjusted
with changes in supply and transport efficiency. As a consequence, variation in
bedload concentration was minimized.

There is no obvious reason to expect channels to maintain constant bedload
concentration. However, it is reasonable to assume that grain-to-grain interactions
among bedload particles, which should be directly related to bedload concentration,
would oppose the buildup of particles in the channel center by driving lateral bedload
transport. I speculate that the width of the zone of bedload transport and incision thus
reflects a balance, on the one hand, between the feedbacks that to tend to focus
transport and incision, and on other hand, concentration-driven grain-to-grain
interactions that drive particles away from the channel center.

I calculate a non-dimensional bedload concentration, C^*, as follows:

$$C^* = \frac{3Q_s}{2D_s\rho_s WU_s} \tag{1}$$

where Q_s is bedload flux by mass, D_s is sediment diameter, ρ_s sediment density, W is
the width of active bedload transport and incision, and U_s is average downstream

bedload velocity. Equation 10 from Sklar and Dietrich (2004), an empirical fit to available saltation data, states that U_s can be predicted by,

$$U_s = 0.83(R_b g D_s)^{1/2}(\tau^*/\tau^*_c)^{0.83}$$ (2)

where R_b is the non-dimensional buoyant sediment density, g is the acceleration due to gravity, τ^* is the non-dimensional bed shear stress, and τ^*_c is the critical non-dimensional bed shear stress at the threshold of particle motion. Substitution of equation 2 into equation 1 yields

$$C^* = k_1 \frac{Q_s}{D_s^{3/2} W \left(\tau^*/\tau^*_c\right)^{5/6}}$$ (3)

where $k_1 = \dfrac{9}{5\rho_s(R_b g)^{1/2}}$.

Equation 3 is an expression for non-dimensional bedload concentration in terms of boundary shear stress, width, sediment supply, and grain size. Essentially, this conceptualizes bedload flux as a diffuse carpet of grains moving downstream at the saltation velocity, U_s. Physically, C^* is the ratio of the bed area occupied by bedload to the total bed area. It is obtained by projecting the active bedload into the plane of the bed and assumes grains do not overlap and that there is no alluvial cover. Despite the nearly six-fold variation in sediment supply and the two-fold variation in transport stage encompassed by my data, there is essentially no accompanying variation in C^* within measurement error. The value of C^* from the experiments is 0.048 +/- 0.007 (mean plus or minus standard deviation), which is obtained by averaging C^* from the data split between the upstream and downstream halves of the

flume, and averaged over 12 hours of incision. Notably, this suggests that changes in bedload concentration were minimal during the experiment.

Capitalizing on the fact that C^* remained relatively constant in our experiments, equation 3 can be solved for W and non-dimensionalized by grain size to obtain an explicit non-dimensional expression for the width of an incising slot in terms of bedload supply, grain size, and bed shear stress,

$$\frac{W}{D_s} = k_1 \frac{Q_s}{D_s^{5/2} C^* \left(\tau^*/\tau_c^*\right)^{5/6}} \qquad (4).$$

In Figure 18A, I plot the slot width data from the two halves of the flume as a function of bed slope, showing a trend between slot width and bed slope for a given sediment supply. In Figure 18B, I plot the same dataset against equation 4, using the value of C^* as reported above. The figure illustrates the excellent non-dimensional collapse in the data resulting from equation 4. Width was determined for these figures as follows. I first identified an incision depth threshold that exceeded the noise in the laser scan data. For incision data averaged over 12 hours, this threshold incision value corresponded to 10 mm. At every 5 mm increment along the channel, I then calculated the width of the channel over which active incision exceeded this threshold value. Finally, I averaged width values over the upper and lower halves of the flume in order to obtain reach-averaged slot widths. These data are reported in Table 2.

Equation 4 indicates that for the range of data available there is a unique width over which bedload transport (and hence incision) will take place for a given combination of sediment supply, grain size, and bed shear stress. Equation 4 assumes

channels maintain a constant bedload concentration where bedload transport is active in the channel. Therefore, an increase in bedload velocity or a reduction in the rate of bedload supply will decrease the width of the bed necessary for active bedload transport, in order to maintain constant concentration. In contrast, a decrease in bedload velocity or an increase in the rate of bedload supply will enlarge the width of the bed necessary for active transport, again given a constant concentration constraint. Equation 4 thus may provide an important clue into how channels change width. When channels are largely cover free, the width over which incision takes place is sensitive to the rate of sediment supplied to the channel, the bed shear stress, and sediment grain size. When cover is thick enough to impede incision of the bed, however, equation 4 is no longer strictly valid. In this case, incision appears to be concentrated in two zones where alluvial cover borders on exposed bedrock, but some of the mobile sediment may also pass over patches of alluvial cover rather than bedrock.

3.5.0 Implications for Bedrock Channel Width

What ultimately sets the width of channels, and how does this relate to incision rate? Extending experimental observations to addressing these questions is challenging because it requires integrating all of the magnitude and frequency variation in sediment supply and water flux experienced by a typical river. The experiments described herein suggest that variation in sediment supply relative to

transport capacity results in complex patterns of incision within a channel related to the changing width of bedload transport and due to formation of alluvial cover. Given natural hydrologic and sediment supply variability in most channels, both the width and location of incision in natural bedrock channels should change on a storm-by-storm basis, as observed by Hartshorn et al. (2002). My results therefore underscore the realization that natural stochasticity in both river stage and sediment delivery, although difficult to recreate in the laboratory, is likely to be essential to understanding the dynamics of natural channels (e.g., Snyder et al., 2003; Tucker, 2004; Lague et al., 2005; Molnar et al., 2006). Because the time scale of a single storm is small relative to the time scale of adjustment for an entire channel cross-section, hydraulic geometry must reflect a complex averaging of antecedent storm conditions (Stark, 2006).

In the experiment presented above, bedload supply varied at a much shorter timescale than the timescale of adjustment for the whole channel. Consequently, a channel with a single width never evolved. Rather, the channel was a composite of the initial channel and the slots formed under the various bedload supply rates (Figure 19A). Figure 19B shows a reach of Watkins Glen, NY at low flow. Watkins Glen, like the experimental channel, has experienced a reduction in sediment supply as its mantle of glacially-derived sediments has been stripped away during the late Pleistocene and early Holocene (Mullins, 1989). In both examples, remnants of abandoned, wider channel segments are still visible above the active channel.

Finally, in extending observations of slot incision to the problem of channel incision, it is necessary to consider the fundamental differences in the dynamics of slot incision observed in these experiments compared to the dynamics of channel incision. The important difference lies in the fact that in the experiments a slot never grew to accommodate the entire flow cross section.   Experimental results show that the slot incision rate was independent of slot width (Figure 11C). However, had the slot actually grown to accommodate the entire flow, it would have significantly increased flow depth in the channel and led to increased boundary stresses in the slot. According to experimental observations, this would, in turn, narrow the width of incision, which would drive up shear stress further. It is therefore possible to imagine a positive feedback wherein the channel would experience runaway narrowing until eventually it narrowed to the point where increasing wall drag inhibited sediment transport on the bed (e.g., Wohl et al., 1999). Although this is an appealing mechanism to explain slot canyon formation, it suggests a fundamental problem in using equation 4 to simulate channel width in most settings. Equation 4 requires another mechanism, such as the development of roughness, to stabilize channel width. It is therefore unclear whether in natural channels width simply responds passively to imposed sediment supply and transport efficiency, or whether via feedbacks with flow depth, width may actually help govern incision rate.

Thus, many reasons exist for why slot width and channel width are unlikely to be equivalent, and that suggest caution in using equation 4 to understand the channel

width of rivers. However, at the core of equation 4 is the notion that bedload transport tends to occur over a width that is unique for a given shear stress, grain size, and sediment supply. Seen in this light, the equation provides a useful jumping off point for exploring the interaction of bedload transport, incision, and channel width in bedrock rivers. To the extent that shear stress, discharge, and sediment flux can be defined in terms of characteristic reference values that meaningfully integrate their inherent natural variation, equation 4 may be cast in terms of quantities typical to hydraulic scaling. Below I derive a scaling relationship for channel width after making a number of simplifications to equation 4. I do this in the spirit of exploring the extent to which my experimental observations may help understand the role bedload plays in setting channel width scaling in natural channels.

By assuming constant sediment density, water density, roughness, τ^*_c, C^*, and gathering constants, equation 4 states:

$$W \propto \frac{Q_s}{D_s^{2/3}\tau^{5/6}} ,$$

(5)

where τ is mean bed shear stress. Using a wide, rectangular channel approximation and solving for flow depth from the Manning equation yields:

$$h = \frac{(Q_w n)^{3/5}}{W^{3/5}S^{3/10}}$$

(6)

where h is flow depth, Q_w is water discharge, n is an empirical roughness coefficient, W is channel width and S is channel slope. Via the same assumptions used to obtain equation 7, mean bed shear stress, τ, is given by:

$$\tau = \rho_w g h S \tag{7}$$

where ρ_w is the density of water. Substituting equations 6 into 7 and the resulting

equation for shear stress into equation 5, and solving for W yields:

$$W \propto \frac{Q_s^2}{Q_w S^{7/6} D_s^{4/3} n} \tag{8}$$

Equation 8 thus states that changes in the width of active bedload transport and

hence vertical incision would be driven either by variation in sediment supply or in the

ability of the channel to move sediment (slope, discharge, grain size or roughness).

Equation 8 is appealing because it provides a mechanistic basis for why channel width

is often inversely correlated with slope (Lavé and Avouac, 2001; Finnegan et al.,

2005a). Additionally, it provides a framework for evaluating the effects of, for

instance, orographic precipitation (Roe et al., 2002), spatially non-uniform sediment

delivery (Brandon and Gasparini, 2005), or downstream breakdown of bedload (Sklar

et al., 2006) on channel width scaling in watersheds. Testing equation 8 in a well-

constrained natural setting would provide a needed next step in validating its

applicability to natural channels. Additionally, equation 8 provides motivation for

exploring how dynamic adjustments in channel width might change sediment flux

dependent bedrock incision models that otherwise assume a fixed width.

Equation 8 also indicates that assuming constant channel width-to-depth ratio

(i.e. scale invariance), as has been suggested as a closure for channel width scaling

models (Finnegan et al., 2005a), may not be appropriate where there are large

gradients in transport stage along channels. A channel with a uniform bedload flux that steepens downstream will, according to equation 8, narrow as bedload transport is focused in the channel center by higher river gradients. This narrowing will in turn force higher flow depths in the channel to accommodate water flux. Therefore channels may deepen where they narrow, which is a violation of constant aspect ratio scaling suggested by Finnegan et al. (2005a).

Indeed, data from Watkins Glen, NY show a high degree of correlation between channel aspect ratio and channel slope (Figure 20), indicating channel deepening and narrowing at high gradients in a manner consistent with equation 8. The data in Figure 20 are taken from a 3 km section of river that represents a small fraction of the entire drainage basin. Therefore bedload supply is likely to be constant through this small section. The three-order of magnitude variation in channel slope appears to drive changes in the efficiency of bedload transport and hence in the area over which bedload transport takes place. This is manifested in the narrowing and deepening of channels that is correlated with increasing channel slope.

3.6.0 Conclusions

I used a laboratory flume to investigate experimentally how bedrock channel slope, width, roughness, alluvial cover, and incision rate, collectively evolved during the transient incision of an initially smooth channel with a varying bedload supply rate.

My results indicate that when channels are free of alluvial cover, incision is focused over a fraction of the bed that varies as a function of both the imposed bedload supply and the intrinsic transport capacity of the channel. However, I have shown that after alluvial cover deposition occurs on a bedrock channel bed, incision will be focused in the lateral and higher regions of the channel and along the margins of alluvial deposits. Building on a non-dimensionalization of slot width data collected in the experiment, I offer a new scaling relationship for bedrock channel width that explicitly incorporates bedload supply rate, sediment grain size, and bed shear stress. My scaling relationship and experimental observations provide insight into how channel width adjusts to accommodate variation in discharge and sediment supply in natural settings. Additionally, my proposed scaling relationship permits exploration of saltation-abrasion dynamics where width is free to adjust dynamically.

Because increases in sediment supply widened the band of active bedload sediment transport and thus the width over which incision took place, mass removal from the experimental bed scaled with sediment supply when the bed was free of cover during the experiment. However, bed roughness growth due to the progressive incision of the bed during the experiment eventually forced deposition of alluvial cover and thereby led to the suppression of incision on the bed at high sediment supply rates. The dynamics of roughness creation and alluvial cover deposition can therefore drive both negative and positive feedbacks on incision rate change following sediment supply perturbations.
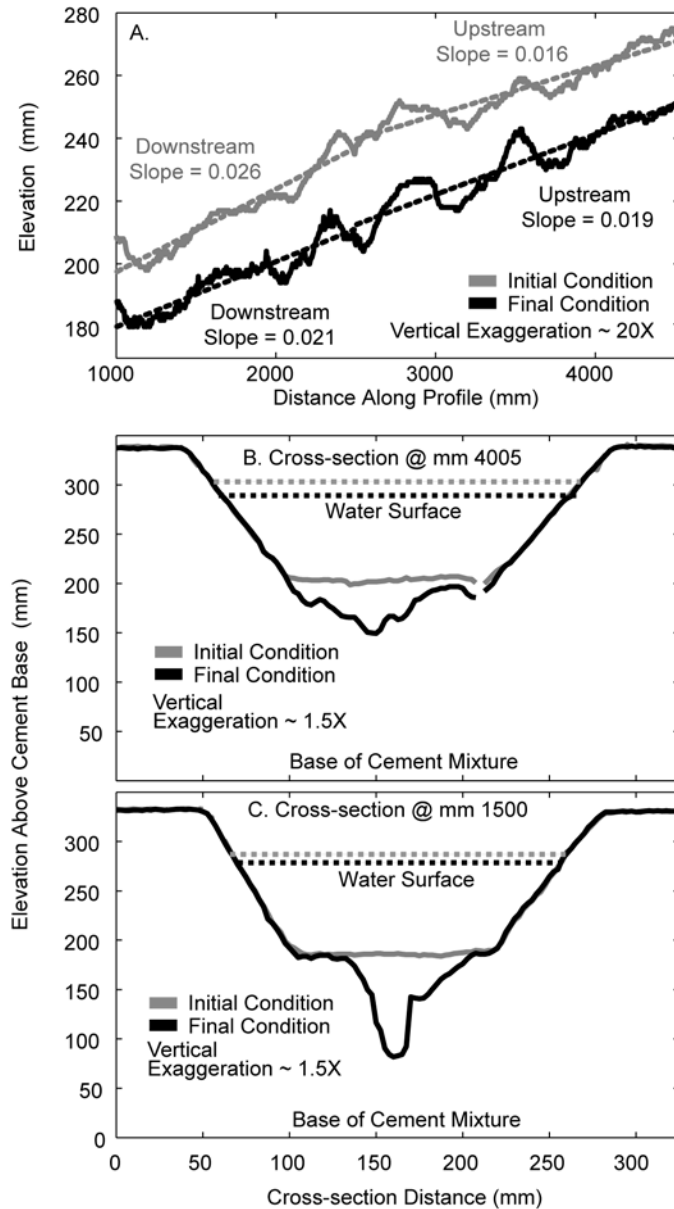
Figure 4: Initial and final conditions of the experimental channel
(A) Channel bed elevation profiles at the initial and final stage of the experiment. Dotted lines show linear fits to the upper and lower halves of the flume bed. (B & C) Elevation cross-sections and water surface elevations measured at 2 locations in the flume at the initial and final stages of the experiment.
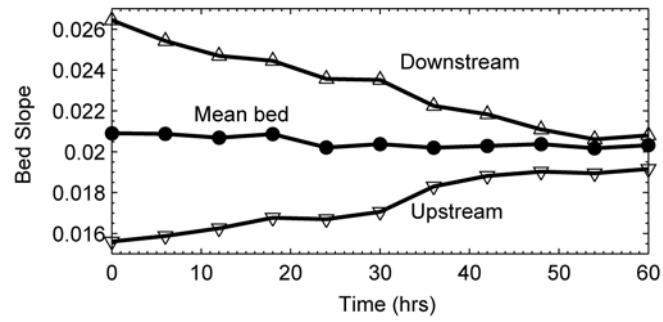
Figure 5: Channel slope
Evolution of mean bed slope, upstream bed slope, and downstream bed slope during the experiment.
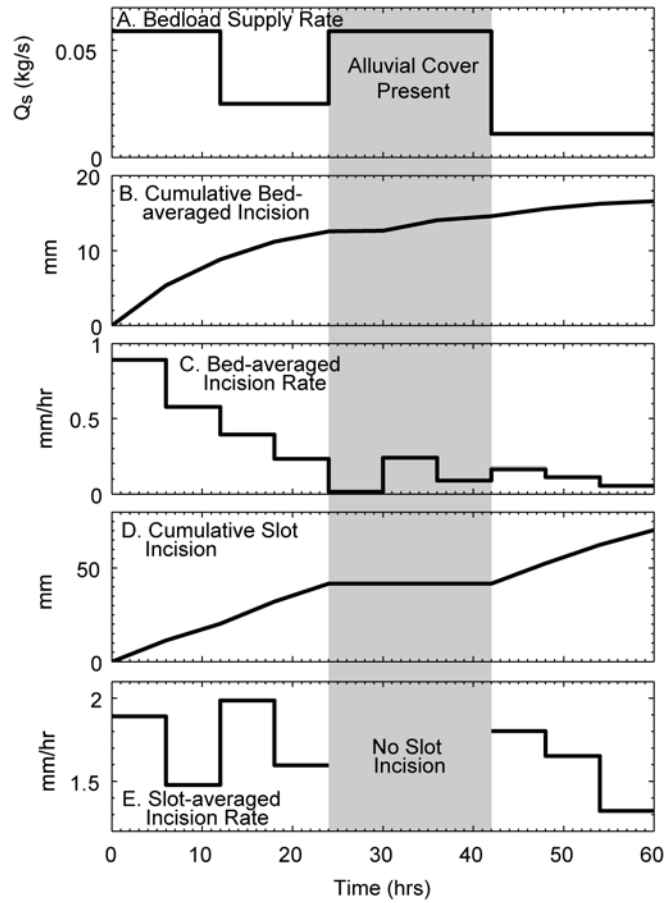
Figure 6: Channel incision rate
(A) The rate of bedload supply to the channel during the experiment. (B) Cumulative bed-averaged incision during the experiment. (C) Bed-averaged incision rate during the experiment. (D) Cumulative slot-averaged incision during the experiment. (E) Slot-averaged incision rate during the experiment. Grey bar indicates time interval with significant alluvial cover.
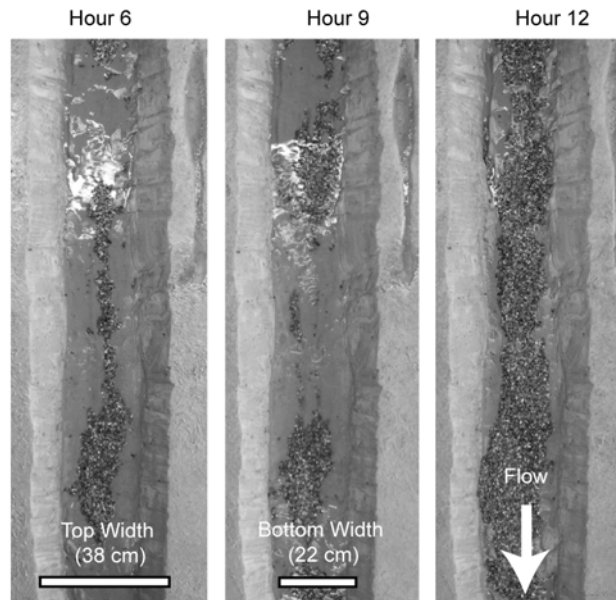
Hour 6   Hour 9   Hour 12

Top Width (38 cm)   Bottom Width (22 cm)   Flow

Figure 7: Alluvial cover
Snapshots of alluvial cover from the upper ~ 2 meters of the flume during hours 6 to 12 of the experiment highlighting the rapid transition from sparse alluvial cover to continuous alluvial cover. Bedload supply rate is 0.59 kg/s in each photograph.
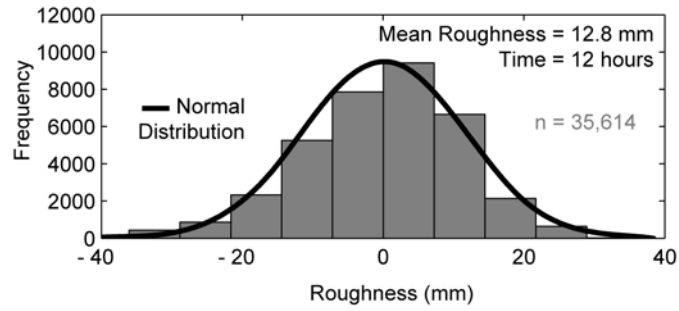
Figure 8: Example roughness histogram
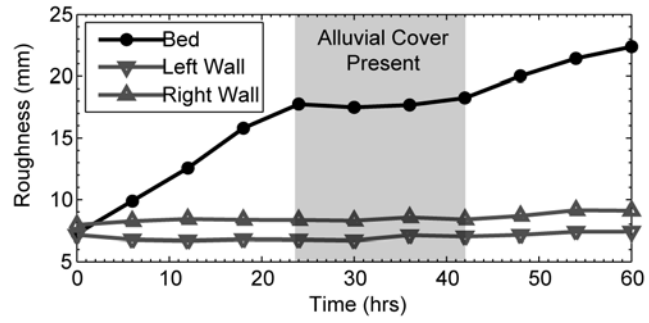Histogram of roughness at hour 12 of the experiment.

Figure 9: Bed roughness
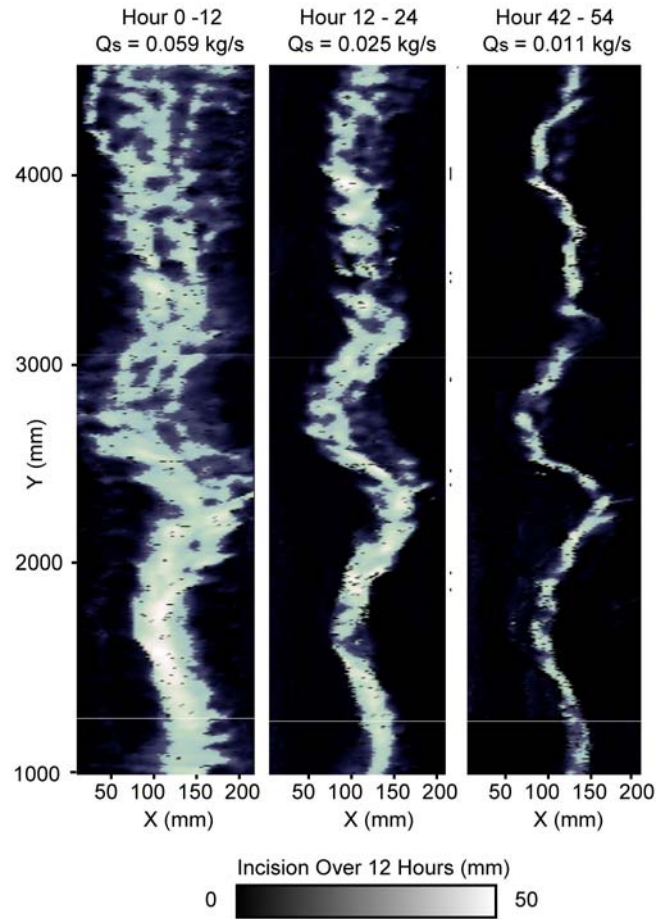The growth of bed roughness and wall roughness during the experiment.

Figure 10: Spatial patterns of bed incision at different sediment supply rates
Spatial patterns and magnitudes of bedrock incision on the bed of the flume for 12-
hour periods of time at (A) 0.059 kg/s sediment supply rate, (B) 0.025 kg/s sediment
supply rate, and (C) 0.011 kg/s sediment supply rate. Note, in the figures horizontal
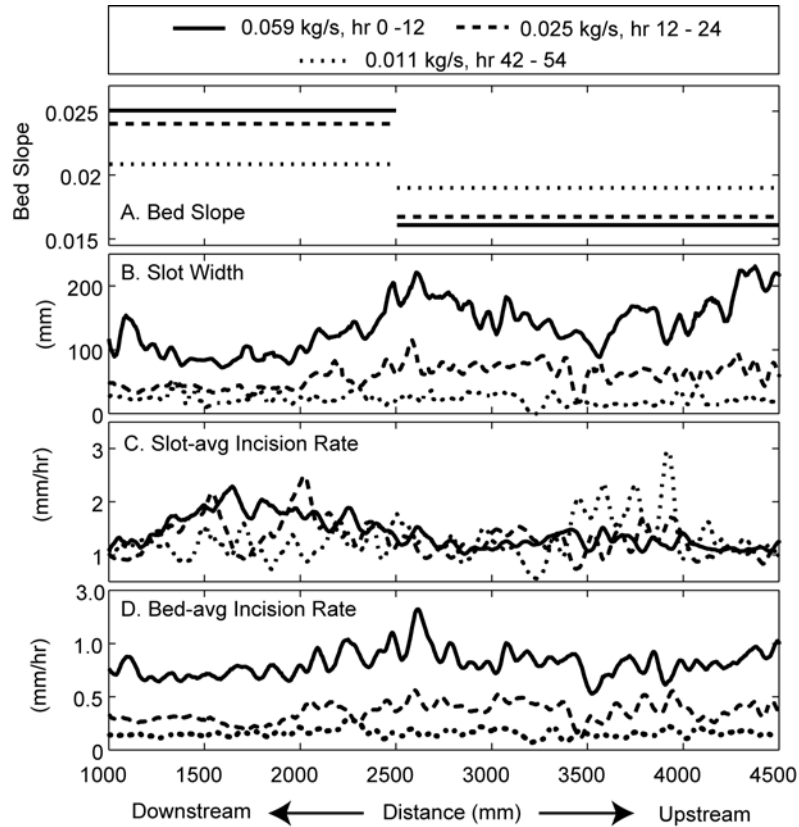exaggeration is approximately 5:1

Figure 11: Longitudinal patterns of incision rate, slot width and slope
(A) Bed slope at three time intervals with different bedload supply rates. (B) Slot
width versus channel distance for the three time intervals. (C) Rate of slot-averaged
incision versus channel distance for the three time intervals. (D) Rate of bed-averaged
incision versus channel distance for the three time intervals. A 5 cm smoothing
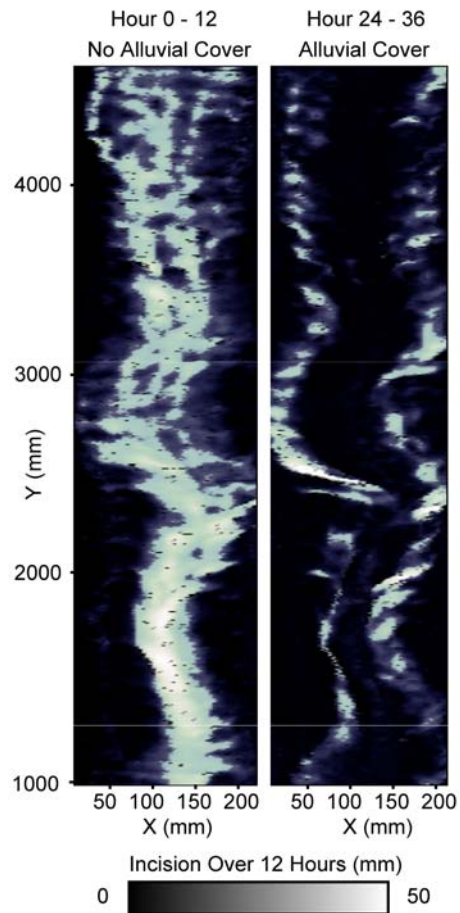window has been applied to the data in panels B-D.

Figure 12: Spatial patterns of bed incision with and without bed cover
Spatial patterns and magnitudes of bedrock incision on the bed of the flume for (A) a predominately alluvial cover-free bed at 0.059 kg/s bedload supply rate and (B) a bed with alluvial cover at 0.059 kg/s bedload supply rate. Note, in the figures horizontal exaggeration is approximately 5:1
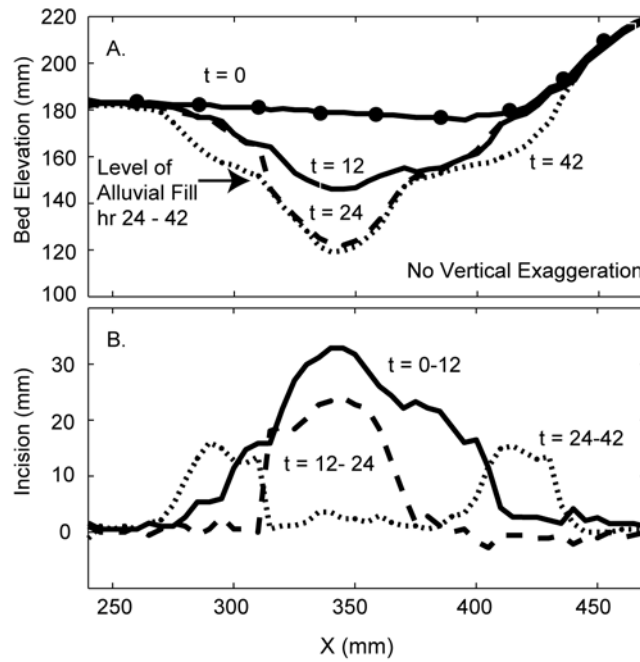
Figure 13: Cross-sectional incision rate patterns
(A) Evolution of a channel cross-section under variable sediment supply rate and
alluvial cover. Black arrows indicate the approximate level of alluvial fill that formed
between hours 24 and 42 of the experiment. (B) Patterns of vertical incision
calculated from differencing the elevation transects shown in 10A.
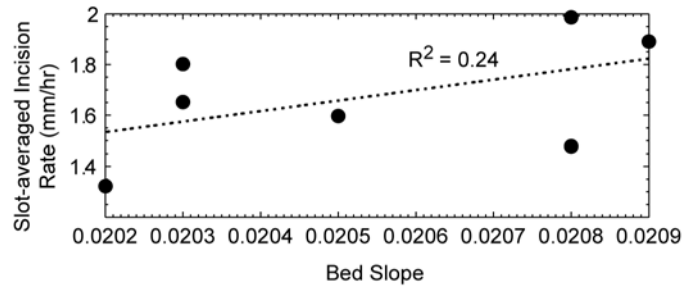
Figure 14: Slot-averaged incision rate versus bed slope
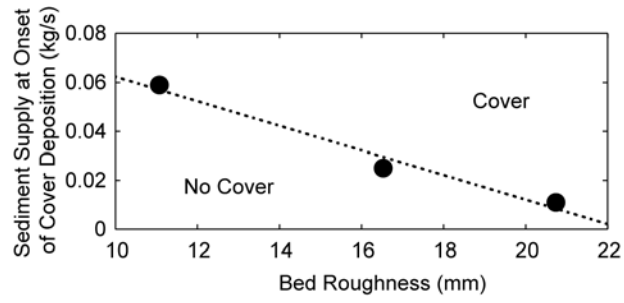
Figure 15: Bedload supply rate, roughness, and cover deposition
Bedload supply rate versus bed roughness at the onset of alluvial cover deposition
during the experiment.
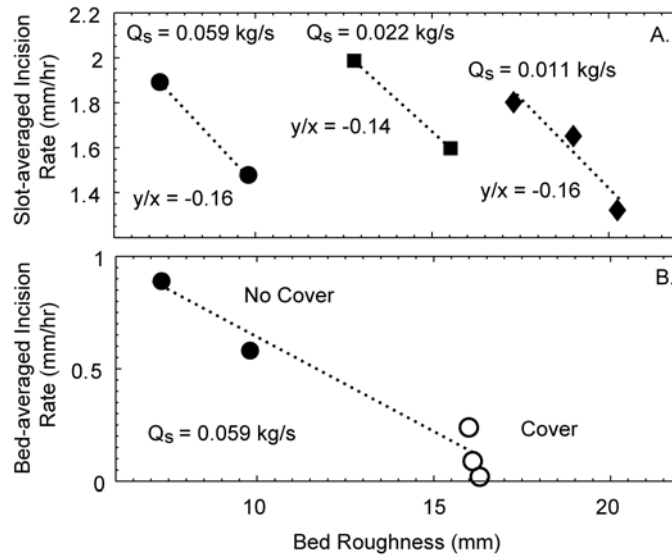
Figure 16: Roughness and incision rate
(A) Slot-averaged incision rate versus bed roughness for three sediment supply rates.
(B) Bed-averaged incision rate versus roughness at 0.059 kg/s bedload supply rate.
Open circles refer to data that reflect incision when alluvial cover was present on the bed.
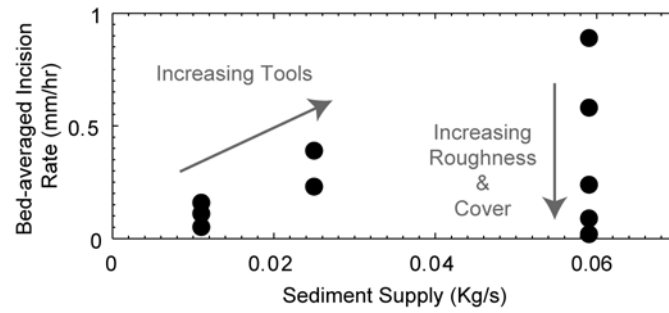
Figure 17: Bedload supply rate and incision rate
Bed-averaged incision rate versus bedload supply rate. Arrows in the figure show
both tools and cover effects on the incision rate of the channel.

83
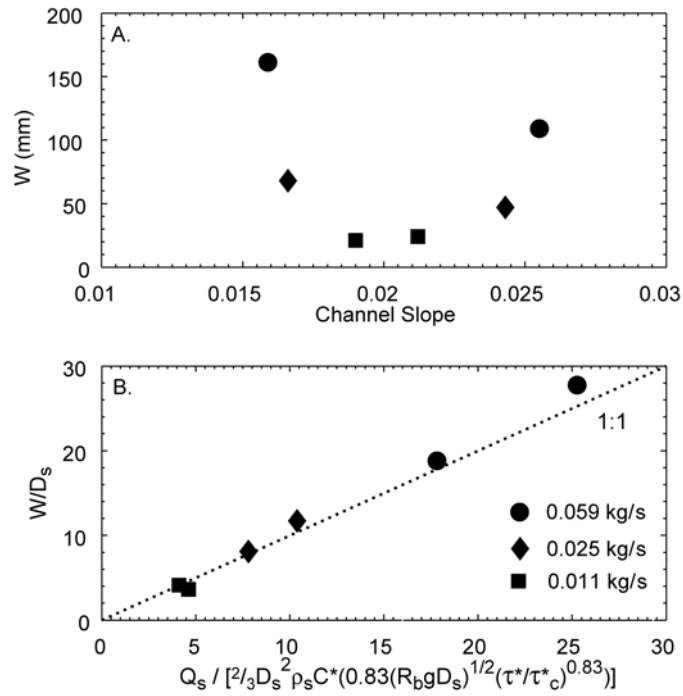
Figure 18: Slot width
(A) Slot width versus channel slope for different sediment supply rates. (B) Non-dimensional collapse of the slot width using equation 4, dotted line denotes line of 1:1 correspondence. In panels A and B, the data are drawn from the upstream and downstream halves of the flume, rather than averaged over the whole bed.

84
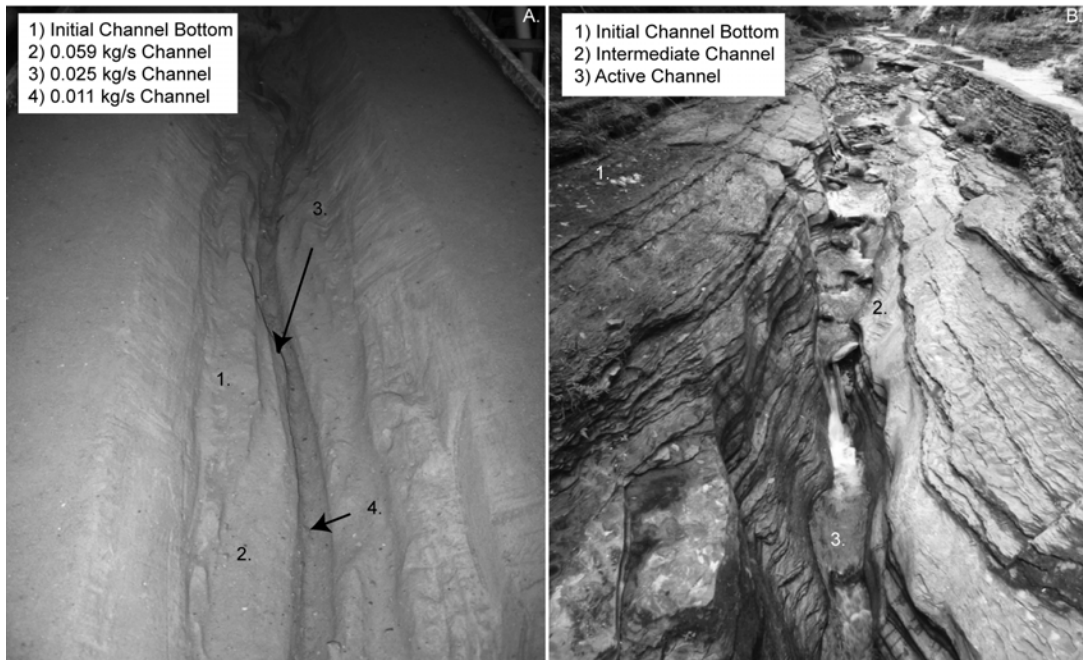
Figure 19: Comparison of experimental channel to Watkins Glen, NY
(A) Composite experimental channel formed after 60 hours of incision at bedload
supply rates between 0.011 kg/s and 0.059 kg/s. Numbers identify regions of the
composite channels incised at specific bedload supply rates at different times in the
experiment. (B) Photograph from Watkins Glen, NY showing progressive reduction
in channel width with ongoing incision. Watersheds in the region have experienced a
drop in sediment supply as glacial sediments have been excavated throughout the late
Pleistocene and early Holocene (Mullins, 1989).
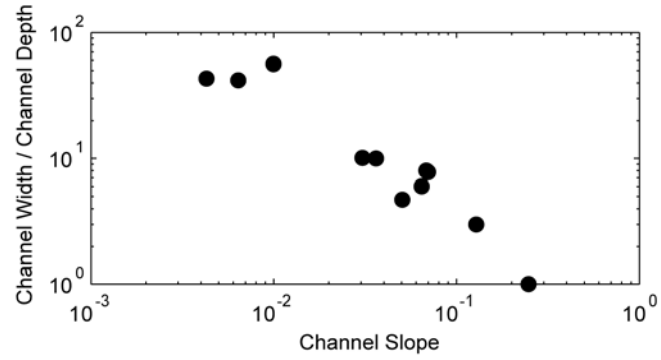
Figure 20: Channel aspect ratio versus channel slope, Watkins Glen, NY
(A) Channel width-to-depth ratio versus channel slope for a 3 km reach of Watkins Glen, NY.

Table 1: Experimental results
* Standard error is < 0.5% and is not shown in the table.

Time Interval (hrs)	Mean Bed Roughness (mm)	Mean Bed Slope	Mean Hydraulic Radius (mm)	Bedload Suppy Rate (kg/s)	Slot-Avg Incision Rate (mm/hr)*	Bed-Avg Incision Rate (mm/hr)*	τ^*
0-6	7.3	0.0209	68	0.059	1.89	0.89	0.148
6-12	9.8	0.0208	71	0.059	1.48	0.58	0.154
12-18	12.8	0.0208	71	0.025	1.99	0.39	0.154
18-24	15.5	0.0205	70	0.025	1.60	0.23	0.150
24-30	16.3	0.0203	72	0.059	-	0.02	0.153
30-36	16.0	0.0203	73	0.059	-	0.24	0.155
36-42	16.1	0.0202	70	0.059	-	0.09	0.148
42-48	17.3	0.0203	65	0.011	1.80	0.16	0.139
48-54	19.0	0.0203	63	0.011	1.65	0.11	0.135
54-60	20.2	0.0202	64	0.011	1.32	0.05	0.135

Table 2: Experimental results used in slot width analysis
The data are divided between the upstream and downstream portions of the channel.

Time Interval (hrs)	Region of Flume	Mean Bed Slope	Mean Hydraulic Radius (mm)	Mean Slot Width (mm)	Bedload Suppy Rate (kg/s)	τ^*
0-12	Upstream	0.0159	74	161 +/- 2	0.059	0.123
12-24	Upstream	0.0166	73	68 +/- 1	0.025	0.127
42-54	Upstream	0.0190	64	21 +/- 1	0.011	0.126
0-12	Downstream	0.0255	70	109 +/- 2	0.059	0.187
12-24	Downstream	0.0243	71	47 +/- 1	0.025	0.180
42-54	Downstream	0.0212	65	24 +/- 1	0.011	0.144

Chapter 4

Coupling of rock uplift and river incision in the Namche Barwa-Gyala Peri massif, Tibet.

4.1.0 Introduction

The potential for spatial patterns in erosion to influence the location of deformation in active mountain belts is well established in numerical models (e.g., Willett, 1999; Beaumont et al., 2001; Koons, 2002). Additionally, the tendency for rivers to grow steeper, convey more water, and become more erosive with higher rates of tectonic uplift is also documented in numerical models (Whipple and Tucker, 1999; Anders, 2005). Such work has lead to wide acknowledgment of the idea that rates of rock uplift with respect to the geoid and surface erosion should be driven towards a dynamic balance in actively uplifting ranges. Coupling between rock uplift and surface erosion has important implications for geodynamics because patterns in topography and climate can potentially reveal information about spatial gradients in rock uplift rates, which can lack clear surface expression in heavily dissected and hard to access terrain (Finlayson et al., 2002; Wobus et al., 2003; Kirby et al., 2003). Additionally, recent models demonstrate that the width and height of active mountain ranges may be controlled by rates of erosion (Whipple and Meade, 2004; Stolar et al., 2006; Roe et al., 2006, Willett et al., 2006). Finally, coupled surface, thermal, and mechanical models show that focused erosion, even on the scale of a large river valley system, can have dramatic consequences for the deformation of the lithosphere,

leading to localized feedbacks between erosion, deformation, and rock uplift (Koons et al., 2002).

The latter scenario, dubbed a "tectonic aneurysm," arises due to the dynamic interactions of localized erosion, topographic stresses, rock uplift, thermal weakening of the lithosphere, and deformation (Koons et al., 2002). The Nanga Parbat-Haramoosh massif in Pakistan exhibits the interconnected geomorphic, geophysical, petrologic, and geochemical evidence that initially inspired the aneurysm model (Zeitler et al., 1993; Meltzer et al.1998, Park and Mackie, 2000): A large, powerful and rapidly incising river, the Indus, cutting a deep gorge adjacent to an isolated, high-relief massif with extremely rapid cooling, and an upwardly bowed Moho. Nanga Parbat's eastern counterpart, the Namche Barwa-Gyala Peri massif, punctuates the eastern terminus of the Himalaya arc. The major east flowing orogen-parallel river, the Yarlung Tsangpo-Brahmaputra, wraps around the Himalayan arc here, cutting a spectacular gorge into the easternmost high Himalaya. Field observations, analysis of coarse-scale digital elevation data, and mineral cooling age data suggest that the superposition of the 5 km deep Yarlung Tsangpo-Brahmaputra river gorge and the rapidly cooled and deeply incised Namche Barwa-Gyala Peri massif is consistent with local coupling between erosion and crustal deformation in this region (Burg et al., 1998, Zeitler et al., 2001; Koons et al., 2002). However, until now neither the geomorphology nor the thermal history of the eastern syntaxis has been characterized

with sufficient detail to confirm such coupling with any satisfaction, and hence to begin to address the unique geodynamics of this region.

The first of the two goals of this chapter, therefore, is to assess the extent of coupling between fluvial incision and rock uplift in the eastern Himalayan syntaxis and thereby investigate the tectonic aneurysm hypothesis. To this end, I present an overview of newly published biotite ^{40}Ar/^{39}Ar ages, zircon (U-Th)/He ages, and structural geology from the syntaxis. Using measured channel width, TRMM satellite-derived river discharges, and channel slopes determined from 90 meter-resolution digital elevation data from the syntaxis, I then compute spatial patterns in river power to provide an index of the rate of detachment-limited fluvial incision within the field area. However, acknowledging the important duel role of sediment in both sustaining and suppressing channel incision, I also use river power as an index of bedload transport capacity within the framework of the saltation-abrasion model of Sklar and Dietrich (2004). In combination with mapped patterns in valley-bottom sediment storage, which I use as a proxy for low excess transport capacity, channels with high power and no apparent sediment storage can be inferred as having high excess transport capacity. Dividing the river network in this fashion allows for determination of where perturbations in sediment supply from proglacial fluvial sedimentation and bedrock landslides, the primary mechanisms of sediment delivery to channels in the field area, are likely to amplify incision and where they are likely to suppress incision. I then compare patterns in these two indices of fluvial incision rate to patterns in

mineral cooling and mapped structures to assess the accord between apparent recent river incision, deformation, and exhumation over the Quaternary. I also discuss the implications of this coupling in light of models for the geodynamics of this region.

The second and more general goal of this paper is to provide additional insight into how sustained high erosion rates are expressed topographically and geomorphically in active mountain belts. Despite considerable attention, there is still little consensus on which, if any, fluvial metrics are likely to reflect adjustment to long-term rates of rock-uplift, and to what extent patterns in precipitation, alone, control exhumation (Reiners et al., 2003; Burbank et al., 2003). The eastern Himalayan syntaxis is ideally suited as a natural laboratory to advance understanding of the field expression of coupling between erosion and rock-uplift in active mountain belts. This is because the study area is characterized by large and now well-constrained gradients in exhumation, precipitation, fluvial power, excess sediment transport capacity, and topographic relief. Thus, the likelihood of discerning a signal in both exhumation and topography that is above inherent noise levels is arguably higher here then elsewhere in the Himalaya. Based on synthesis of zircon (U-Th)/He ages and biotite ^{40}Ar/^{39}Ar ages, inferred incision rate patterns, and field observations, I discuss the two approaches I have taken to inferring spatial patterns in long-term river incision. Additionally, as it is widely speculated that patterns in precipitation, by themselves, drive exhumation in the Himalaya (e.g., Wobus et al., 2003; Thiede et al.,

2004), I also examine patterns in precipitation, independently of patterns in river incision potential, to assess their spatial relationship to exhumation.

4.2.0 Overview of Geology, Tectonics and Geomorphology

The eastern Himalayan syntaxis is one of the terminations of the great Himalayan arc. As such, it spans the transition from dip-slip thrust sense tectonics along the Himalayan front to the largely dextral strike-slip tectonics responsible for accommodating the northern motion of India relative to SW China and Myanmar (Burg et al., 1997). The syntaxis is the NE corner of the indenting Indian plate, and is so named because rocks are folded around its prow along a nearly vertical axis. As the Indian plate corner plows into Asia, Asian crust is forced away from the leading edge of the indentor and into a pattern of clockwise rotation around the syntaxis (Tapponnier et al., 1982; Royden et al., 1997; Zhang et al., 2004).

In accord with intense northward-directed convergence here, field mapping and thermochronometry indicate that the tip of the syntaxis is cross-cut by a major north-dipping crustal-scale shear zone and fault, the Nam-la thrust zone (Ding et al., 2001) (Figure 21A). The Nam-La thrust bounds to the south an antiformal crustal pop-up (Burg et al., 1997) that contains the two highest peaks for several hundreds kilometers: 7782 m Namche Barwa and 7294 m Gyala Peri. Cooling ages drop to the north across this inferred structure, indicating that the Namche Barwa-Gyala Peri antiform has been recently and rapidly exhumed relative to the surrounding terrain

(Burg et al., 1997). The antiform itself is complexly folded, but shows fabrics and fold axes consistent with N-S to NW-SE compression (Burg et al., 1998; Ding et al., 2001)

To the north, the Namche Barwa-Gyala Peri antiform is truncated by the Jiali Fault Zone, a SE – NW oriented dextral strike-slip fault accommodating clockwise crustal rotation around the syntaxis (Armijo et al., 1989; Burg et al., 1998). Recent activity on the fault is evident in much of the topography in the vicinity of the syntaxis (Figure 21A and 21B), however slip rates are unconstrained and the presence of the fault is inferred on the basis of topographic expression and juxtaposition of differing lithologies.

An interesting consequence of the geography of an indenting plate corner is that it will tend to entrain major orogen parallel rivers that have been forced to flow behind the mountain front as peaks have uplifted (Zeitler et al., 2001). On a much smaller scale is is analogous to a river being diverted by a growing anticline and forced to flow around its tip. In the case of the eastern syntaxis, the Yarlung Tsangpo-Brahmaputra turns to the south here after flowing east for over 1200 km across the southern portion of the Tibetan plateau. It is worth noting that it is also speculated that an ancestral Yarlung Tsangpo-Brahmaputra river flowing to the east and out through the Irrawaddy drainage was captured at the syntaxis (Clark et al., 2004). In either case, the result is the same, and that is that the largest river in the Himalaya is now incorporated within the complex deformational regime of the syntaxis.

Where the Nam-la thrust crosses the Yarlung Tsangpo-Brahmaputra, the river accelerates over the top of a prominent knickpoint as the sand-bedded river abruptly transitions to a boulder-strewn channel. Approximately 30 km downstream of the Nam-La thrust, the river undergoes a second abrupt transition, entering a narrow bedrock gorge centered between the summits of Namche Barwa and Gyala Peri. At this point the river drops 2 km in less than 100 river km over one of the most spectacular knickpoints in the world.

The spatial coincidence of the Yarlung Tsangpo gorge and the Namche Barwa-Gyala Peri antiform initially lead Burg et al. (1997) to suggest that erosion by the Yarlung Tsangpo-Brahmaputra passively paced rock uplift associated with an east-west trending crustal-scale buckle fold (also recognized by Ding et al., 2001) within the syntaxis, thereby enabling nearly 30 km of uplift and exhumation since the late Miocene (Burg et al., 1997). More recently, Zeitler et al. (2001) and Koons et al. (2002) have suggested that instead of acting passively to accommodate rock uplift within the syntaxis, erosion by the Yarlung Tsangpo has itself triggered and localized the rock uplift of the Namche Barwa-Gyala Peri antiform. According to the tectonic aneurysm hypothesis, focused erosion by a river gorge removes the upper few kilometers of the crust along the leading edge of the indenting corner, leaving hot, weak crust near the surface of a region under intense N-S to NW-SE directed compression. The reduced strength of the exhumed, thermally weakened crust in combination with the increase in gravitational stress inherent to the creation of large

valleys spontaneously localizes strain precisely where exhumation is greatest. This leads, in turn, to continued deformation, exhumation, and focused coupling between vertical rock advection and erosion at the surface (Koons et al., 2002).

4.3.0 Constraints and Observations

4.3.1 He and Ar Thermochronometry

I evaluate the patterns in long-term exhumation within the eastern syntaxis using an extensive suite of (U-Th)/He and ^{40}Ar/^{39}Ar cooling ages on zircon and biotite from terranes in SE Tibet (Zeitler et al., 2006). A mineral cooling age records the time since a particular thermochronometer crossed its closure isotherm. Hence, old cooling ages indicate slow cooling, whereas young ages indicate fast cooling. By assuming a thermal gradient in the crust, mineral cooling rates, in turn, are commonly used to estimate exhumation rates, which are equivalent to rock uplift rates with respect to the surface if the surface elevation does not change and remains, on average, isothermal. However, in regions of high relief and unknown topographic history, establishing a geothermal gradient is difficult (e.g., Stuwe, 1994). Therefore, I interpret patterns in cooling ages only as proxies for patterns in relative exhumation rates. In particular, I use (U-Th)/He in zircon to determine the time since a sample cooled from 200 - 230 degrees C (Reiners et al., 2002), and ^{40}Ar/^{39}Ar in biotite to record the time since a mineral cooled from 300 - 440 degrees C (Fuller et al., 2006). In order to illustrate gradients in exhumation in the field area, I have highlighted young cooling ages in the

study area in Figures 22 and 23. Because (U-Th)/He in zircon closes at roughly half

the temperature of ^{40}Ar/^{39}Ar in biotite, I have designated young biotites as those with

less than 2 Ma ^{40}Ar/^{39}Ar ages, while young zircons are designated as those with (U-

Th)/He ages less than 1 Ma. Under highly idealized time-invariant thermal conditions

and a linear temperature gradient in the upper crust, biotite ^{40}Ar/^{39}Ar ages of less than

2 Ma and zircon (U-Th)/He ages less than 1 Ma should thus represent similar

exhumation rates.

The cooling age data are summarized in Figures 22 and 23. For further

description of the data acquisition and analysis, see Zeitler et al. (2006). The mineral

cooling data reveal a "bullseye" pattern of young ages confined to within and adjacent

to the Namche Barwa-Gyala Peri massif that is dominant in both the (U-Th)/He and

^{40}Ar/^{39}Ar datasets. However, there are important differences between the patterns

revealed by the two datasets. Young biotite ages (0.9 - 2 Ma) are contained within the

mapped, bounding structures of the Namche Barwa-Gyala Peri massif. In contrast,

extremely young Zircon helium ages (0.3 – 1) Ma extend across terranes and

structures, expanding the region of apparently rapid exhumation into the lower

Parlung River watershed, as compared to the pattern of ^{40}Ar/^{39}Ar cooling ages.

4.3.2 Topographic Relief and Catchment Erosion Rates

Rock uplift drives relief production in active orogens, and in the Himalaya high relief is associated with high rock uplift rates (e.g., Bilham and Bendick, 2001; Wobus et al., 2006a). A relationship between relief and erosion rate, in turn, is expected in active orogens where rates of surface erosion and rock uplift have had sufficient time to equilibrate, such as is likely for the Himalaya where convergence has been ongoing for 50 Ma (e.g., Hodges, 2000). In the vicinity of the Namche Barwa-Gyala Peri antiform, Finnegan et al. (2005b) report [10]Be-derived erosion rates in river sediments that clearly increased $(R^2 = 0.81)$ with topographic relief. This trend, corrected for the effects of snow and ice cover, holds over an order of magnitude of erosion rates (0.1 – 4 mm/yr) and over a 3000 m range of mean relief. The trend is also consistent with [10]Be-derived catchment erosion rates from the western Himalaya and various erosion rate measurements elsewhere indicating that erosion rate increases non-linearly with relief (Vance et al., 2002; Montgomery and Brandon, 2002).

In figure 24, I plot regional patterns in relief, calculated as the difference between maximum and minimum elevation within a ~ 10 km radius circle on the GTOPO 30 digital elevation dataset. Figure 24 shows the close correspondence between areas of rapid erosion inferred from [10]Be analyses (Finnegan et al., 2005b), and areas of high local relief. The topographic pattern revealed by Figure 24, much

the same as the pattern in cooling ages, is a "bullseye" of high relief centered on the

Namche Barwa-Gyala Peri massif.

4.3.4 Precipitation

In the Himalaya, the extent to which orographic precipitation patterns directly

influence patterns in long-term exhumation rates is debated. Although it is speculated

that orographic precipitation patterns are likely to be important to the geodynamics of

the Himalayan front (Beaumont et al., 2001; Wobus et al., 2003), actual comparisons

of precipitation patterns and exhumation rates along the Himalaya yield conflicting

pictures of the influence of precipitation, alone, on rock uplift (Burbank et al., 2003;

Thiede et al., 2004). In order to explore the roll of precipitation in influencing

exhumation within the syntaxis, I define precipitation patterns with the TRMM

(Tropical Rainfall Measuring Mission) Satellite. As described in 4.2, I also use the

TRMM satellite data to generate river discharges that are faithful to patterns in

orographic precipitation as well as to the drainage basin architecture.

The TRMM satellite (http://trmm.gsfc.nasa.gov/) uses radar reflectivity to

remotely estimate precipitation rates within its ~ 6 X 4 km instrumental footprint.   At

the latitude of the eastern syntaxis, measurements are made approximately every 30

hours. By averaging all TRMM measurements between 1998 – 2001, I generated a

map of mean annual precipitation for the study area that is calculated from

approximately 1100 independent precipitation rate estimates (Figure 25). I note that

TRMM estimates precipitation in all forms, so the measurements are not restricted exclusively to rainfall.

The gross pattern of precipitation in the field area is closely related to the topography of the syntaxis (Anders et al., 2006). The lower Yarlung Tsangpo-Brahmaputra valley appears to funnel moisture up valley until the first major northward bend in the river, at which point precipitation falls off steeply to below 1 m/year. Heavy precipitation therefore appears restricted to the region to the south and downstream of the high topography of the Namche Barwa-Gyala Peri massif. Importantly, the TRMM data indicate that heavy rainfall does not appear to penetrate the rapidly cooled core of the syntaxis.

4.4.1 River Incision

The detachment-limited stream power model (Howard, 1994) provides an index of the rate of fluvial incision where the mechanism of incision scales with the magnitude of mean bed shear stress or stream power, such as is expected where erosion is dominantly due to the plucking of jointed bedrock (Whipple et al., 2000). Although this simple approach overlooks a number of important dynamics in many mountain channels (e.g., Stock and Montgomery, 1999; Sklar and Dietrich, 2004; Molnar et al., 2006), as I discuss later, approaches to modeling river incision with a linear dependence of incision on power, shear stress or excess shear stress have

nevertheless been validated in many settings (e.g., Stock and Montgomery, 1999;

Kirby and Whipple, 2001; Lavé and Avouac, 2001; Wobus et al., 2003).

Commonly, stream power approaches assume that the variables key to incision

scale in a simple way with either slope or drainage area, and then via a series of

further assumptions and substitutions (e.g., Whipple and Tucker, 2001) cast incision as

a function of quantities that can be obtained from a digital elevation model. In this

way, spatial patterns in incision rates can be inferred over broad geographic domains

(e.g., Finlayson et al., 2002; Wobus et al., 2003). Wide acknowledgment of the

importance of orographic precipitation gradients (Lavé and Avouac, 2001; Roe et al.,

2002) and channel width variation (e.g., Lavé and Avouac, 2001; Montgomery and

Gran, 2001) in modifying spatial patterns in channel shear stress has lead to more

refined approaches to inferring spatial incision rate patterns (e.g., Lavé and Avouac,

2001; Finnegan et al., 2005a). In keeping with these approaches, I compute spatial

patterns in river power for the large rivers within the syntaxis using direct

measurements of channel width and TRMM satellite-derived river discharges, in

addition to measurements of channel slope determined from 90 meter-resolution

digital elevation data. The combination of TRMM data and channel width

measurements allow us to compute river power in a manner that incorporates

pronounced orographic precipitation patterns (Figure 25) and the rich variation in

channel width observed within the syntaxis (Finnegan et al., 2005a).

I calculate river power for the Yarlung Tsangpo and its major tributaries in the eastern syntaxis as follows:

$$\Omega = \rho g Q S / W ,\qquad\qquad\qquad\qquad (1)$$

where ρ is the density of water, g is the acceleration due to gravity, Q is river discharge, S is channel slope, and W is channel width.

I obtain estimates of mean annual river discharge throughout the field area by routing annually accumulated TRMM satellite-derived rainfall on the 30-arc second GTOPO 30 DEM of Asia. Anders et al. (2006) show that estimates of river discharge using TRMM data agree with gauged mean annual discharges for 21 Himalayan catchments to within 20%.

Channel slopes and elevation profiles for the Jiggong Tsangpo, Yarlung Tsangpo and most of the Parlung Tsangpo were calculated from the 3-arc second (~90 m) Defense Mapping Agency Digital Terrain Elevation Data (DTED) for Asia. Due to the inherent noise in digital elevation data, I averaged river elevation data by 10 km reaches in order to obtain smooth and statistically significant river elevation profiles and channel slopes. The vertical resolution of the 3-arc second data is estimated to be 7 m (EROS Data Center, 2000), which means theoretically that maximum errors in slope data are approximately $< \sim 0.1\%$ when averaged over 10 km reaches.

3-arc second data were unavailable for the Po Tsangpo, lower Parlung and the Dongxiu river system. I therefore used the HYDRO1K 1 km resolution Digital Elevation Model of Asia to determine river slopes for these rivers, again by averaging

the data into 10 km reaches to smooth noise in the data. Although the 1 km data are far lower resolution than the 90 m data, I note that the reaches where it was necessary to substitute 1 km data all exceeded 2% in slope. Over 10 km, a 2% drop corresponds to a vertical change of 200 m. Given the nominal vertical resolution of the HYDRO1K data of 18 m (Gesch and Larson, 1998), Hydro1K slope data have a maximum uncertainty of $< \sim 0.2$ % averaged over a 10 km reach. Therefore, for all of reaches where Hydro1K was used to calculate slope, the maximum uncertainty in slope was less than 10% of the measured slope.

I measured channel width for all of the rivers in the analysis directly from satellite imagery. For the Yarlung Tsangpo, Jiggong Tsangpo and Parlung Tsangpo, channel width was sampled every 100 m from a continuous map of channel width created by digitizing channels from 28.5 m pixel resolution Landsat 7 Thematic Mapper images of the rivers at high flow, thereby providing an estimate of bankfull width. Like elevation, these width values were then averaged over 10 km to obtain a reach-mean channel width. For the Po Tsangpo, lower Parlung and the Dongxiu river system, I measured channel width directly from Google Earth (earth.google.com/) for every 1 km of channel. A reach-averaged channel width was then obtained by averaging these measurements over 10 km. Because the pixel resolution of the Landsat imagery for all of the measurements of width is 28.5 m, channels widths are known to, at best, within 1 pixel. Therefore the uncertainty in these measurements is +/- 28.5 m. However, I emphasize that as the width analysis was restricted to

relatively large channels with widths typically larger than 100 m, width error was generally no more than 30%.

In figure 26, I plot the spatial pattern in river power across the eastern Syntaxis. Overall, mean annual river power varies from less than 10 watts/m^2 in the more distal regions of the syntaxis, and away from the Namche Barwa-Gyala Peri Massif to a maximum of over 3000 watts/m^2 in the heart of the Tsangpo Gorge. The analysis shows that high river power is centered in the region of the high topography and extreme relief within the Namche Barwa-Gyala Peri massif. The reaches of high power along the Yarlung Tsangpo-Brahmaputra and the Po Tsangpo together dissect the region of rapid cooling within the syntaxis, and therefore suggest that exhumation rates scale with river power.

An alternative framework for modeling the dynamics of bedrock channel incision is provided by the saltation-abrasion model proposed by Sklar and Dietrich (2004), which provides an explicit treatment of sediment-modulated river incision, as described below. Where bedload abrasion is the dominant incision mechanism, coarse sediment carried by rivers – depending on sediment supply relative to transport capacity – can either promote incision by providing tools, or inhibit incision when deposited as a protective alluvial cover (Gilbert, 1877; Sklar and Dietrich, 1998). The Sklar and Dietrich saltation-abrasion model incorporates this essential non-linearity imposed on incision by sediment dynamics, and thereby frames the argument that

moderate sediment supplies are likely to optimize incision by both providing the

required tools and avoiding burial of the bed.

Strictly speaking, the saltation abrasion model requires, at a minimum, direct

constraints on both sediment supply and transport capacity, in addition to

measurements of channel morphology. Although I lack direct constraints on bedload

supply within the syntaxis, I suggest that the spatial extent of valley-bottom sediment

storage within the syntaxis provides a proxy for regions of the channel network with

low excess transport capacity, where sediment supply is at or near the intrinsic

capacity of a channel to convey it. Long-term storage of sediment, fundamentally,

reflects sediment supply rates that exceed transport rates, so I argue that the

distribution of incised alluvial terraces and currently braided channel reaches provides

a measure of supply relative to transport capacity integrated over the recent geologic

past. Figure 27 depicts the spatial pattern of valley bottom deposits throughout the

syntaxis. The striking pattern of deposition indicates that the heart of the syntaxis

lacks long-term sediment storage altogether, whereas the distal regions of the syntaxis

appear far less capable of evacuating supplied sediment. I note that in the gorge

significant sediment deposition is absent despite 8 glaciers feeding into the Yarlung

Tsangpo-Brahmaputra River, and documented peaks in regional rates of bedrock

landsliding here (Bunn et al., 2004). Just as the presence of valley bottom alluvial

deposits provides an index of low excess transport capacity channels, I further argue

that the absence of alluvial deposits provides an index of channels with relatively higher excess transport capacity.

Within the framework of the saltation-abrasion model, patterns in river power, in turn, provide an index not of incision rate, but rather of gross bedload transport capacity. Thus comparison of figures 26 and 27 reveals that areas of high sediment transport capacity (i.e. power) within the syntaxis are generally spatially coincident with reaches of high excess transport capacity, whereas reaches of low and intermediate power are associated with extensive sedimentation and incised alluvial terraces, both indicative of low excess transport capacity.

Insight into relative rates of bedrock incision is then provided via recognition of the fundamentally different dynamics of channels that are at or near transport capacity compared to channels that are well below transport capacity, such as is apparently the case in the heart of the Yarlung Tsangpo gorge. Channels with low excess transport capacity, Sklar and Dietrich (2004) argue, will be cover limited and therefore subject to negative feedbacks on channel incision rates from perturbations in sediment supply. For example, a landslide delivered to a channel that is already at capacity will lead to rapid deposition of alluvial cover and suppression of channel incision. Importantly, in such an example, continued relative base-level fall and channel steepening may provide the only means for a channel to evolve out of such a condition (e.g., Korup, 2005). An example of such a negative feedback is apparent in the before and after images from a landslide delivered to the Yiggong Tsangpo in

2000 that triggered extensive alluvial deposition (Figure 28). The images, which

bracket the event in time, show the total inundation of the formerly narrow channel

with a thick blanket of alluvial cover delivered from the landslide.

In contrast, according to the saltation-abrasion model, channels with excess

transport capacity will be tools limited, and therefore subject to positive feedbacks on

incision rate from perturbations in sediment supply (Sklar and Dietrich, 2004). This is

because in the tools regime the supply of sediment, rather than the extent of alluvial

cover, dictates channel incision rates. Hence an excess transport capacity channel in

the tools regime will experience enhanced incision when supplied with, for example,

landslide debris. Figure 29 shows a reach of the Yarlung Tsangpo-Brahmaputra River

within the Yarlung Tsangpo gorge. Note that despite numerous, large bedrock

landslide scars in the photo, sediment storage is minimal within the channel and the

valley bottom, confirming that the channel is capable of evacuating supplied landslide

debris.

Importantly, whereas low excess transport capacity channels can experience a

virtual shut down of erosion due to an influx of sediment, high excess transport

channels may be able to sustain incision indefinitely, provided they are supplied with

sediment. Thus, in regions of extensive bedrock landsliding, low excess transport

capacity channels are likely to be unstable over geologic time, oscillating between

periods of alluvial deposition and renewed incision due to on-going base-level fall.

This effect will also be reinforced by the fact that alluvial channels are typically wider

and therefore less powerful than bedrock channels for the same slope and discharge (Finnegan et al., 2005a), suggesting that channels may become less capable of transport following sediment deposition. With regard to channel morphology and incision rates, this further suggests that for low excess transport capacity channels a snapshot of channel morphology at a given time may be unrepresentative of its long-term incision rate.

Although landsliding and high sediment supply rates (Figure 24) are prevalent throughout the study area, I argue that the effects of landslides will tend to amplify river incision in the gorge, whereas landslide debris will retard channel incision in the regions with lower river power. Thus the regions of high power and excess transport capacity shown in Figure 26 and 27 will incise efficiently over geologic timescales, compared to regions of low power and low excess transport capacity

4.5.0 Discussion

4.5.1 Evidence for Coupling of River Incision and Rock Uplift

Taken together, the patterns in zircon (U-Th)/He ages, biotite ^{40}Ar/^{39}Ar ages, topography, and river morphology indicate a striking spatial coincidence of: (1) extreme topographic relief, (2) river incision potential, (3) efficient bed load transport and (4) rapid cooling centered on the Namche Barwa-Gyala Peri massif over the last ~1 Ma (Figure 30). Because of this close spatial association of patterns in river incision potential determined independently in two ways, sediment transport

108

efficiency, relief, and mineral cooling, I infer that the exhumation of the Namche

Barwa-Gyala Peri massif is related primarily to intense, focused incision and efficient

sediment transport by the Yarlung Tsangpo and Po Tsangpo. The over-steepened

slopes and pervasive bedrock landsliding within the gorge (Bunn et al., 2004), in turn,

provide direct independent evidence that landscape lowering is driven by river incision

within the gorge (e.g., Burbank et al., 1996).

Given the tens of kilometers of exhumation within the syntaxis since the

Pliocene (Burg et al., 1997; Booth et al., 2004), it is unlikely that young mineral ages

in valley bottoms reflect only cooling due to recent valley incision (e.g., Clark et al.,

2005). Moreover, bedrock mapping in the syntaxis indicates that peaks are

structurally continuous with rapidly cooled and deeply exhumed rocks in the gorge

(Burg et al., 1997), suggesting that deep exhumation is continuous across peaks and

valleys. Additionally, if reset thermal ages in valley bottoms are related simply to

headward cutting of the Yarlung Tsangpo-Brahmaputra into Tibet, it is anticipated that

downstream of the knickpoint's current location, there would be a trail of young

cooling ages corresponding to the former location of the propagating knickpoint. This

scenario however is inconsistent with the older cooling ages present downstream of

the knickpoint (Figures 22 and 23).

Exhumation of the Namche Barwa-Gyala Peri massif is also unlikely to be

related to extensional faulting, which is often invoked as the exhumational mechanism

for isolated metamorphic massifs. Where extensional faulting is responsible for un-

roofing deep crustal rocks, there is no reason to expect a close correspondence between erosion and exhumation because faulting itself is the primary mechanism of mass removal above a core complex. Additionally, the thrust motion along faults bounding the Namche Barwa-Gyala Peri massif (Burg et al., 1998; Kidd et al., 2006) and the structural fabric mapped in detail by Burg et al. (1998) are both inconsistent with extensional exhumation.

Prior studies have recognized the importance of the Yarlung Tsangpo to the geodynamics of the syntaxis (Burg et al., 1998; Zeitler et al., 2001; Koons et al., 2002). Zeitler et al. (2001) and Koons et al. (2002) attribute uplift of the Namche Barwa-Gyala Peri massif directly to the influence of river incision via the tectonic aneursym hypothesis. In contrast, Burg et al. (1998) have suggested that the Yarlung Tsangpo and its tributaries, although vital to the exhumation of the massif, are nevertheless antecedent to what is fundamentally a lithospheric buckling instability. It is challenging to distinguish between these end-member models for the tectonic development of the syntaxis because both require a close correspondence between river incision and rock uplift. However, a number of features of the region discussed below are well explained by dynamic coupling between river incision and rock uplift.

From the perspective of a buckle fold origin for the Namche Barwa-Gyala Peri massif (Burg et al., 1998), the patterns of relief, river morphology and cooling ages shown in figure 30 would require a fortuitous coincidence of the location of maximum buckle folding and the location of the Yarlung Tsangpo knickpoint. As noted earlier,

high topographic relief is closely associated with high rates of rock uplift inferred

from cooling ages (Wobus et al., 2003; 2006a) and surface uplift measured by GPS

(Bilham and Bendick, 2001) along the Main Himalayan Thrust (MHT). However,

whereas high relief forms a more or less continuous band along the Himalayan front in

response to uplift along the MHT, in the eastern syntaxis high relief, rapid cooling and

by inference rock uplift are extremely localized within a region of rapid inferred river

incision. Given the apparently very localized nature of rock uplift within the syntaxis,

it is therefore striking that the steepest portion of the Yarlung Tsangpo-Brahmpatura,

the largest river in the Himalaya and Tibet, is centered precisely on the Namche

Barwa-Gyala Peri uplift. This is particularly notable because rivers tend to be

deflected around actively uplifting antiforms (e.g., Van der Beek et al., 2002), rather

than incorporated within their structural or topographic culminations. That is, unless

the rivers themselves are responsible for the location of the structure (e.g., Oberlander,

1985; Zeitler et al., 2001; Koons, 2002; Simpson, 2004; Montgomery and Stolar,

2006)

A longitudinal perspective of the river reveals that the great knickpoint of the

Yarlung Tsangpo and its zone of inferred high incision are centered directly on the

region of rapid zircon and biotite cooling, as well as extreme local relief (Figure 31).

This superposition of patterns in power, relief, and cooling rates indicates that the

location of rapid incision and rock uplift on the Tsangpo has been pinned for at least 1

million years. Without compensatory uplift of the Namche Barwa-Gyala Peri massif

during this time, the Yarlung Tsangpo knickpoint would have propagated rapidly into Tibet, causing a mismatch between the location of rapid current incision and the location of rapid exhumation in the past as revealed by the cooling age data. In considering the coincidence of the Tsangpo gorge and the Namche Barwa-Gyala Peri massif, therefore, one might ask how what is widely regarded as the most erosive river in the Himalaya (Finlayson et al., 2002) became superimposed on the one structure apparently capable of balancing its incision?

4.5.2   Inferring River Incision from Geomorphology and Topography

Prior field studies investigating evidence for coupling between tectonic uplift and surface erosion have focused on the relationship of fluvial geomorphology to a variety of exhumation rate data (e.g., Burbank et al., 2003; Wobus et al., 2003; Vannay et al., 2004; Mitchell and Montgomery, 2006). Wobus et al. (2003) and Vannay et al. (2004) report spatial correlations of river steepness and muscovite $^{40}Ar/^{39}Ar$ age in the central Nepal Himalaya and Sutlej Valley, India. In contrast, Mitchell and Montgomery (2006) and Burbank et al. (2003), respectively, illustrate that trends in river power are not well correlated with those in apatite ages from the western Cascades of Washington State, and from the central Nepal Himalaya. Additionally, Tomkin et al. (2003) show that apart from even agreeing with cooling ages, patterns in river power are also un-correlated with incision rates.

112

The results reported in this analysis suggest that spatial patterns in detachment-limited river incision rate, as inferred from stream power, and saltation-abrasion rates, as inferred from patterns in river power and excess fluvial transport capacity, provide reasonably accurate and complementary pictures of the spatial patterns in long-term erosion inferred from mineral cooling data. Although stream-power approaches are often criticized for neglecting the complicating dynamics of sediment transport, in the eastern syntaxis there is a strong correspondence of incision rates inferred from river power and those inferred from taking sediment transport explicitly into account. However, I emphasize that within the framework of the saltation-abrasion model, the pattern of river power alone provides no insight into incision rates without additional constraints on sediment supply and excess transport capacity (Brandon and Gasparini, 2005), as I have tried to provide. Therefore I suggest that, in addition to patterns of river power, mapping alluvial terraces and other indicators of relative excess transport capacity can provide insight into spatial patterns in the dynamics of incision in active orogens.

From the standpoint of the saltation-abrasion model, the Yarlung Tsangpo, because of its extremely large range of river power, may present a relatively unique example of a river that transitions from a cover-limited regime to a tools-limited regime over a short distance. One of the virtues of the framework provided by considering the effects of tools and cover on incision is that a much richer and more

realistic perspective on river incision immerges, as compared to using digital elevation and precipitation data alone.

For example, despite considerable overlap between regions of high inferred incision rate and rapid mineral cooling in the study area, two regions along the lower Parlung River and the upper Yarlung Tsangpo (Figures 22, 26 and 27) are observed to have low river power and rapid mineral cooling in a manner locally inconsistent with a detachment-limited view of long term river incision. Notably, both of these reaches are relatively steep, but have sediment choked channels and thick flights of incised fill terraces at present, as shown in Figure 32. As discussed in section 4.1, due to the negative feedbacks inherent to low excess transport capacity channels, perturbations in sediment supply can lead to a virtual shut down of erosion that only continued relative base-level fall can eventually reactivate. Again, this suggests that in regions of active landsliding where channels are near transport capacity, they can be expected to oscillate between periods of alluvial deposition and renewed incision due to on-going base-level fall or climate-induced increases in the sediment transport capacity . I suggest that such a dynamic can explain the rapid mineral cooling observed in two river reaches with relatively low power and evidence for recent aggradation.

4.5.5 Precipitation and Exhumation

Although patterns in orographic precipitation have been found to control patterns in exhumation of the Himayalan front (Thiede et al., 2004) and the

Washington Cascades (Reiners et al., 2003), there is no clear spatial relationship

within the syntaxis between patterns in precipitation and cooling ages (Figure 33). In

the syntaxis, this may be due to the fact that river incision by the Yarlung Tsangpo,

which drains 200,000 km^2 of the Tibetan Plateau, is driving regional erosion and

deformation. Because of the complex pattern of drainage within the syntaxis, it would

be naïve to expect a straightforward relationship between precipitation and erosion by

rivers. This is because discharge at a given point in a catchment reflects a

combination of locally sourced precipitation from small tributaries and water

originating from distant sources. In the case of the syntaxis, the huge volume of water

carried into the gorge by the Yarlung Tsangpo-Brahmaputra and the Po Tsangpo

overwhelms local contributions of water due to orographic precipitation. The addition

of locally derived orographic precipitation to the Yarlung Tsangpo gorge accounts for

only about 10 % of the combined discharge of the Po Tsangpo and Yarlung Tsangpo-

Brahmaputra, and is therefore unlikely to be of primary importance in driving river

incision along mainstem channels here.

4.6.0 Conclusions

I have compared spatial patterns in inferred detachment-limited incision and

sediment-modulated incision potential to patterns in topographic relief, precipitation,

and exhumation rates reflected by zircon and biotite cooling ages across the eastern

Himalayan syntaxis. Mapping indicates a spatial co-location of high incision rate

potential, sediment transport efficiency, relief, and mineral cooling rates focused on the Namche Barwa-Gyala Peri antiform. Only patterns in precipitation appear uncorrelated with those in mineral cooling ages, suggesting it is not directly tied to exhumation within the syntaxis. Taken together, these observations suggest strongly that river incision combined with efficient sediment evacuation within the region of the Yarlung Tsangpo-Brahmaputra gorge is closely coupled with vertical rock uplift. Within the study region there are two exceptions to this detachment-limited view of long-term river incision; they are along the lower Parlung Tsangpo and the upper Yarlung Tsangpo. However, these exceptions clearly arise from the abundance of sediment bordering these river reaches and its likely effects on long-term incision.

Isolated, active, high-relief metamorphic massifs spatially co-located with large and erosive rivers is an expected consequence of erosional, thermal, and mechanical coupling in an active orogen (Koons et al., 2002). A number of features of the eastern syntaxis suggest that the Yarlung Tsangpo-Brahmaputra river plays a significant role in controlling lithospheric dynamics here: (1) Along much of the Himalaya front, areas of high relief and young cooling ages form a continuous band related to active rock uplift along the Main Himalayan Thrust. However, high relief in the syntaxis is restricted to a "bullseye" pattern precisely in the region cut by the largest river in the Himalaya, the Yarlung Tsangpo-Brahmaputra, suggesting rock uplift is equally localized. This is confirmed by patterns in zircon and biotite cooling ages. (2) The coincidence of high river power, high relief, and young cooling ages

requires that the location of rapid incision on the Tsangpo be pinned for at least 1 million years. Without a close balance between the uplift of the Namche Barwa-Gyala Peri massif and the incision of the Yarlung Tsangpo knickpoint, a wave of headward incision would have propagated rapidly into Tibet. Because the Yarlung Tsangpo-Brahmaputra gorge is the most powerful reach of river in the Himalaya (Finlayson et al., 2002), it is striking that it is co-located with the one structure that is apparently capable of balancing it's incision.
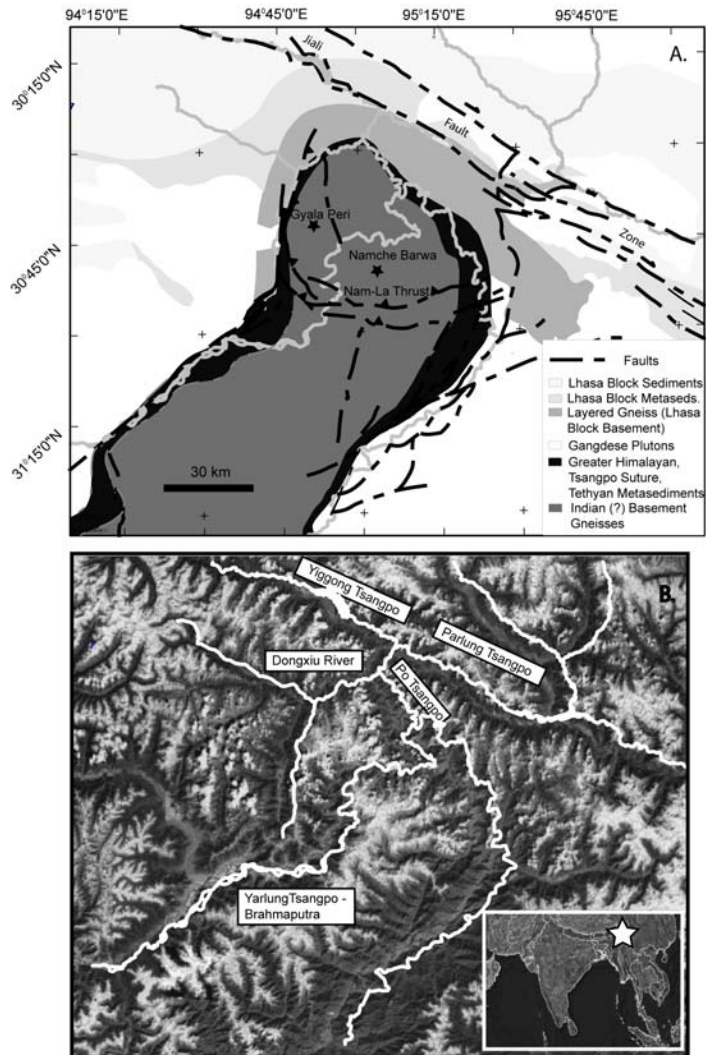
Figure 21: Geologic setting of the eastern Himalayan syntaxis
(A) Geologic and tectonic map of the eastern syntaxis. (B) Satellite overview of the syntaxis showing the location of major rivers.
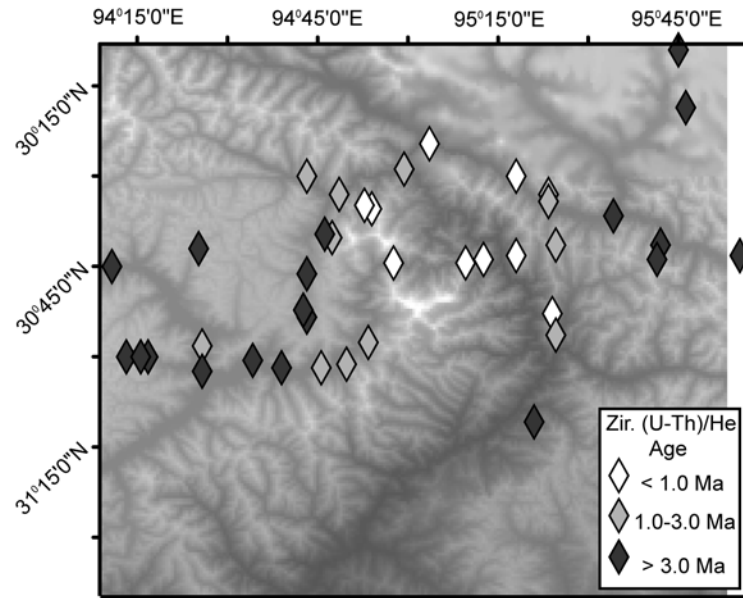
118

Figure 22: (U-Th)/He thermochronometry
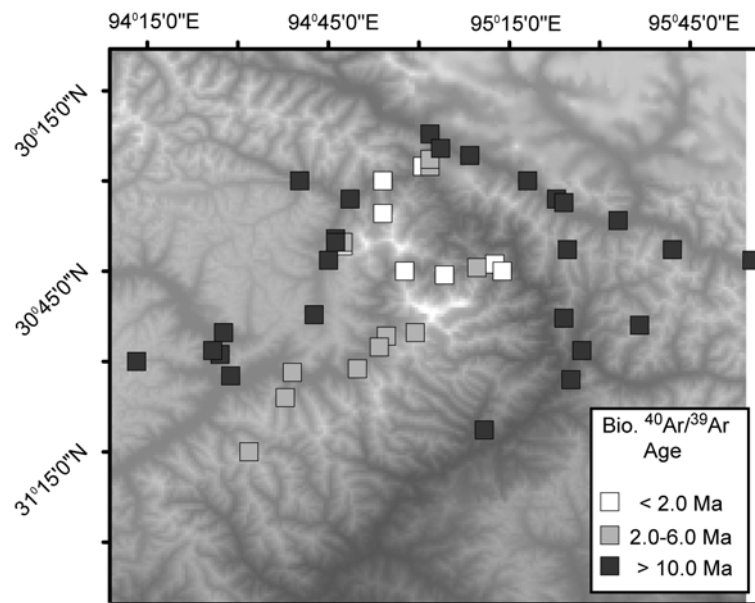Spatial distribution of zircon (U-Th)/He ages within the eastern syntaxis.

Figure 23: ^{40}Ar/^{39}Ar thermochronometry
Spatial distribution of biotite ^{40}Ar/^{39}Ar ages within the eastern syntaxis.
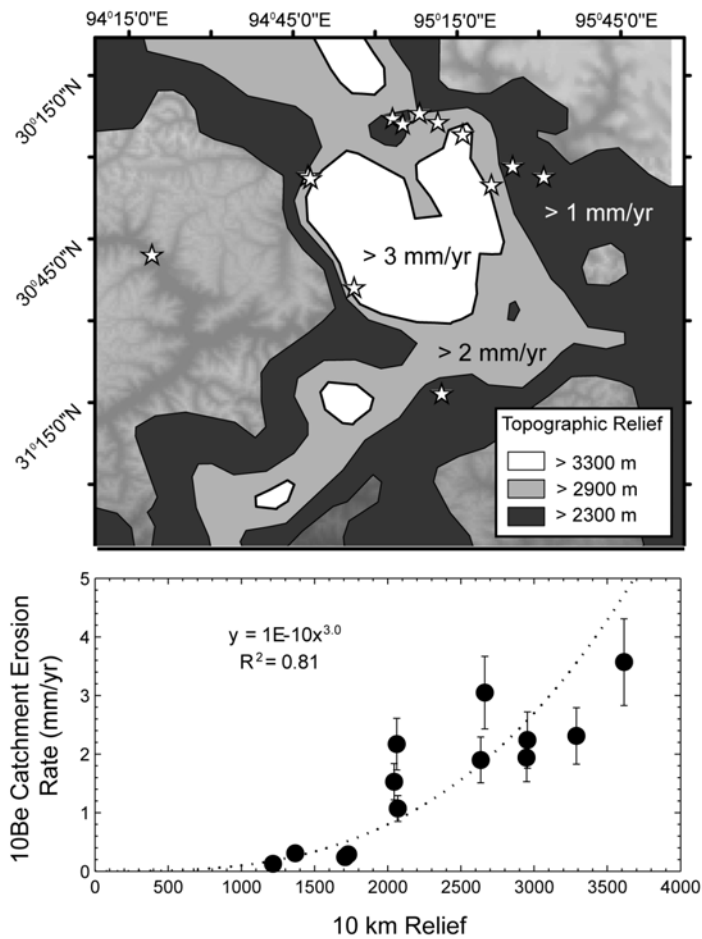
Figure 24: Topographic relief and erosion rates
(A) Patterns in topographic relief within the eastern syntaxis and corresponding inferred [10]Be basin averaged erosion rates. Stars denote the mouths of catchments sampled for [10]Be analyses in Finnegan et al. (2005b). (B) Regression of [10]Be basin-averaged erosion rate versus mean topographic relief.
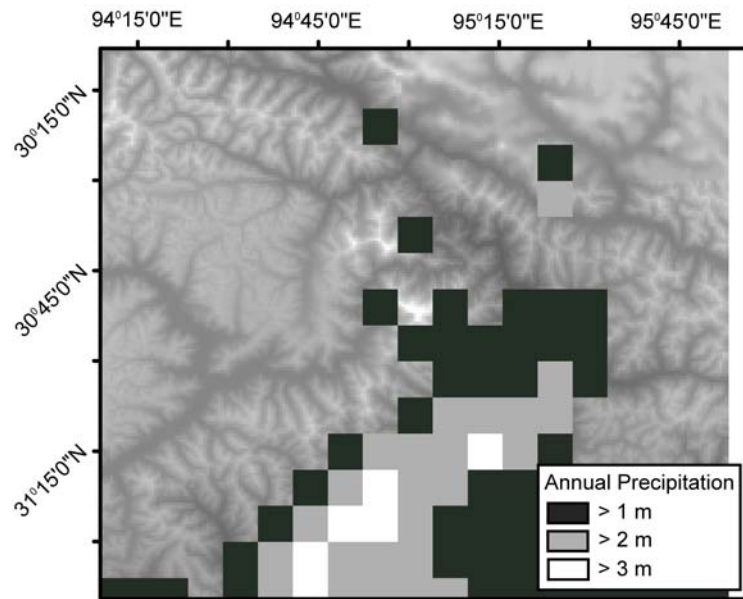
Figure 25: Precipitation patterns
Patterns in mean annual precipitation within the eastern syntaxis. Areas with no
coverage are those with less than 1 m of precipitation annually.
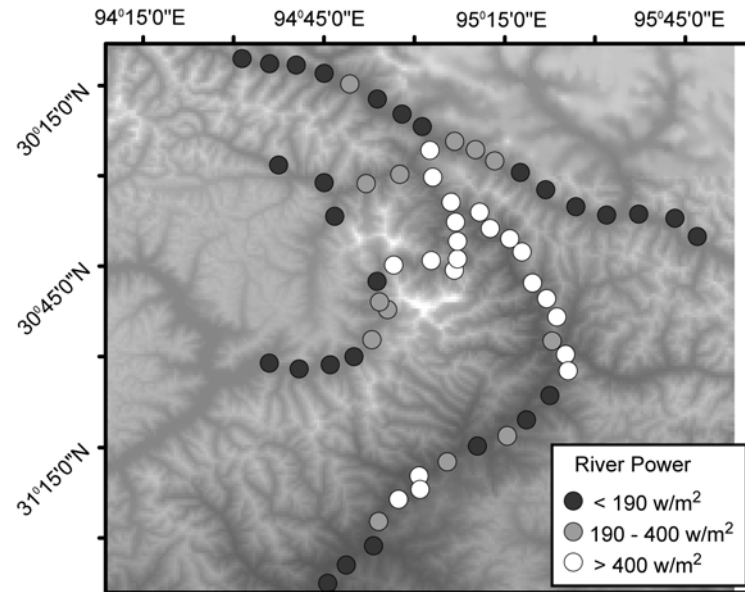
Figure 26: River power
Patterns in mean annual river power within the eastern syntaxis.

123
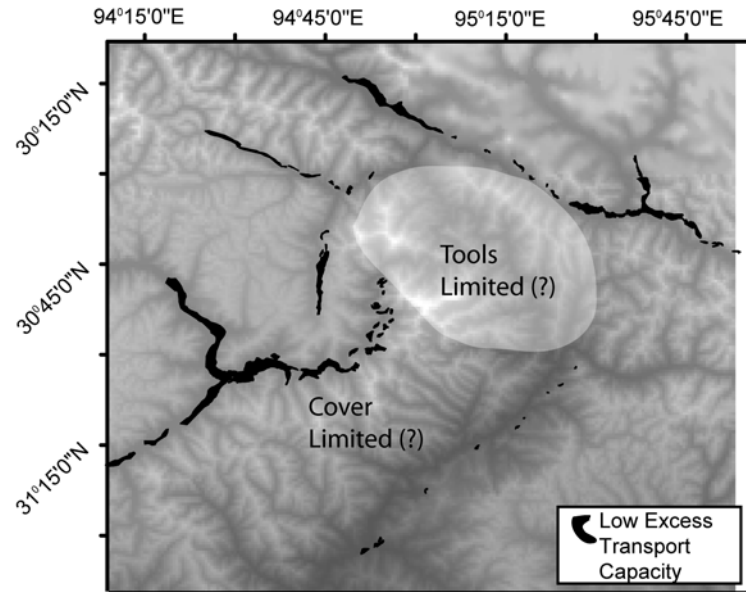
Figure 27: Sediment storage
Valley-bottom sediment storage within the eastern syntaxis, a proxy for low excess transport capacity channels.
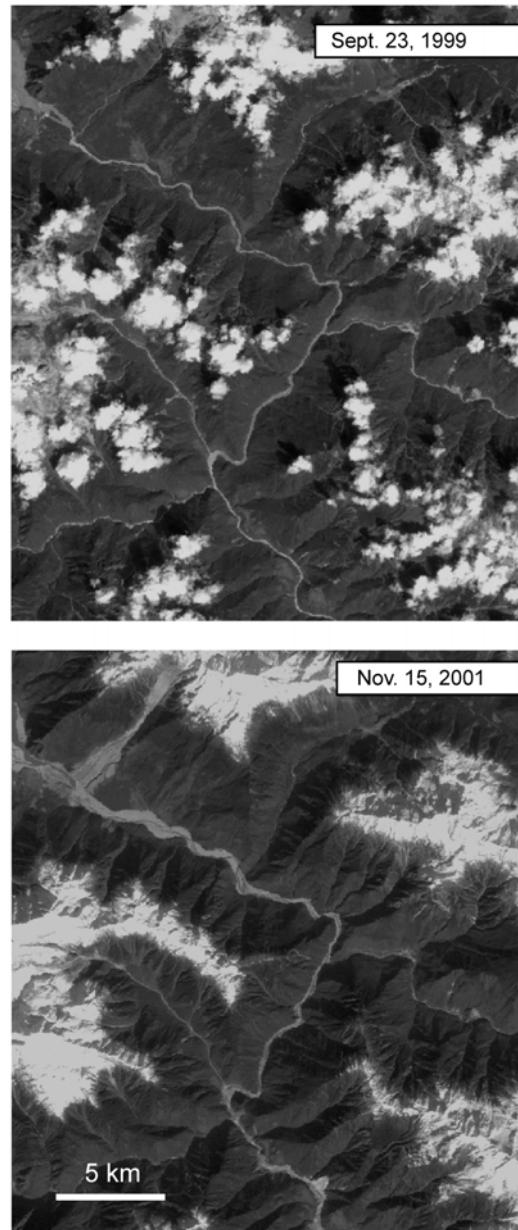
Figure 28: Example of a cover limited channel
Paired landsat images showing the Yiggong Tsangpo before and after a massive
bedrock landslide in 2000.

Photo Credit: Allan Ellard
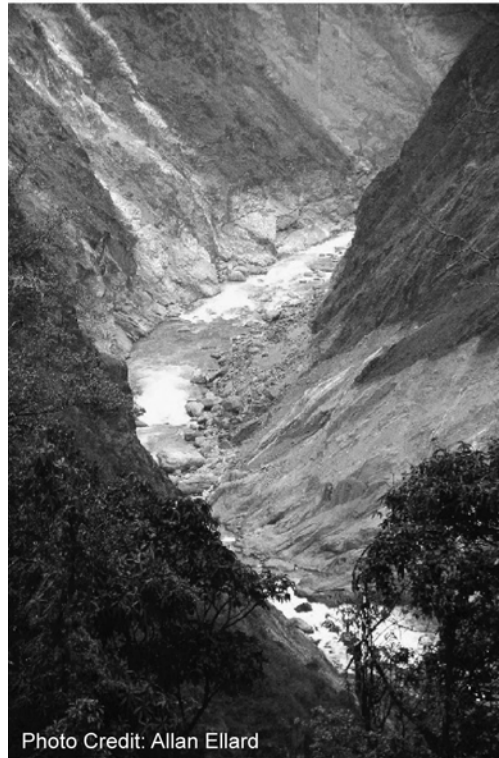
Figure 29: Example of a tools limited channel
Photograph of the Yarlung Tsangpo-Brahmaputra within the Yarlung Tsangpo gorge showing numerous large bedrock landslide scars and minimal sediment storage in the channel.
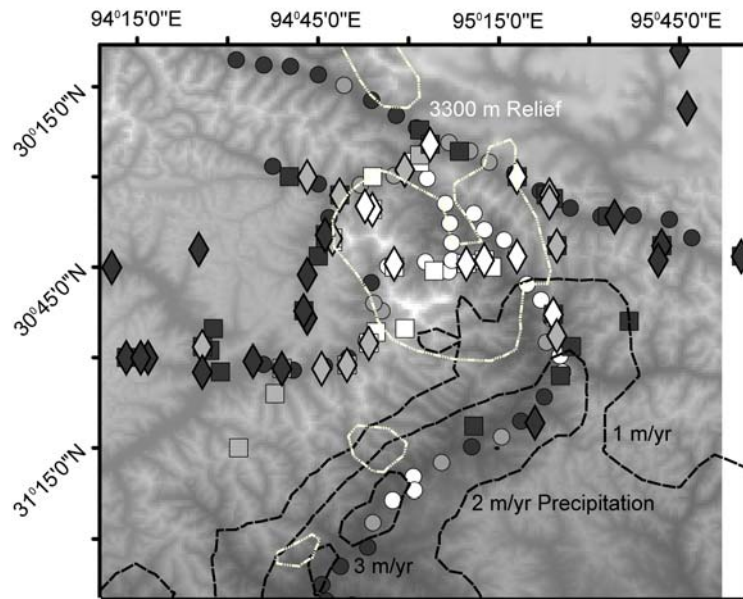
Figure 30: Data synthesis
Superimposed patterns in topographic relief, precipitation, river power, zircon ages, and biotite ages. The color scheme for each dataset is the same in this figure as in Figures 22 – 27.
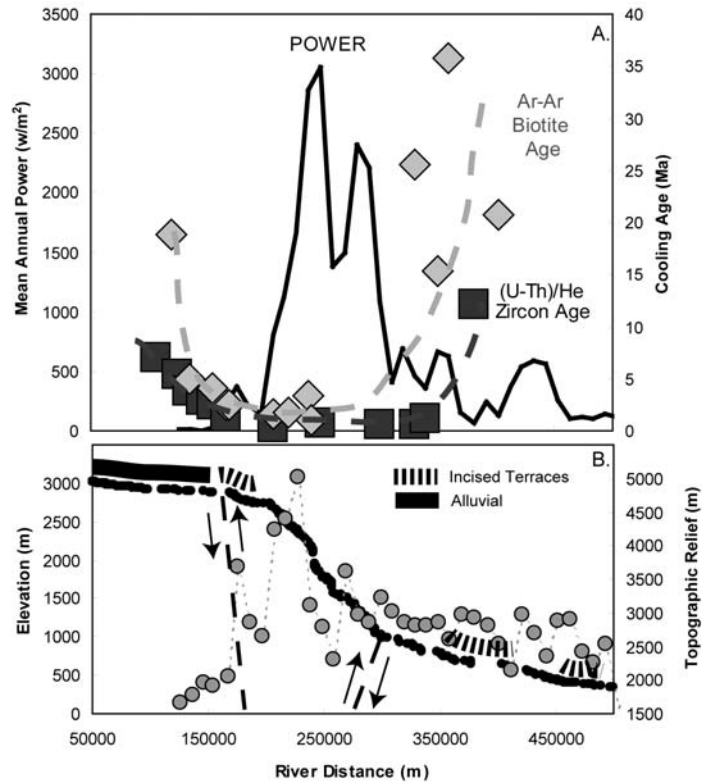
Figure 31: Coupling of river incision and rock uplift
(A) Longitudinal profile of zircon (U-Th)/He ages, biotite ^{40}Ar/^{39}Ar ages, and river power through the Tsangpo gorge. (B) Elevation, topographic relief, and sediment storage through the Yarlung Tsangpo gorge.

Figure 32: Recently aggraded channels with young cooling ages
(A) A sediment choked reach of the Yarlung Tsangpo-Brahmaputra above the gorge
showing signs of extensive recent aggradation inferred from fill terraces in the
background. (B) A sediment choked reach of the Parlung Tsangpo showing signs of
recent aggradation, again inferred from fill terraces along the far bank. Both channels
segments have young cooling ages but relatively low river power.
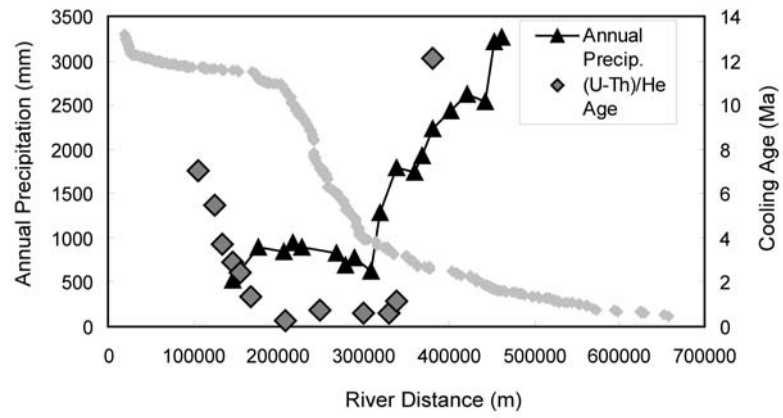
Figure 33: Precipitation and exhumation
Profiles of elevation, precipitation, and zircon (U-Th)/He ages through the Yarlung Tsangpo gorge.

Chapter 5

Erosion rate patterns and sediment provenance within the Yarlung Tsangpo river basin from cosmogenic [10]Be

5.1.0 Introduction

The eastern Himalayan syntaxis is the termination of the great Himalayan arc. As the NE corner of the indenting Indian plate, it spans the transition from the E-W oriented thrust tectonics of the Himalayan front to the largely N-S oriented transpressional tectonics of the Indo-Burmese ranges (Zeitler et al., 2001). The core of the eastern syntaxis exposes high-grade Indian basement rocks (Booth et al., 2004), some exhumed 30 km since the Pliocene (Burg et al., 1998). Cutting through this zone of rapid exhumation is the 5 km deep Yarlung Tsangpo gorge, where the river threads a tortuous path between 7782 m Namche Barwa and 7294 m Gyala Peri. The spatial coincidence of the unparalleled erosive potential of the Tsangpo gorge (Finlayson et al., 2002) and the extremely rapid exhumation of the Namche Barwa-Gyala Peri Massif has motivated the hypothesis that vigorous erosion by the Yarlung Tsangpo and its tributaries helps localize crustal uplift and deformation in this unique geodynamic setting (Zeitler et al., 2001).

Previous chemical and mineral mass-balance studies (Singh and France-Lanord, 2002; Stewart and Hallet, 2004; Tibari et al., 2005) collectively indicate that the core of the eastern syntaxis contributes 40 – 50 % of the sediment load carried by

the Brahmaputra in India, while a variety of mineral cooling data suggest exhumation rates of 3 – 7 mm/yr in the region of the syntaxis (Burg et al., 1998; Stewart and Hallet, 2004; Tibari et al., 2005). However, sediment mass-balances provide only an indication of the relative contributions of different regions to a given sediment sample, while exhumation rate estimates are extremely sensitive to assumptions made about the thermal structure of the upper few kilometers of the crust. Consequently, it is only certain that a source of rapidly cooled zircon and apatite exists in the vicinity of the Tsangpo gorge, and that these minerals comprise 40-50% of the zircon and apatite in the sediment load of the Yarlung Tsangpo in India. The spatial extent of the inferred erosional hotspot and the mass flux associated with it are uncertain.

Knowledge of spatial patterns in erosion rates across the eastern syntaxis, in particular, would provide a necessary field-test of the tectonic aneurysm hypothesis because the hypothesis requires a tight coupling of erosion, exhumation and deformation. Additionally, geodynamic models of this complex area require accurate surface erosion boundary conditions. More generally, the topographic controls on erosion rates in tectonically active regions remain vigorously debated (Montgomery and Brandon, 2002; von Blanckenburg, 2005) and more erosion rate data spanning regions of active erosion such as the Himalaya are needed to evaluate the extent to which topography may be used to infer erosion rates. Finally, because of the importance of Himalayan erosion to chemical weathering and carbon uptake (Raymo and Ruddiman, 1992; France-Lanord and Derry, 1997) accurate estimates of mass

fluxes in Himalyan rivers over millenial time scales are desirable for climate modeling.

In order to constrain spatial gradients in erosion rates from the Tibetan plateau to the high Himalaya in the vicinity of the eastern Himalayan syntaxis, I measured in-situ, cosmic ray produced ^{10}Be in quartz sand from tributaries of the Yarlung Tsangpo entering the eastern syntaxis, as well as along the mainstem Yarlung Tsangpo itself. Cosmogenic ^{10}Be accumulates in quartz while it resides in the upper ~ 1 m of the earth's surface (Lal, 1991). Consequently, ^{10}Be measurements in quartz river sediments provide the most direct estimate of basin scale erosion rates averaged over centuries to millennia (Granger et al., 1996; von Blanckenburg, 2005).

Below I present measurements of cosmogenic ^{10}Be from river sediments in the eastern Himalayan syntaxis. These measurements are used (1) to map the spatial pattern of erosion across the eastern Himalayan syntaxis, (2) to make an estimate of the volumetric sediment flux of the Brahmaputra river near where it exits the Himalaya, (3) to examine the relationship between topography and erosion rates within the sampled region, and (4) to assess the relative contributions of the Tibetan plateau, Tsangpo Gorge and Nyainqentangla Range to the sediment load of the Brahmaputra River.

5.2.0 Setting

The study region spans the southern Tibetan Plateau, and a prominent series of mountains in the Nyainqentangla Range and Namche Barwa-Gyala Peri Massif (Figures 34A and 34B). These mountains comprise a continuous band of high topography characterized by extreme local relief, heavy glaciation, threshhold slopes, pervasive landsliding and episodic flooding related to landslide and glacier dam failures (Montgomery et al., 2004). The Southern Tibetan Plateau drained by the Yarlung Tsangpo, in contrast, is relatively arid and is generally soil-mantled, with more subdued relief and few glaciers (Figure 35). The Nyainqentangla Range and Namche Barwa-Gyala Peri Massif are easily distinguished physiographically from the surrounding Tibetan Plateau in Figure 34B as the extensively dissected, snowy NW-SE trending band of mountainous topography. Figure 35, shows the study area from the edge of the Tibetan plateau looking towards the Namche Barwa-Gyala Peri massif. It highlights the topographic transition from the relatively gentle topography of the Tibetan Plateau to the extreme relief of the Namche Barwa-Gyala Peri massif. The Nyainqentangla Range and Tibetan Plateau within the vicinity of the syntaxis are comprised mainly of Lhasa block meta-sediments, paleozoic sediments and plutonic rocks of the Trans-Himalayan Batholith (Figure 34A). The Namche Barwa-Gyala Peri massif is an exposed, deeply exhumed core of underthrust Indian basement rocks (Figure 34A).

5.3.0 Methods

[10]Be measurements in quartz grains separated from river sand can be used to infer basin average erosion rates by:

$$E = \Lambda P / N \rho, \tag{1}$$

where E is basin-averaged erosion rate, P is the production rate of [10]Be by spallation, N is [10]Be concentration in a sample, Λ is the effective attenuation length for spallation, and ρ is the density of the eroding material (Granger et al., 1996). To use the above equation, a number of conditions have to be met (Brown et al., 1995; Bierman and Steig, 1996; Granger et al., 1996). Equation 1 assumes uniform quartz distribution in a catchment and a sand sample that is well-mixed and representative of the entire catchment. The sample's residence time in the catchment, following erosion, must be neglible compared to its residence time in the upper ~1 m of the earth's surface. The equation assumes steady-state where the accumulation of [10]Be at the catchment surface is balanced by its erosional removal. It also assumes that radiogenic decay of [10]Be (half-life of 1.51 Ma) is neglible over the residence time of [10]Be in the catchment, a good assumption for all but the most slowly eroding terrains. Finally, Equation 1 assumes only production of [10]Be via spallation; the small contribution of production due to muons is well within the error of the results presented below.

I calculated the [10]Be production rate (Stone, 2000) in each catchment using the hypsometric mean elevation of each catchment. This production rate is corrected for topographic shielding effects using the methodology of Balco (2001). Because the

region of interest is heavily glaciated, I also corrected basin-averaged [10]Be production

rates for areas covered by permanent snow and ice and thus contributing sediment

with, in theory, no [10]Be. I mapped glaciers and permanent snow cover from available

Landsat 7 images of the field area. By assuming these areas contributed sediment to

their respective catchments in proportion to their area, I was able to correct the basin-

averaged production rate for the effects of snow and ice cover. Spectral estimates of

snow and ice-cover suffer from uncertainties due to shadowing of snow and ice

covered areas by large peaks, failure to map debris-covered ice as ice cover, and

failure to record seasonal variation in the snow line. Consequently, there is

considerable uncertainty in the production rate corrections, which were as high as 40%

for some catchments. In order to reflect this uncertainty, I have assigned a 20% error

for all production rate estimates made from the Landsat imagery. These production

rate uncertainties were then propagated through the various erosion rate calculations

presented below.

In the field, I sampled sand directly from the rivers and streams draining the

catchments of interest, and tried to sample sandy areas of the bed where transport

appeared to have been recent or was active at the time of the sampling. Sediments

were initially bathed in 2% nitric acid to remove carbonate and organic material, and

then sieved to the size fraction of interest. After magnetic separation and heavy liquid

separations, samples were etched repeatedly in 2% hydroflouric acid for quartz

purification. I extracted [10]Be from quartz according to previously published standard

procedures (Stone et al., 2004). Beryllium isotope ratios were measured at the

Lawrence Livermore National Laboratories Center for Accelerator Mass

Spectrometry. Combined process and carrier blanks were 2725 +/- 1159, 4808 +/-

1606, and 7328 +/- 1677 atoms of ^{10}Be. The total amount of ^{10}Be introduced during

processing was never more than 3% of the total atoms measured for the lowest sample.

Figure 34B shows the locations of the larger catchments sampled over the

2002 and 2004 field seasons. The sampling strategy in this analysis reflects a balance

between on the one hand covering a wide area geographically and on other hand trying

to evaluate spatial gradients in erosion across the landscape. Hence sand was

collected from predominately medium-sized catchments of order $\sim 10^9$ m^2 and larger.

However, I also sub-sampled tributaries of the Parlung River with areas of $10^6 - 10^7$

m^2. These extremely steep, landslide dominated catchments provided an opportunity

to explore the relationship between the erosion rate measured in small 1st and 2nd order

catchments and the erosion rate measured at the mouth of the catchment within which

they are nested. Additionally, the catchments enabled us to evaluate the variability in

cosmogenic isotope derived erosion rates for catchments dominated by landslides.

All topographic data presented below are based on analyses of the 30 arc-

second GTOPO-30 DEM of Asia. Although higher resolution data were available for

portions of the study region, for the sake of consistency I only use the relatively coarse

30 arc-second data for this study because it is continuous across the study region.

5.4.0 Results

Table 3 lists the results of the [10]Be measurements and erosion rate calculations.

Samples NB-8-04, NB-7-04, and NB-5-04 all drain regions with mean local relief

below 2000 m, measured on a 10 pixel radius for each pixel in the watershed (i.e. 10

cells on the GTOPO 30 DEM). NB-8-04 was collected at Gyala, from the mainstem

of the Yarlung Tsangpo river where it transitions from a low gradient sand and gravel

bed along the Tibetan Plateau to the steep bedrock gorge it cuts through the Namche

Barwa-Gyala Peri Massif. Hence quartz in the sample is expected to be primarily

derived from sand carried by the Yarlung Tsangpo during its 1200 km traverse of the

arid, low relief Tibetan plateau. As anticipated, sample NB-8-04 has the highest

concentration of [10]Be measured in the field area, indicating an erosion rate of the

southern portion of the Tibetan Plateau of 0.13 +/- 0.03 mm/yr. Sample NB-7-04

from the Nyang River – the last major tributary of the Yarlung Tsangpo before it

descends off of the Tibetan Plateau - has a similar erosion rate of 0.24 +/- 0.05 mm/yr.

Additionally, sample NB-5-04, a tributary of the Po-Tsangpo (Figure 36) - the major

tributary of the Yarlung Tsangpo in the gorge – has an erosion rate of 0.29 +/- 0.06

mm/yr.

In constrast, the three samples with mean local relief in excess of 2000 m all

exhibit erosion rates greater than 1 mm/yr. Samples NB-3-04 and NB-4-04, the

Parlung Tsangpo and Yiggong Tsangpo, collectively drain the Nyainqentangla Range

and when joined become the Po Tsangpo River system. The erosion rates of the

Parlung Tsangpo and Yiggong Tsangpo are 1.07 +/- 0.22 mm/yr and 2.17 +/- 0.44 mm/yr respectively. NB-6-04 is sampled from a catchment that drains the southern flank of the Nyainqentangla Range, and yields an erosion rate of 1.53 +/- 0.31 mm/yr.

I also analyzed quartz sand from Medoc, a small village at the lower end of the Yarlung Tsangpo gorge. From where the Yarlung Tsangpo plunges off the Tibetan Plateau in Gyala, Tibet, to where it begins to emerge from its gorge in Medoc, 2 vertical kilometers downstream, in-situ ^{10}Be concentrations in quartz sand diminishes 2-fold from 390293 +/- 19954 atoms/g to 157453 +/- 4885 atoms/g due to dilution of plateau sediments by locally-derived low-^{10}Be quartz. The apparent erosion rate of the Yarlung Tsangpo basin increases from 0.13 +/- 0.03 mm/yr at Gyala to 0.31 +/- 0.06 mm/yr at Medoc, due to the addition of locally derived sediments to the Yarlung Tsangpo.

Finally, I measured ^{10}Be in sand from six 1st and 2nd order catchments entering the lower Parlung River. These catchments ranged in size from 1 km^2 to 36 km^2, in mean relief from 2635 to 3614 m, and in permanent snow and ice cover from 7% to 29%. All of these catchments showed signs of active landsliding. The erosion rates of these catchments range between 1.9 and 3.6 mm/yr, reflecting less than a two-fold variability in the erosion rate measured among the six catchments.

5.5.0 Discussion

5.5.1 The erosion rate of Southern Tibet

The erosion rate of the southern Tibetan plateau has been directly measured with cosmogenic isotopes at several isolated bedrock exposures (Lal et al., 2004) and from ^{10}Be and ^{26}Al in river sediments for the 1.7 x 10^9 m^2 of the upper Ganges that drains the Tibetan Plateau (Vance et al., 2002). The estimate of the erosion rate of the southern Tibetan Plateau by these methods differs by two orders of magnitude from 0.013 mm/yr (Lal et al., 2004) to 1.2 mm/yr (Vance et al., 2002), suggesting, unsurprisingly, considerable heterogeneity in erosion rates across the vast region. The 0.13 +/- 0.03 mm/yr erosion rate that reported herein integrates 2.0 x 10^{11} m^2 of the southern Tibetan plateau, and represents an intermediate value between the two previous estimates. Cosmogenic isotope measurements from larger catchments more faithfully record long-term erosion rates when compared to smaller catchments (Matmon et al., 2003; Niemi et al., 2005) and isolated bedrock samples (Niemi et al., 2003). Consequently, my sampling strategy – which yields a 0.13 mm/yr erosion rate – is more likely to be a reasonable erosion rate for southern Tibet. Additionally, based on 20 years of suspended sediment and water flux measurements from just upstream of where I sampled the mainstem of the Yarlung Tsangpo, I compute an erosion rate of 0.03 mm/yr for southern Tibet. This suggests that the current rate of sediment export from the Tibetan plateau is within a factor of 3 or 4 of what I infer from ^{10}Be in river sediments, again suggesting that my estimate from ^{10}Be is a

relatively accurate assessment of the mass flux from southern Tibet. This data point

therefore provides a unique benchmark for geochemical and geodynamic studies in

this region that require quantification of erosional fluxes for the southern Tibetan

plateau.

5.5.2 Erosion Rate Patterns and Topography

The results reported in Table 3 indicate that the topographic transition from the

Tibetan Plateau to the Nyainqentangla Range and Namche Barwa-Gyala Peri Massif is

accompanied by an order of magnitude increase in erosion rates (Figure 36). In Figure

37, I show erosion rate as a function of the average relief of a given catchment, where

relief is computed within a 10-pixel radius for every pixel in each watershed. The data

indicate a clear trend of increasing erosion rate with increasing relief for the studied

catchments. The erosion rate data generally conform to previously reported empirical

relationships indicating a non-linear relationship between relief and catchment erosion

rate (Montgomery and Brandon, 2002; Vance et al., 2002)

5.5.3 Sub-catchment erosion rates

Data from 1st and 2nd order catchments sampled along the Parlung conform

with observations in the Smokie Mountains, USA that show the coherence of basin-

wide erosion rate data to break down at small catchment sizes (Matmon et al., 2003).

Similarly, the data indicate a two-fold variation in measured basin-averaged erosion

rates at the scale of $1 - 30$ km^2 catchments in the Himalaya. Numerical models

(Niemi et al., 2005) demonstrate that ^{10}Be erosion rate estimates for small-order,

landslide dominate catchments will tend to systematically underestimate basin-

averaged erosion rates because large and infrequent landslides dominate the erosion of

these catchments, but typically are not sampled. My data, however, indicate that the

small 1st and 2nd order catchments draining the Parlung exhibit uniformly higher

erosion rates, 1.9 +/- 0.39 to 3.57 +/- 0.74 mm/yr, than for the whole Parlung basin,

1.07 +/- 0.22 mm/yr.

That the Parlung collectively has a lower apparent erosion rate than its first

order tributaries may be due to the mean topographic relief of the Parlung catchment

as a whole being much lower than the mean relief of the six tributaries sampled in this

study. The six sub-catchments sampled within the Parlung Tsangpo watershed are all

located entirely within the lower, more deeply dissected portion of the Parlung

Tsangpo watershed and all have mean relief in excess of 2600 m, while the Parlung

drainage basin itself has mean relief (measured over the same length-scale) of 2070 m.

I therefore infer that the lower relief upper catchment is eroding slowly and thus

enriching the Parlung river sediment with high-^{10}Be sand that mixes with low ^{10}Be

sand from the higher-relief portion of the catchment. The mixing of these two source

regions yields basin-averaged erosion rates that are lower than what I measure in sub-

catchments from the lower Parlung. This result thus reinforces Figure 37, indicating a

strong correlation between topographic relief and erosion rate within the sampled region.

5.5.4 Sediment Provenance and Fluxes

My data also provide constraints on the provenance of sediment carried by the Yarlung Tsangpo as it exits the Himalayan front. I divide the sampled area into two regions: (1) the region draining the Tibetan Plateau – essentially the Yarlung Tsangpo above Gyala, sample NB-8-04, and (2) the region draining the Nyainqentangla Range – essentially the Po Tsangpo drainage, comprised of samples NB-3-04 through NB-6-04. Combining all of the samples for the Po Tsangpo drainage, I estimate an erosion rate of 1.55 +/- 0.22 mm/yr for the Po Tsangpo. The Yarlung Tsangpo above Gyala has an erosion rate of 0.13 +/- .03 mm/yr. Taken together, erosion rate estimates and catchment drainage areas indicate a volume flux of 4.34×10^7 +/- 0.82×10^7 m^3/year from the Po Tsangpo and 2.67×10^7 +/- 0.55 m^3/year for the Yarlung Tsangpo above Gyala. This suggests that 38 +/- 9 % of the sediment flux of Yarlung Tsangpo below where the rivers join is sourced from the Tibetan Plateau, while 62 +/- 9% is sourced from the Po Tsangpo drainage. In other words, roughly 2/3 of the sediment carried by the Yarlung Tsangpo is sourced from the 14% of the catchment draining the Nyainqentangla Range. This estimate is consistent with previous mass-balance work (Singh and France-Lanord, 2002; Stewart and Hallet, 2004; Tibari et al., 2005) that collectively suggests 40-50% of the sediment flux of the Brahmaputra is sourced

locally in the region of the eastern syntaxis. However, my estimate differs

considerably from cosmogenic work based on isolated bedrock samples (Lal et al.,

2004) that concludes material eroded from the Tibetan Plateau represents less than

0.1% of the sediment load of the great Asian rivers originating on the Tibetan plateau.

5.5.5 The Erosion Rate of the Tsangpo Gorge

The ^{10}Be measurement from Medoc should reflect mixing of sediment derived

from the Po Tsangpo and Tibetan Plateau with sediment sourced from the region

downstream of these locations and upstream of Medoc. This region, roughly 3% of

the entire Yarlung Tsangpo catchment above Medoc, is the heart of the Yarlung

Tsangpo Gorge, and is characterized by extremely young zircon and apatite ages and

exhumation rates of 3-7 mm/yr (Stewart and Hallet, 2004; Tibari et al., 2005). Thus

despite its small area, I expect that a large volume of low ^{10}Be quartz enters the gorge

in this 3 % of the catchment. I therefore calculate mixing between these three source

regions in order to test the sensitivity of the measurement of ^{10}Be at Medoc to the

erosion rate of the Tsangpo Gorge. The concentration of ^{10}Be in a mixture of

sediment between the Tsangpo Gorge, Po Tsangpo and Tibetan plateau is calculated as

follows:

$$N_{Tibet}Vf_{Tibet} + N_{PoTsangpo}Vf_{PoTsangpo} + N_{TsangpoGorge}Vf_{TsangpoGorge} = N_{mix} \quad\quad (2)$$

where N is sediment ^{10}Be concentration and Vf is volume fraction contributed from a

given catchment:

$$Vf_i = (A_i \varLambda P_i / N_i \rho) \; / \; \sum_{i=1}^{3} (A_i \varLambda P_i / N_i \rho) \hspace{3cm} (3)$$

Although the concentration of sediment sourced on the Tibetan Plateau and from the Po Tsangpo are known, the concentration of sediment sourced from the Tsangpo Gorge itself is unknown. This concentration, via equation 1, determines the erosion rate of the gorge and therefore influences the respective volume fractions of each of the three terms in equation 2. In Figure 38, I plot equation 2 for a series of assumed erosion rates for the Tsangpo gorge, along with the concentration of ^{10}Be measured at Medoc. The figure indicates that the ^{10}Be measurement at Medoc will fall within the uncertainty of the mixing model for a range of assumed erosion rates for the Tsangpo Gorge between 0 and 6 mm/yr. Obviously changes to the assumed production rate uncertainty of 20% would enable considerable refinement of the bounds on the erosion rate of the Tsangpo Gorge. However as there has been no study yet to systematically address the problem of glacial shielding and its effect on calculated basin-averaged cosmogenic erosion rates, I feel that the relatively liberal uncertainty estimates for production rate are warranted.

Consequently, without a more direct measurement of erosion from within the Tsangpo Gorge, such as from tributaries draining into the gorge itself, it is difficult to constrain the erosion rate in this region. This is mainly due to the combination of the relatively small area of the Yarlung Tsangpo Gorge relative to the catchment area sampled in this study and the large uncertainty in production rate estimates.

145

5.6.0 Conclusions

Measurements of cosmogenic ^{10}Be in river sediments from the eastern Himalaya reveal an order of magnitude increase in erosion rates from 0.13 – 0.24 mm/yr from the southern Tibetan plateau to 1.07 – 3.57 mm/yr for the Namche Barwa-Gyala Peri massif and Nyainqentangla Range. This acceleration of erosion is accompanied by an increase in local topographic relief, suggesting that within the study region relief is a useful proxy for erosion rate. The estimate of the erosion rate of the southern Tibetan Plateau reflects an intermediate value compared to previous cosmogenic estimates for the erosion rate of the Tibetan plateau. However this erosion rate measurement integrates far more geographic area than previous estimates, and agrees within a factor of 4 with erosion rates inferred from suspended sediment measurements.

Based on my data, 62 +/- 9 % of the flux of the Yarlung Tsangpo at Medoc, Tibet (el. 700m) is sourced from the 14 % of the catchment within the Nyainqentangla Range. This estimate compares favorably to previous mass-balance studies that find 40-50 % of the sediment flux of the Tsangpo/Brahmaputra to be sourced locally within the syntaxis. Given uncertainties in basin-averaged ^{10}Be production rates due to glaciers within the study region, my analysis allows for as much as 6 mm/yr of erosion within the Tsangpo Gorge. This estimate accommodates previous exhumation rate estimates for the region of 3-7 mm/yr.
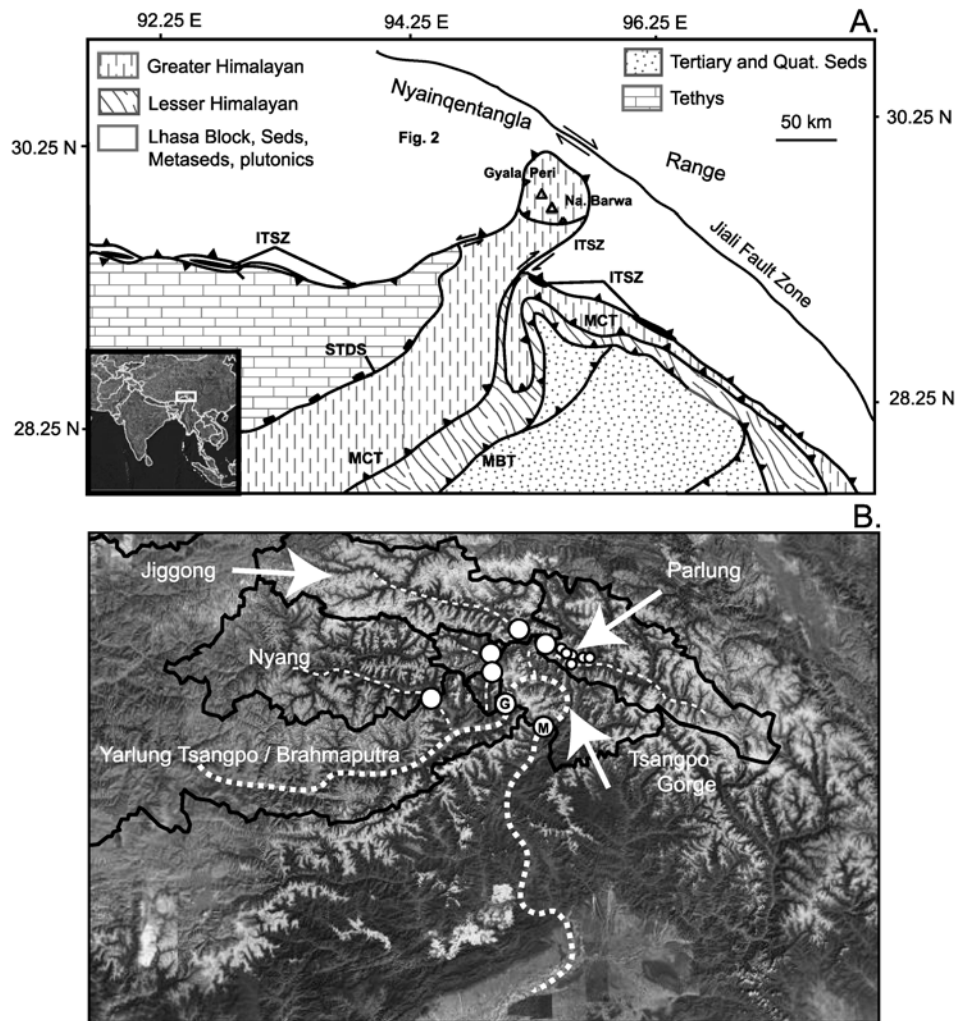
Figure 34: Geologic setting
(A) Bedrock geology and simplified tectonic map (Booth et al., 2004) for the eastern Himalayan syntaxis. MCT = Main Central Thrust, MBT = Main Boundary Thrust, ITSZ = Indus Tsangpo Suture Zone, STDS = South Tibetan Detachment System. (B) Satellite overview of the field area. Dotted lines indicate major river courses, solid lines indicate the boundaries of sampled catchments. Large white circles mark sample locales for principal catchments, small white circles mark sample locales for sub-catchments. G = Gyala, M = Medoc.
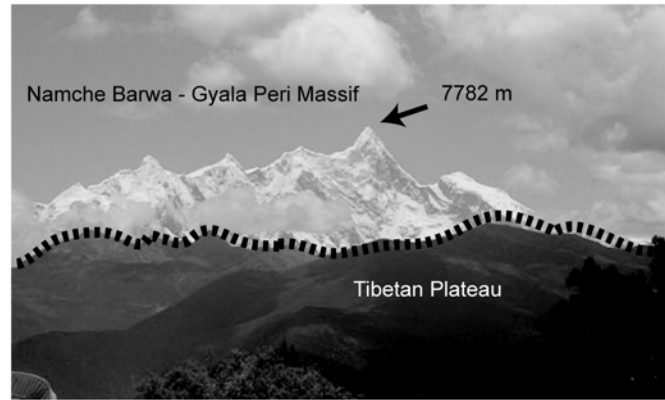
Figure 35: The transition from the Tibetan Plateau to the High Himalaya
Namche Barwa summit massif seen from the west. Note distinct topographic
transition from the Tibetan Plateau to the Namche Barwa-Gyala Peri massif. Photo
Credit B. Zurek.
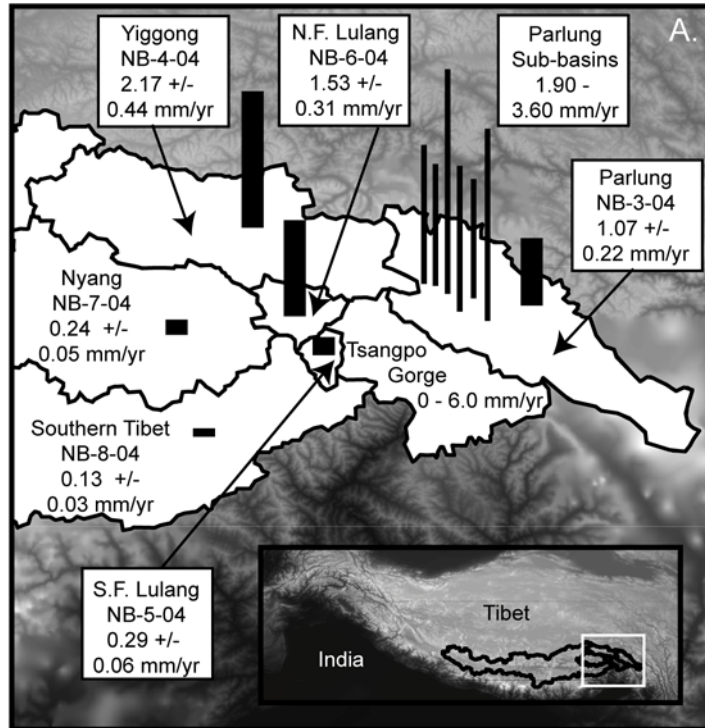
Figure 36: [10]Be-derived erosion rates for the eastern Himalayan syntaxis
Bars are proportional to erosion rate. Thick bars indicate erosion rates for principal catchments, thin bars indicate erosion rates for sampled sub-catchments.

149
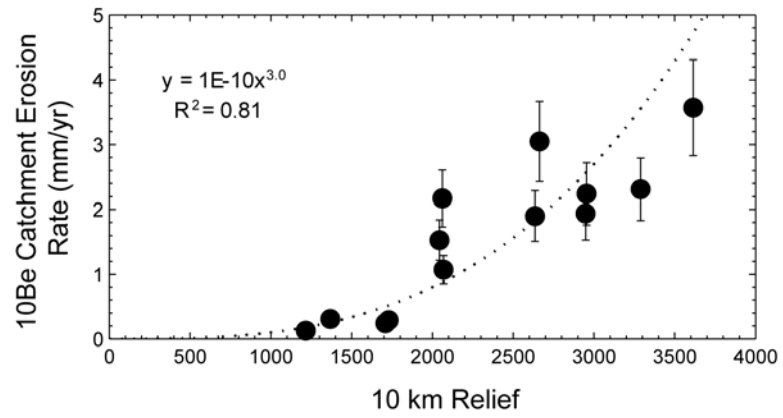
Figure 37: Relief and erosion rates
Basin-averaged erosion rate as a function of mean topographic relief for all sampled catchments.
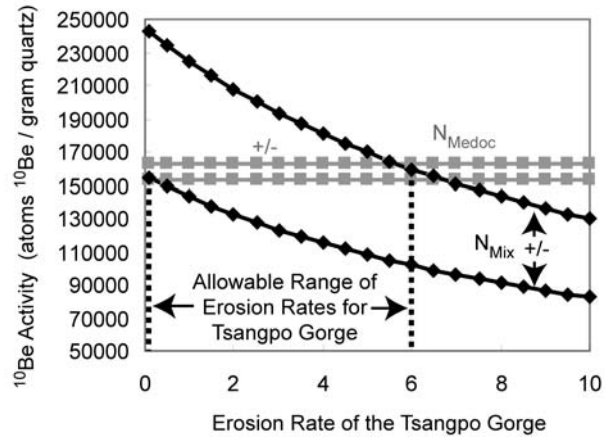
Figure 38: Mixing model results
Calculated concentration of [10]Be in sediment (black lines) sourced from a mixture of Tibetan Plateau, Nyainqentangla Range, and Yarlung Tsangpo Gorge sediment for different assumed erosion rates of the Yarlung Tsangpo Gorge. Line spacing shows the upper and lower bounds on uncertainty for the concentration of the mixture. Grey lines show the measured value of [10]Be in sediment from Medoc which theoretically mixes sediment sourced from the Tibetan Plateau, Nyainqentangla Range, and Yarlung Tsangpo. Dotted vertical lines show the range of allowable erosion rates for the Yarlung Tsangpo Gorge.

Table 3: ^{10}Be sample information

Sample	Description	Latitude	Longitude	Grain Size (μm)	N^{10}Be (atoms/g Qtz)	δ N^{10}Be (atoms/g Qtz)	production rate (atoms ^{10}Be/g qtz/yr)	apparent age (yrs)	Erosion Rate (mm/yr)	error (mm/yr)
NB-8-04	Yarlung Tsangpo Above Gyala	29.604056	94.936878	250-500	390239	19954	86	4538	0.13	0.03
NB-4-04	Yiggong Tsangpo (Po Tsangpo)	30.096703	95.06468	250-500	19641	776	71	277	2.17	0.44
NB-3-04	Parlung Tsangpo (Po Tsangpo)	30.095569	95.06624	250-500	22349	960	40	559	1.07	0.22
NB-6-04	North Fork Lulang (Po Tsangpo)	29.948215	94.800577	250-500	23554	949	60	393	1.53	0.31
NB-5-04	South Fork Lulang (Po Tsangpo)	29.945375	94.803485	250-500	127553	4669	61	2091	0.29	0.06
NB-7-04	Nyang River	29.709889	94.327901	250-500	195657	4999	79	2477	0.24	0.05
P-6-02	Parlung Sub-Catchment	29.94964444	95.38325833	500-850	10630	531	41	259	2.31	0.48
NB-5-02	Parlung Sub-Catchment	30.066032	95.179558	500-850	15810	990	51	310	1.94	0.41
NB-7-02	Parlung Sub-Catchment	30.04484444	95.26316111	500-850	7226	353	43	168	3.57	0.74
NB-13-02	Parlung Sub-Catchment	29.90863611	95.51360556	500-850	15818	564	50	316	1.90	0.39
NB-14-02	Parlung Sub-Catchment	29.94671667	95.41108333	500-850	12374	449	63	196	3.05	0.62
NB-23-02	Parlung Sub-Catchment	30.102062	95.111448	500-850	11761	855	44	267	2.24	0.48
MEDOC	Yarlung Tsangpo at Medoc	29.326442	95.311501	250-500	157453	4885	81	1944	0.31	0.06

Sample	Mean Elv. (m)	relief (max - min)	Area (m²)	glacial cover / total area
NB-8-04	4849	1216	2.02E+11	0.07
NB-4-04	4758	2061	1.21E+10	0.17
NB-3-04	4533	2069	1.35E+10	0.41
NB-6-04	4350	2044	1.68E+09	0.12
NB-5-04	4196	1729	7.74E+08	0.04
NB-7-04	4718	1708	1.57E+10	0.06
P-6-02	3563	3289	1.26E+06	0.07
NB-5-02	3968	2949	1.75E+07	0.13
NB-7-02	3880	3614	1.09E+07	0.25
NB-13-02	3797	2635	3.51E+07	0.29
NB-14-02	3648	2663	4.78E+06	0.21
NB-23-02	3642	2954	2.86E+07	0.19
MEDOC	4820	1368	6.94E+09	0.14

Chapter 6.

Conclusion

6.1 Conclusion

      The dynamics of incising bedrock rivers are a central focus of geomorphology and geodynamics because of the primary importance of river incision in the coupling of surface and tectonic processes, and because of the capacity of river morphology to reveal information about tectonics. Bedrock channel morphology also remains a challenging fluid dynamical problem in its own right. The components of channel morphology: width, shape, slope, depth, roughness, and bed cover are central to channel incision because they collectively determine the magnitude and variation of fluid stresses on the bed. However, of these variables, only the controls on channel slope are at all well constrained. In this dissertation, I have taken two approaches, one experimental and one theoretical, to investigate the controls on the morphology of incising bedrock channels. I then apply the results of this work to the problem of estimating the spatial variation of river incision rates throughout the eastern Himalayan syntaxis.

      In chapter 1 I develop a scaling relationship for the width of river channels that depends on channel slope, river discharge, roughness, and channel width-to-depth ratio. A simplified version of this relationship is used to explore channel width scaling for two longitudinally simple, uniformly concave bedrock rivers and one more complex river traversing a pronounced rock uplift gradient. In the former case, our relationship is

indistinguishable from traditional width-discharge relations that scale river width with only the square-root of discharge. However, our equation is considerably more versatile as it also describes river width trends in the more complex terrain undergoing spatial variable rock uplift, where traditional empiricisms are shown to fail.

I further demonstrate that in the Yarlung Tsangpo gorge, unit stream-power calculated with a common discharge-based power-law for channel width is as much as 40% lower than estimates made from satellite-based width measurements and from our model. My analysis thus shows that modeling of bedrock channel incision can be improved simply by accounting for adjustments in channel width that result from the fact that water flows faster through steeper reaches and thus occupies smaller channels.

In chapter 2, I use a laboratory flume to investigate experimentally how the components of channel morphology (bedrock channel slope, width, roughness, alluvial cover) and incision rate collectively evolved during the transient incision of an initially smooth channel with a varying bedload supply rate. The results of this analysis indicate that when channels are free of alluvial cover, incision is focused over a fraction of the bed that varies as a function of both the imposed bedload supply and the intrinsic transport capacity of the channel. However, after alluvial cover deposition occurs on a bedrock channel bed, incision will be focused in the lateral and higher regions of the channel and along the margins of alluvial deposits. I non-dimensionalize slot width data collected in the experiment, and I offer a new scaling

relationship for bedrock channel width that explicitly incorporates bedload supply rate, sediment grain size, and bed shear stress. The scaling relationship and experimental observations provide insight into how channel width adjusts to accommodate variation in discharge and sediment supply in natural settings.

Because increases in sediment supply widened the band of active bedload sediment transport and thus the width over which incision took place, mass removal from the experimental bed scaled with sediment supply when the bed was free of cover during the experiment. However, bed roughness growth due to the erosional destruction of the bed during the experiment eventually forced deposition of alluvial cover and thereby led to the suppression of incision on the bed at high sediment supply rates. The dynamics of roughness creation and alluvial cover deposition can therefore drive both negative and positive feedbacks on incision rate change following sediment supply perturbations

In chapter 3, I compare patterns in inferred detachment-limited incision and saltation abrasion potential to topographic relief, precipitation and exhumation rate patterns reflected by zircon and biotite cooling ages across the eastern Himalayan syntaxis. The coincidence of high incision potential, sediment transport efficiency, relief, and mineral cooling rates focused on the Namche Barwa-Gyala Peri antiform suggests a tight coupling between rock uplift and surface erosion over at least the last 1 Ma. Only patterns in precipitation are uncorrelated with those in mineral cooling ages, indicating that it does not directly influence exhumation within the syntaxis.

I highlight two regions along the lower Parlung Tsangpo and the upper Yarlung Tsangpo with high river power and rapid mineral cooling in a manner locally inconsistent with a detachment-limited view of long-term river incision. However, using the framework of the saltation-abrasion model (Sklar and Dietrich, 2004), I reconcile this apparent conflict in a manner that is self-consistent with both the model and field observations of these reaches.

A number of features of the eastern syntaxis suggest that the Yarlung Tsangpo – Brahmaputra plays a role in controlling lithospheric dynamics here. High relief in the syntaxis is restricted to a "bullseye" pattern in the region cut by the largest river in the Himalaya, the Yarlung Tsangpo-Brahmaputra, suggesting rock uplift is equally localized. This is confirmed by patterns in zircon and biotite cooling ages. Notably, despite the localized nature of the Namche Barwa-Gyala Peri uplift, the Yarlung Tsangpo-Brahmaputra is not deflected around the structure, but instead cuts through it. 2) The superposition of high river power, high relief, and young cooling ages indicates that the location of rapid incision on the Tsangpo has been pinned for at least 1 million years. Without uplift of the Namche Barwa-Gyala Peri massif during this time to balance the incision in the Yarlung Tsangpo gorge, its knickpoint would have propagated rapidly into Tibet. The Yarlung Tsangpo-Brahmaputra gorge is the most powerful reach of river in the Himalaya (Finlayson et al., 2002). Thus its co-location with a one structure that is apparently capable of balancing it's incision is striking.

In chapter 4, I present measurements of cosmogenic ^{10}Be in river sediments from the eastern Himalayan syntaxis in order to constrain regional erosion rates. These are used, in turn, in the analysis of river incision presented in chapter 3. The ^{10}Be data reveal an order of magnitude increase in erosion rates from 0.13 – 0.24 mm/yr for the southern Tibetan plateau to 1.07 – 3.57 mm/yr for the Namche Barwa-Gyala Peri massif and Nyainqentangla Range. Patterns in regional relief closely correlate with patterns in erosion rates inferred from ^{10}Be. I calculate that 62 +/- 9 % of the flux of the Yarlung Tsangpo-Brahmaputra at Medoc, Tibet (el. 700m) is sourced from the 14 % of the catchment within the eastern syntaxis. This compares favorably to previous mass-balance studies that find the eastern syntaxis to contribute 40-50% of the sediment load of the Yarlung Tsangpo-Brahmaputra.

REFERENCES

Anders, A.M., Montgomery, D., and Hallet, B., 2002, Comparing spatial variations in precipitation and erosion index to differences in long term exhumation along the European Alps, Abstracts with Programs - Geological Society of America, v. 34, p. 108.

Anders, A.M., 2005, The co-evolution of precipitation and topography: Ph.D thesis, University of Washington.

Anders, A. M., Roe, G.H., Hallet, B., Montgomery, D.R., Finnegan, N. J., and Putkonen, J., 2006, Spatial patterns of precipitation and topography in the Himalaya, in Willett, S.D., Hovius N., Brandon, M.T., and Fisher, D.M., eds., Tectonics, Climate and Landscape Evolution: Special Paper - Geological Society of America, v. 398, p. 39-53.

Balco, G., 2001, Topographic shielding and cosmogenic nuclide production rates over large areas, http://depts.washington.edu/cosmolab/math.html

Beaumont, C., Jamieson, R.A., Nguyen, M.H., and Lee, B., 2001, Himalayan tectonics explained by extrusion of a low-viscosity crustal channel coupled to focused surface denudation, Nature, v. 414, p. 738–742.

Bendick, R., and Bilham, R., 2001, How perfect is the Himalayan arc?, Geology, v. 29, p. 791–794.

Bierman, P., and Steig, E.J., 1996, Estimating rates of denudation using cosmogenic isotope abundances in sediment, Earth Surface Processes and Landforms, v. 21, p. 125–139.

Booth, A.L., Zeitler, P.K., Kidd, W.S.F., Wooden, J., Liu, Y., Idleman, B., Hren, M., and Chamberlain, C.P., 2004, U-Pb zircon constraints on the tectonic evolution of southeastern Tibet, Namche Barwa Area, American Journal of Science, v. 304, p. 889-929.

Brandon, M.T., and Gasparini, N.M., 2005, A power-law approximation for fluvial incision by tools and bed-coverage processes, Eos Transactions AGU, v. 86, Fall Meeting Supplement, Abstract H53D-0515.

Brown, E.T., Stallard, R.F., Larsen, M.C., Raisbeck, G.M., and Yiou, F., 1995, Denudation rates determined from the accumulation of in situ-produced ^{10}Be in the

Luquillo Experimental Forest, Puerto Rico, Earth and Planetary Science Letters, v. 129, p. 193–202.

Buffington, J. M., and D. R. Montgomery, 1997, A systematic analysis of eight decades of incipient motion studies, with special reference to gravel-bedded rivers, Water Resources Research, v. 33, p. 1993-2030.

Buffington, J. M., and Montgomery, D.R., 1999a, Effects of sediment supply on surface textures of gravel-bed rivers, Water Resources Research, v. 35, p. 3523-3530.

Buffington, J.M. and D.R. Montgomery, 1999b, Effects of hydraulic roughness on surface textures of gravel-bed rivers, Water Resources Research, v. 35, p. 3507-3521.

Bunn, J.T, Finnegan, N.J., and Montgomery, D.R., 2004, Landsliding and stream power in the vicinity of the Tsangpo River gorge at Namche Barwa, eastern Tibet, Abstracts with Programs, Geological Society of America, v. 36, p. 33.

Burbank, D.W., Leland, J., Fielding, E., Anderson, R.S., Brozovic, N., Reid, M.R., and Duncan, C., 1996, Bedrock incision, rock uplift and threshold hillslopes in the northwestern Himalayas, Nature, v. 379, p. 505-510.

Burbank, D.W., Blythe, A.E., Putkonen, J., Pratt-Sitaula, B., Gabet, E., Oskin, M., Barros, A., and Ojha, T.P., 2003, Decoupling of erosion and precipitation in the Himalayas, Nature, v. 426, p. 652–655.

Burg, J.P., Davy, P., Nievergelt, P., Oberli, F., Seward, D., Diao, Z., and Meier, M., 1997, Exhumation during crustal folding in the Namche Barwa syntaxis, Terra Nova, v. 9, p. 117–123.

Burg, J.P., Nievergelt, P., Oberli, F., Seward, D., Davy, P., Maurin, J.C., Diao, Z., and Meier, M., 1998, The Namche Barwa syntaxis; evidence for exhumation related to compressional crustal folding, Journal of Asian Earth Sciences, v. 16, p. 239-252.

Carter, C.L., and R.S. Anderson, 2006, Fluvial erosion of physically modeled abrasion-dominated slot canyons, Geomorphology, v. 81, p. 89-113.

Clark, M. K., Schoenbohm, L.M., Royden, L.H., Whipple, K.X., Burchfiel, B.C., Zhang, X., Tang, W., Wang, E., Chen, L., 2004, Surface uplift, tectonics, and erosion of eastern Tibet from large-scale drainage patterns, Tectonics, v. 23, TC1006, doi:10.1029/2002TC001402.

Clark, M.K., House, M.A., Royden, L.H., Whipple, K.X., Burchfiel, B.C., Zhang, X., and Tang, W., 2005, Late Cenozoic uplift of southeastern Tibet, Geology, v. 33, p. 525–528.

Daly, C., Neilson, R.P., and Phillips, D.L., 1994, A statistical-topographic model for mapping climatological precipitation over mountainous terrain, Journal of Applied Meteorology, v. 33, p. 140-158.

Davis, J.R., Sklar, L.S., Demeter, G.I., Johnson, J.P., and Whipple, K.X., 2005, The influence of bed roughness on partial alluviation in an experimental bedrock channel, Eos Transactions AGU, v. 86, Fall Meeting Supplement, Abstract H53D-0508

Davis, W.M., 1889, The rivers and valleys of Pennsylvania, National Geographic Magazine, v. 1, p. 183-253.

Davis, W.M., 1899, The geographical cycle, Geographical Journal, v. 14, p. 481-504.

Demeter, G.I., Sklar, L.S., Davis, J.R., 2005, The influence of variable sediment supply and bed roughness on the spatial distribution of incision in a laboratory bedrock channel, Eos Transactions AGU, v. 86, Fall Meeting Supplement, Abstract H53D-0519

Dietrich, W.E., J.W. Kirchner, H. Ikeda, F. Iseya, 1989, Sediment supply and the development of the coarse surface layer in gravel-bedded rivers, Nature, v. 340, p. 215-217.

Ding, L., Zhong, D., Yin, A., Kapp, P., and Harrison, T.M., 2001, Cenozoic structural and metamorphic evolution of the eastern Himalayan syntaxis (Namche Barwa), Earth and Planetary Science Letters, v. 192, p. 423-438.

Dingman, S.L., 1984, Fluvial Hydrology, 383 p., W.H. Freeman and Co., New York, NY.

Dingman, S.L., and Sharma, K.P., 1997, Statistical development and validation of discharge equations for natural channels, Journal of Hydrology, v. 199, p. 13-35.

Duvall A., Kirby, E., and Burbank, D., 2004, Tectonic and lithologic controls on bedrock channel profiles and processes in coastal California, Journal of Geophysical Research, v. 109, F03002, doi:10.1029/2003JF000086.

EROS Data Center, 2000, U.S. GeoData Digital Elevation Models, USGS Fact Sheet 040-00, http://erg.usgs.gov/isb/pubs/factsheets/fs04000.html (April, 2000).

Finlayson, D.P., Montgomery, D.R., and Hallet, B., 2002, Spatial coincidence of rapid inferred erosion with young metamorphic massifs in the Himalayas, Geology, v. 30, p. 219-222.

Finnegan, N.J., Roe, G.H., Montgomery, D.R., and Hallet, B., 2005a, Controls on the channel width of rivers: implications for modeling fluvial incision of bedrock: Geology, v. 33, p. 229-232.

Finnegan, N.J., Stone, J.O., Hallet, B., Montgomery, D.R., and Liu, Y., 2005b, Cosmogenic Nuclide Determination of the Source of Sediment to the Brahmaputra River, Eos Transactions AGU, v. 86, Fall Meeting Supplement, Abstract U32A-04.

Flint, J.J., 1974, Stream gradient as a function of order, magnitude, and discharge: Water Resources Research, v. 10, p. 969-973.

France-Lanord, C., and Derry, L.A., 1997, Organic carbon burial forcing of the carbon cycle from Himalayan erosion, Nature, v. 390, p. 65–67.
Fuller, C.W., Willett, S.D., Fisher, D., and Lu, C.Y., Lu, 2006, A thermomechanical wedge model of Taiwan constrained by fission-track thermochronometry, Tectonophysics, v. 425, p.1-24.

Gasparini, N.M., R.L. Bras, and K.X. Whipple, 2006, Numerical modeling of non-steady-state river profile evolution using a sediment-flux-dependent incision model, in Willett, S.D., Hovius N., Brandon, M.T., and Fisher, D.M., eds., Tectonics, Climate and Landscape Evolution: Special Paper - Geological Society of America, v. 398, p. 127-141.

Gesch, D.B., and Larson, K.S., 1998, Techniques for development of global 1-kilometer digital elevation models, in Proceedings, Pecora Thirteen, Human Interactions with the Environment--Perspectives from Space, 13th, Sioux Falls, South Dakota, August 20-22, 1996: Bethesda, Maryland, American Society of Photogrammetry and Remote Sensing, CD-ROM, 1 disc.

Gilbert, G. K., 1877, Report on the Geology of the Henry Mountains, U.S. Government Print Office, Washington, D. C., 160 pp.

Granger, D.E., Kirchner, J.W., and Finkel, R., 1996, Spatially averaged long-term erosion rates measured from in situ produced cosmogenic nuclides in alluvial sediments, Journal of Geology, v. 104, p. 249–257.
Griffiths, G.A., 2003, Downstream hydraulic geometry and hydraulic similitude, Water Resources Research, v. 39, no.4, 1094, doi:10.1029/2002WR001485.

Grujic, D., Coutand, I., Bookhagen, B., Bonnet, S., Blythe, A., and Duncan, C., 2006, Climatic forcing of erosion, landscape, and tectonics in the Bhutan Himalayas, Geology, v. 34, p. 801–804.

Hack, T.J., 1960, Interpretation of erosional topography in humid temperate regions, American Journal of Science, v. 248A, p. 80-97.

Hartshorn, K., Hovius, N., Dade, W. B., and Slingerland, R. L., 2002, Climate-driven bedrock incision in an active mountain belt, Science, v. 297, p. 2036–2038.

Hodges, K. V., 2000, Tectonics of the Himalaya and southern Tibet from two perspectives, Geological Society of America Bulletin, v. 112, p. 324–350.

Howard, A.D., and Kerby, G., 1983, Channel changes in badlands, Geological Society of America Bulletin, v. 94, p. 739-752.

Howard, A. D., 1994, A detachment-limited model of drainage basin evolution, Water Resources Research, v. 30, p. 2261–2285.

Howard, A. D., 1998, Long profile development of bedrock channels: Interaction of weathering, mass wasting, bed erosion, and sediment transport, in Rivers Over Rock: Fluvial Processes in Bedrock Channels, Geophysical Monograph Series, vol. 107, edited by K. J. Tinkler and E. E. Wohl, pp. 297–320, AGU, Washington, D. C.

Huang, C., I. White, E.G. Thwaite, and A. Bendeli, 1988, A noncontact laser system for measuring soil surface topography, Soil Society of America Journal, v. 52, p. 350-355.

Ikeda, H., and F. Iseya, 1988, Experimental study of heterogeneous sediment transport, Paper 12, Environmental Research Center, University of Tsukuba, Tsukuba, Japan.

Johnson, J.P., and K.X. Whipple, 2004, Experimental bedrock channel incision: Scaling, sculpture and sediment transport, Eos Transactions AGU, v. 85, Fall Meeting Supplement, Abstract H41G-07.

Kidd, W. S., Lim, C., Zeitler, P.K., Enkelmann, E., Booth, A.L., Chamberlain, C.P., Tang, W., Liu, Y., and Craw, D., 2006, Structural and Tectonic Geology of the Namche Barwa-Gyala Peri Antiform, Southeastern Tibet, Eos Transactions AGU, v. 87, Fall Meeting Supplement, Abstract T32B-02.

Kirby, E., and Whipple, K.X., 2001, Quantifying differential rock-uplift rates via stream profile analysis, Geology, v. 29, p. 415–418.

Kirby, E., Whipple, K.X., Tang, W., and Chen, Z., 2003, Distribution of active rock uplift along the eastern margin of the Tibetan Plateau: Inferences from bedrock channel longitudinal profiles, Journal of Geophysical Research, v. 108, no. B4, 2217, doi:10.1029/2001JB000861.

Kirchner, J.W, W.E. Dietrich, F. Iseya, and H. Ikeda, 1990, The variability of critical shear stress, friction angle, and grain protrusion in water-worked sediments, Sedimentology, v. 37, p. 647-672.

Knighton, D.A., 1998, Fluvial Forms and Processes, Edward Arnold, London, 377 p.

Kooi, H., and Beaumont, C., 1994, Escarpment evolution on high-elevation rifted margins: Insights derived from a surface processes model that combines diffusion, advection, and reaction, Journal of Geophysical Research, v. 99, p.12,191–12,209.

Koons, P.O., Zeitler, P.K., Chamberlain, C.P., Craw, D., and Meltzer, A.S., 2002, Mechanical links between erosion and metamorphism in Nanga Parbat, Pakistan Himalaya, American Journal of Science, v. 302, p. 749–773.

Korup, O., Geomorphic imprint of landslides on alpine river systems, southwest New Zealand: Earth Surface Processes and Landforms, v. 30, p.783-800.

Lague, D., Hovius, N., and Davy, P., 2005, Discharge, discharge variability, and the bedrock channel profile, Journal of Geophysical Research, v. 110, F04006, doi:10.1029/2004JF000259.

Lal, D., 1991, Cosmic ray labeling of erosion surfaces; in situ nuclide production rates and erosion models, Earth and Planetary Science Letters, v. 104, p. 424–439.

Lal, D., Harris, N.B.W., Sharma, K.K., Gu, Z., Ding, L., Liu, T., Dong, W., Caffee, M.W., and Jull, A.J.T., 2004, Erosion history of the Tibetan Plateau since the last interglacial: constraints from the first studies of cosmogenic [10]Be from Tibetan bedrock, Earth and Planetary Science Letters, v. 217, p. 33-42.

Lavé, J., and Avouac, J.P., 2001, Fluvial incision and tectonic uplift across the Himalayas of central Nepal, Journal of Geophysical Research, v. 106, p. 26,561–26,592.

Leopold, L.B., and Maddock, T. Jr., 1953, The hydraulic geometry of stream channels and physiographic implications, U.S. Geological Survey Professional Paper 252, 57 p.

Manga, M. and J.W. Kirchner, 2000, Stress partitioning in streams by large woody debris, Water Resources Research, v. 36, p. 2373-2379.

Manning, R., 1891, On the flow of water in open channels and pipes, Transactions of the Institute of Civil Engineers of Ireland, v. 20, p. 161 - 207.

Matmon, A., Bierman, P.R., Larsen, J., Southworth, S., Pavich, W., and Caffee, M., 2003, Temporally and spatially uniform rates of erosion in the southern Appalachian Great Smoky Mountains, Geology, v. 31, p. 155–158.

Meltzer, A.S., Sarker, G.L., Seeber, L., and Armbruster, J., 1998, Snap, crackel, pop! Seismicity and crustal structure at Nanga Parbat, Pakistan, Himalaya, Eos Transactions AGU, v. 79, Fall Meeting Supplement, p. F. 909.

Meyer-Peter, E., and Muller, R., 1948, Formulas for bed-load transport: Proceedings, 2nd meeting, IAHR, Stockholm, Sweden, p. 29-64.

Mitchell, S. G., and Montgomery, D. R., Influence of a glacial buzzsaw on the height and morphology of the central Washington Cascade Range, USA, Quaternary Research, v. 65, p. 96-107.

Molnar, P., and England, P., 1990, Late Cenozoic uplift of mountain ranges and global climatic change: Chicken or egg?, Nature, v. 346, p. 29–34.

Molnar, P., Anderson, R.S., Kier, G., and Rose, J., 2006, Relationships among probability distributions of stream discharges in floods, climate, bed load transport, and river incision: Journal of Geophysical Research, v. 111, doi:10.1029/2005JF000310.

Montgomery, D. R., 1994, Valley Incision and the uplift of mountain peaks, Journal of Geophysical Research, v. 99, p. 13,913-13,921.

Montgomery, D. R., Abbe, T.M., Buffington, J.M., Peterson, N.P., Schmidt, K.M., and Stock, J.D., 1996, Distribution of bedrock and alluvial channels in forested mountain drainage basins, Nature, v. 381, p. 587–589.

Montgomery, D.R., and Gran, K.B., 2001, Downstream variations in the width of bedrock channels, Water Resources Research, v. 37, p. 1841-1846.

Montgomery, D. R., and Brandon, M. T., 2002, Topographic controls on erosion rates in tectonically active mountain ranges, Earth and Planetary Science Letters, v. 201, p. 481-489.

Montgomery, D.R., Finnegan, N., Anders, A., Hallet, B., 2002, Downstream adjustment of channel width to spatial gradients in rates of rock uplift at Namche Barwa, Abstracts with Programs - Geological Society of America,v. 34, p.241.

Montgomery, D.R., 2004, Observations on the role of lithology in strath terrace formation and bedrock channel width, American Journal of Science, v. 304, p. 454 - 476.

Montgomery, D.R., Hallet, B., Yuping, L., Finnegan, N, Anders, A., and Gillespie, A., 2004, Evidence for Holocene megafloods downs the Tsangpo River gorge, Southeastern Tibet, Quaternary Research, v. 62, p. 201-207.

Montgomery, D.R., and Stolar, D. B., 2006, Reconsidering Himalayan river anticlines: Geomorphology, v. 82, p. 4-15.

Mullins, H.T., Erosion and infill of New York's Finger Lakes: Implications for Laurentide ice sheet deglaciation, 1989, Geology, v. 17, p. 622-625.

Niemi, N.A., Oskin, M., Burbank, D.W., Heimsath, A.M., and Gabet, E.J., 2005, Effects of bedrock landslides on cosmogenically determined erosion rates, Earth Planetary Science Letters, v. 237, p. 480–498.

Oberlander, T.M., 1985, Origin of drainage transverse to structures in orogens. In: M. Morisawa and J.T. Hack, Editors, Tectonic Geomorphology, Allen and Unwin, Boston, p. 155–182.

Park, S., and Mackie, R., 2000, Resistive (dry?) lower crust in an active orogen, Nanga Parbat, northern Pakistan: Tectonophysics, v. 316, p. 359–380.

Tapponnier, R; Peltzer, G; Le Dain, A Y; Armijo, Rolando; Cobbold, P, 1982, Propagating extrusion tectonics in Asia; new insights from simple experiments with plasticine, Geology, v. 10, p. 611-616.

Raymo, M.E., and Ruddiman, W.F., 1992, Tectonic forcing of late Cenozoic climate change, Nature, v. 359, p. 117–122.

Reiners, P.W., Farley, K.A., and Hickes, H.J., 2002, He diffusion and (U–Th)/He thermochronometry of zircon: initial results from Fish Canyon Tuff and Gold Butte, Tectonophysics, v. 349, p. 297-308.

Reiners, P., Ehlers, T., Mitchell, S., and Montgomery, D., 2003, Coupled spatial variations in precipitation and long-term erosion rates across the Washington Cascades, Nature, v. 426, p. 645–647.

Roe, G. H., Montgomery, D.R., and Hallet, B., 2002, Effects of orographic precipitation variations on the concavity of steady-state river profiles, Geology, v. 30, p. 143–146.

Roe, G. H., Stolar, D. B., and Willett, S. D., 2006, Response of a steady-state critical wedge orogen to changes in climate and tectonic forcing, in Willett, S.D., Hovius N., Brandon, M.T., and Fisher, D.M., eds., Tectonics, Climate and Landscape Evolution: Special Paper - Geological Society of America, v.398, p. 227-239.

Rosenbloom, N.A., and Anderson, R.S., 1994, Hillslope and channel evolution in a marine terraced landscape, Santa Cruz, California, Journal of Geophysical Research, v. 99, p.14,013-14,029.

Royden, L.H., Burchfiel, B.C., King, R.W., Wang, E., Chen, Z., Shen, F., and Liu, Y., 1997, Surface deformation and lower crustal flow in eastern Tibet, Science, v. 276, p. 788–790.

Seeber, L., and Gornitz, V., 1983, River profiles along the Himalayan Arc as indicators of active tectonics, Tectonophysics, v. 92, p. 335-367.

Seidl, M.A., and Dietrich, W.E., 1992, The problem of channel erosion into bedrock, Catena Supplement, v. 23; p. 101-124.

Seidl, M.A., Dietrich, W.E., Kirchner, J.W., 1994, Longitudinal profile development into bedrock; an analysis of Hawaiian channels, Journal of Geology, v.102, p.457-474.

Sheperd, R. G., and S. A. Schumm, 1974, Experimental study of river incision, Geological Society of America Bulletin, v. 85, p. 257–268.

Simpson, G., 2004, Role of river incision in enhancing deformation, Geology, v. 32, p. 341–344.
Singh, S.K., and France-Lanord, C., 2002, Earth and Planetary Science Letters, v. 202, p. 645-662.

Sklar, L.S. and W.E. Dietrich, 1998, River longitudinal profiles and bedrock incision models: Stream power and the influence of sediment supply, in Tinkler, K.J. and E.E. Wohl, eds., Rivers Over Rock: Fluvial Processes in Bedrock Channels, Geophysical Monograph Series, v. 107, p. 237-260, American Geophysical Union, Washington DC.

Sklar, L.S., and Dietrich, W.E., 2001, Sediment and rock strength controls on river incision into bedrock, Geology, v. 29, p. 1087-1090.

Sklar, L. S., and Dietrich, W.E., 2004, A mechanistic model for river incision into bedrock by saltating bed load, Water Resources Research, v. 40, W06301, doi:10.1029/2003WR002496.

Sklar, L. S., Stock, J.D., Roering, J.J., Kirchner, J.W., Dietrich, W.E., Chi, W., Hsu, L., Hsieh, M., Tsao, S., Chen, M., 2005, Evolution of fault scarp knickpoints following 1999 Chi-Chi earthquake in West-Central Taiwan, Eos Transactions AGU, v. 86, Fall Meeting Supplement, Abstract H34A-06.

Sklar, L.S. and W.E. Dietrich, 2006, The role of sediment in controlling bedrock channel slope: Implications of the saltation-abrasion incision model, Geomorphology, v. 82, p. 58-83.

Sklar, L.S., Dietrich, W.E., Foufoula-Georgiou, E., Lashermes, B., and Bellugi, D., 2006, Do gravel-bed river size distributions record channel network structure?, Water Resources Research, 42, doi:10.1029/2006wr005035.

Snyder, N. P., K. X. Whipple, G. E. Tucker, and D. J. Merritts, 2003, Importance of a stochastic distribution of floods and erosion thresholds in the bedrock river incision problem, Journal of Geophysical Research, v. 108, doi:10.1029/2001JB001655.

Snyder, N. P., Whipple, K.X., Tucker, G.E., and Merritts, D.J., 2000, Landscape response to tectonic forcing; digital elevation model analysis of stream profiles in the Mendocino triple junction region, Northern California, Geological Society of America Bulletin, v. 112, p. 1250-1263.

Stark, C. P., 2006, A self-regulating model of bedrock river channel geometry, Geophysical Research Letters, v. 33, doi:10.1029/2005GL023193.

Stewart, R., and Hallet, B., 2004, Extremely Rapid and Localized Erosion in the Himalaya Recorded in Sediments of the Bengal Fan, Eos Transactions AGU, v. 85, Fall Meeting Supplement, Abstract T53A-0471.

Stock, J.D., and Montgomery, D.R., Geologic constraints on bedrock river incision using the stream power law, Journal of Geophysical Research, v. 104, p. 4983-4993, 1999.

Stock, J., and Dietrich, W.E., 2003, Valley incision by debris flows: Evidence of a topographic signature, Water Resources Research, v. 39, doi:10.1029/2001WR001057.

Stolar, D. B., Willett, S. D., and Roe, G. H, 2006, Climatic and tectonic forcing of a critical orogen, in Willett, S.D., Hovius N., Brandon, M.T., and Fisher, D.M., eds., Tectonics, Climate and Landscape Evolution: Special Paper - Geological Society of America, v. 398, p.241-250.

Stolar, D.B., 2006, Coupling between tectonics and erosion in accretionary wedge settings, Ph.D. Thesis, University of Washington.

Stone, J.O., 2000, Air pressure and cosmogenic isotope production, Journal of Geophysical Research, v. 105, 2000, p. 23753–23759.

Stone, J.O., Todd, C., and Balco, G., 2004, Extraction of Al and Be from quartz for isotopic analysis: Univ. of Washington Cosmogenic Isotope Lab, Methods and Procedures, http://depts.washington.edu/cosmolab/chem.html

Stuwe, K., White, L., and Brown, R., 1994, The influence of eroding topography on steady-state isotherms; application to fission track analysis, Earth and Planetary Science Letters, v. 124, p. 63–74.

Thiede, R.C., Arrowsmith, J.R., Bookhagen, B., McWilliams, M.O., Sobel, E.R., and Strecker, M.R., 2005, From tectonically to erosionally controlled development of the Himalayan orogen, Geology, v. 33, p. 689–692.

Tibari, B., Pik, R., France-Lanord, C., Carignan, J., and Lavé, J., 2005, Extreme uplift and erosion rates in eastern Himalayas (Siang-Brahmaputra Basin) revealed by detrital (U-Th)/He thermochronology, Eos Transactions AGU, v. 86, Fall Meeting Supplement, Abstract T23C-0574.

Tinkler, K.J., 1997, Critical flow in rockbed streams with estimated values for Manning's n, Geomorphology, v. 20, p. 147-164.

Tomkin, J.H., Brandon, M.T., Pazzaglia, F.J., Barbour, J.R., and Willett, S.D., 2003, Quantitative testing of bedrock incision models for the Clearwater River, NW

Washington State, Journal of Geophysical Research, v. 108, doi:
10.1029/2002JB002087.

Tucker, G.E., and Slingerland, R., 1997, Drainage basin responses to climate change,
Water Resources Research, v.33, p.2031-2047.

Tucker, G.E., 2004, Drainage basin sensitivity to tectonic and climatic forcing:
implications of a stochastic model for the role of entrainment and erosion thresholds,
Earth Surface Processes and Landforms, v. 29, p. 185 –205.

Turowski J. M., Lague, D., Crave, A., and Hovius, N., 2006, Experimental channel
response to tectonic uplift, Journal of Geophysical Research, v. 111, F03008,
doi:10.1029/2005JF000306.

van der Beek, P., Champel, B., and Mugnier, J-L., 2002, Control of detachment dip
on drainage development in regions of active fault-propagation folding, Geology, v. 5,
p. 471–474.

van der Beek, P., and P. Bishop, 2003, Cenozoic river profile development in the
Upper Lachlan catchment (SE Australia) as a test of quantitative fluvial incision
models, Journal of Geophysical Research, v. 108, doi:10.1029/2002JB002125.

Vance, D., Bickle, M., Ivy-Ochs, S., and Kubik, P.W., 2002, Erosion and exhumation
in the Himalaya from cosmogenic isotope inventories of river sediments, Earth and
Planetary Science Letters, v. 206, p. 273–288.

Vannay, J.C., Grasemann, B., Rahn, M., Frank, W., Carter, A., and Baudraz, V., 2004,
Miocene to Holocene exhumation of metamorphic crustal wedges in the Himalayan
orogen: Evidence for tectonic extrusion coupled to fluvial erosion, Tectonics, v. 23,
doi: 10.1029/2002TC001429.

von Blanckenburg, F., 2005, The control mechanisms of erosion and weathering at
basin scale from cosmogenic nuclides in river sediment, Earth and Planetary Science
Letters, v. 237, p. 462–479.

Whipple, K. X., and G. E. Tucker, 1999, Dynamics of the stream-power river incision
model: Implications for height limits of mountain ranges, landscape response
timescales, and research needs, Journal of Geophysical Research, v. 104, p. 17,661–
17,674.

Whipple, K. X., Hancock, G.S., and Anderson, R.S., 2000, River incision into bedrock: Mechanics and the relative efficacy of plucking, abrasion, and cavitation, Geological Society of America Bulletin, v. 112, p. 490–503.

Whipple, K. X., and G. E. Tucker, 2002, Implications of sediment-flux-dependent river incision models for landscape evolution, Journal of Geophysical Research, v. 107, doi:10.1029/2000JB000044.

Whipple, K.X, and Meade, B.J., 2004, Controls on the strength of coupling among climate, erosion, and deformation in two-sided, frictional orogenic wedges at steady state, Journal of Geophysical Research, v. 109, p. 1–24.

Whipple, K.X., 2004, Bedrock rivers and the geomorphology of active orogens, Annual Reviews of Earth and Planetary Science, v. 32, p. 151-185.

Willett, S.D., 1999, Orogeny and orography: The effects of erosion on the structure of mountain belts, Journal of Geophysical Research, v. 104, p. 28,957–28,982.

Willett, S.D., Schlunegger, F., and Picotti, V., 2006, Messinian climate change and erosional destruction of the central European Alps, Geology, v. 34, p. 613–616.

Wobus, C.W., Hodges, K.V., and Whipple, K.X., 2003, Has focused denudation sustained active thrusting at the Himalayan topographic front?, Geology, v. 31, p. 861–864.

Wobus, C.W., Whipple, K.X., Hodges, K.V., 2006a, Neotectonics of the central Nepalese Himalaya: Constraints from geomorphology, detrital 40Ar/39Ar thermochronometry, and thermal modeling: Tectonics, v. 25, doi: 10.1029/2005TC00193529 July 2006.

Wobus, C. W., Tucker, G.E., and Anderson, R.S., 2006b, Self-formed bedrock channels, Geophysical Research Letters, v. 33, doi:10.1029/2006GL027182.

Wohl, E.E., 1993, Bedrock channel incision along Piccaninny Creek, Australia, Journal of Geology, v. 101, p. 749-761.

Wohl, E.E., Greenbaum, N., Schick, A.P., Baker, V.R., 1994, Controls on bedrock channel incision along Nahal Paran, Israel, Earth Surface Processes and Landforms, v. 19, p. 1-13.

Wohl, E.E., and Ikeda, H., 1997, Experimental simulation of channel incision into a cohesive substrate at varying gradients, Geology, v. 25, p. 295-298.

Wohl, E.E., and Ikeda, H., 1998, Patterns of bedrock channel erosion on the Boso Peninsula, Japan, Journal of Geology, v. 106, p. 331-345.

Wohl, E.E., Thompson, D.M., and Miller, A.J., 1999, Canyons with undulating walls, Geological Society of America Bulletin, v. 111, p. 949-959.

Wohl, E.E., 2000, Mountain Rivers, Water Resources Monograph series, v. 14, American Geophysical Union, Washington, D.C., 320 p.

Wohl, E.E., and Achyuthan, H., 2002, Substrate influences on incised-channel morphology, Journal of Geology, v. 110, p. 115-120.

Yager, E., Dietrich, W.E., Kirchner, J.W., McArdell, B.W., 2005, Prediction of Sediment Transport and Patch Dynamics in a Steep, Rough Stream, Eos Transactions AGU, v. 86, Fall Meeting Supplement, Abstract H51H-03.
Zeitler, P.K., Chamberlain, C.P., and Smith, H.A., 1993, Synchronous anatexis, metamorphism, and rapid denudation at Nanga Parbat, Pakistan Himalaya, Geology, v. 21, p. 347–350.

Zeitler, P.K., Meltzer, A.S., Koons, P.O., Craw, D., Hallet, B., Chamberlain, C.P., Kidd, W.S.F., Park, S.K., Seeber, L., Bishop, M., and Shroder, J., 2001, Erosion, Himalayan geodynamics, and the geomorphology of metamorphism: GSA Today, v. 11, p. 4–9.

Zeitler, P.K., Malloy, M.A., Kutney, M.P., Idleman, B.D., Liu, Y., Kidd, W.S., and Booth, A.L., 2006, Geochronological Evidence for the Tectonic and Topographic Evolution of SE Tibet, Eos Transactions AGU, v. 87, Fall Meeting Supplement, Abstract T23B-0480

Zhang, P.Z., Shen, Z., Wang, M., Gan, W., Bürgmann, R., Molnar, P., Wang, Q., Niu, Z., Sun, J., Wu, J., Hanrong, S., and Xinzhao, Y., 2004, Continuous deformation of the Tibetan Plateau from global positioning system data, Geology, v. 32, p. 809–812.

VITA

Noah J. Finnegan was born in Lake Forest, Illinois to Robin Engel Finnegan and Gregory Allan Finnegan. At age 10 he moved with his family to Norwich, VT, where he lived until leaving for college at age 18. Noah received a B.A. in geology at Carleton College in June of 1999. He worked for the Appalachian Mountain Club in Gorham, NH, the U.S. Geological Survey in Woods Hole, MA, and the National Marine Fisheries Service in Seattle, WA before starting graduate school at the University of Washington in 2001. Noah married Heidi Anita Guetschow on June 10, 2006.